PhD Program in Biomolecular Sciences

Department of Cellular, Computational and Integrative Biology – CIBIO

XXXIV Cycle

Deciphering mechanisms of resistance to FK866 in cancer cells

Tutor: Prof. Alessandro PROVENZANI

Advisor: Dr. Chiara Zucal

Centre for Integrative Biology, CIBIO

Laboratory of Genomic Screening

Ph.D. Thesis of

Ágata Sofia Assunção Carreira

Centre for Integrative Biology, CIBIO

Laboratory of Genomic Screening

Academic Year 2022-2023

ORIGINAL AUTHORSHIP

I Ágata Sofia Assunção Carreira confirm that this is my own work and the use of all material from other sources has been properly and fully acknowledged.

Ágata Carreira

“A smooth sea never made a skilled sailor.”

F. D. Roosevelt

ABSTRACT

Nicotinamide phosphoribosyltransferase (NAMPT) is a key metabolic enzyme in NAD^+ synthesis pathways which is found upregulated in several tumors, depicting NAD(H) lowering agents, as the NAMPT inhibitor FK866, an appealing approach for anticancer therapy. Like other anticancer small molecules, FK866 triggers chemoresistance, observed in several cancer cellular models, which can prevent its clinical application. Here, we unravel molecular mechanisms sustaining the acquisition of resistance to FK866 in a model of triple-negative breast cancer – TNBC - (MDA-MB-231 – MDA p.), exposed to increasing concentrations of the small molecule (MDA r.). Acquired resistance to FK866 was not explained by the increased activity of efflux pumps or by compensatory mechanisms of NAD^+ production. Additionally, a chemical high-throughput screening approach with FDA-approved drugs failed to identify potentially targetable MDA r. vulnerabilities. Instead, these cells present an increased mitochondrial spare respiratory capacity and a higher mitochondrial mass compared to the FK866-sensitive counterparts, as well as a metabolic dependence on pyruvate and succinate for energy production.

To gain deeper insights into metabolic adaptation in NAD(H) deprived conditions, we focused on the Yes-associated protein (YAP), a cotranscriptional regulator involved in metabolic rewiring. We showed that FK866 induces YAP nuclear translocation in FK866-sensitive but not in FK866-resistant models. Moreover, the up- or down-regulation of YAP levels modulates the sensitivity to the NAD(H) depletion agent, as well as the differential expression of PGC1-α, found upregulated in the TNBC FK866-resistant cells.

Taken together, these results unravel novel mechanisms of cell plasticity to counteract FK866 toxicity, which rely on mitochondrial rewiring. Moreover, we described a correlation between YAP activation and sensitivity to NAMPT inhibition, which can be further explored for clinical use.

ABBREVIATIONS

Only abbreviations that were repeated at least twice throughout the thesis are mentioned in this section

AMPK	AMP-activated protein kinase
AR	Androgen receptor
ATL	Adult T-cell leukemia/lymphoma
CHC	α-cyano-4-hydroxycinnamate
CLL	Chronic lymphocytic leukemia
CsA	Cyclosporin A
CTGF	Connective tissue growth factor
Drp1	Dynamin-related protein 1
ECAR	Extracellular acidification rate
EMT	Epithelial to mesenchymal transition
ETC	Electron Transport Chain
FAO	Datty acids oxidation
FCCP	Carbonyl cyanide-4(trifluoromethoxy) phenylhydrazone
GC	Glucocorticoid
GDH	Glutamate dehydrogenase
glycoPER	Glycolytic proton efflux rate
GLUT	Glucose transporter proteins
GR	Glucocorticoid receptor
G-3-P	Glyceraldehyde 3-phosphate
HDAC	Histone deacetylase
HIF-1	Hypoxia-induced factor 1
HK	Hexokinase

ABBREVIATIONS

LDHA	Lactate Dehydrogenase A
LDHB	Lactate dehydrogenase B
MCT1/4	Monocarboxylate Transporter 1/4
MDR	Multidrug resistance
MMP	Mitochondrial membrane potential
MPC1/2	Mitochondrial pyruvate carrier 1/2
MST1	Mammalian STE20-like protein kinase 1
mtDNA	Mitochondrial DNA
NA	Nicotinic Acid
NAD+	Nicotinamide Adenine Dinucleotide
NADH	Nicotinamide Adenine Dinucleotide Hydrate
NADSYN	NAD synthetase
NAM	Nicotinamide
NAMPT	Nicotinamide Phosphoribosyltransferase
NAPRT	Nicotinic Acid Phosphoribosyltransferase
NMN	Nicotinamide MonoNucleotide
NMNAT	NAM/NA Mononucleotide Adenylyltransferase
NMRK	Nicotinamide Riboside Kinase
NR	Nicotinamide Riboside
nuclearDNA	Nuclear DNA
OCR	Oxygen consumption rate
OMM	Outer mitochondrial membrane
OPA1	Optic atrophy-1
OXPHOS	Oxidative phosphorylation

ABBREVIATIONS

PARP	Poly (ADP-Ribose) Polymerase
PBEF	Pre B-cell colony Enhancing Factor
PDH1EA	Pyruvate dehydrogenase complex subunit 1
PDK1	Pyruvate dehydrogenase kinase 1
PEP	Phosphoenolpyruvate
PFK	Phosphofrutokinase
PGC1-α	Peroxisome proliferator-activated receptor-gamma co-activator
PPP	Pentose phosphate pathway
QA	Quinolinic Acid
QAPRT	Quinolinic acid PhosphoribosylTransferase
ROS	Reactive oxygen species
SDH	Succinate dehydrogenase
SRB	Sulforodamine B
TAZ	transcriptional co-activator with PDZ-binding motif
TBD	TEAD-binding domain
TCA	Tricarboxylic acids
TFAM	Mitochondrial transcriptional factor A
TME	Tumor microenvironment
TNBC	Triple-negative breast cancer
TOMM20	Translocase of outer mitochondrial membrane 20
YAP	Yes-associated protein

CONTENTS

FIGURE INDEX

INTRODUCTION

Cancer metabolism

Hallmarks of cancer: reprogramming of energy metabolism

Neoplastic cells present several distinctive features, gradually acquired by cell transformation. These cells are often characterized by uncontrolled proliferation, sustained by metabolic adjustments to fuel cell growth and division. In fact, the reprogramming of energy metabolism is considered one of the “Hallmarks of cancer”, an essential factor that progressively alter cell physiology until a stage of malignant growth. Importantly, these alterations in cell metabolism can be exploited for therapeutical purposes[1,2]. Despite cancer heterogenicity, malignant transformation at the bioenergetic level triggers alterations in metabolic enzymes or oncogenic signaling that support core functions like anabolism, catabolism and redox balance (Figure 1)[3]. Anabolic processes allow cancer cells use nutrients and ATP for the biosynthesis of essentials macromolecules (like proteins, lipids and nucleic acids).

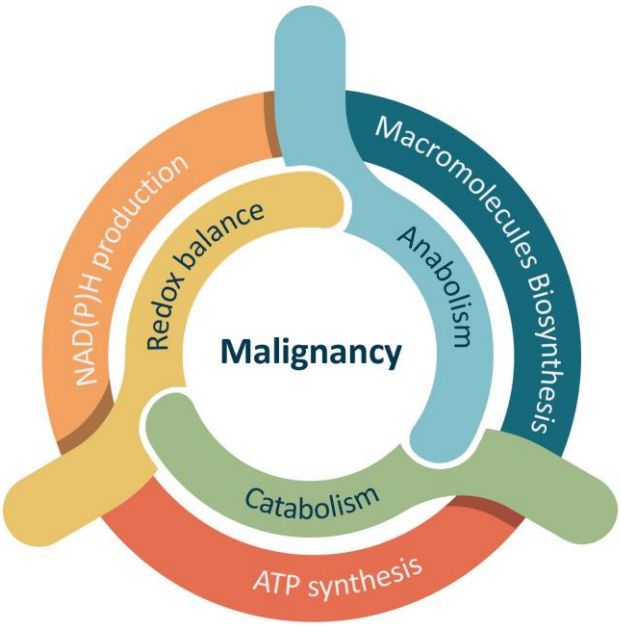

Figure 1 Malignant transformation. Normal cell malignant transformation includes alterations in anabolism (byosinthesis of macromolecules), catabolism (ATP synthesis) and redox balance (production of NAD(P)H equivalents).

Instead, catabolic reactions drive the production of energy transfer molecules as ATP through the oxidation of carbon sources by glycolysis and/or oxidative phosphorylation[4]. Cytoplasmic and mitochondrial NAD(P)H are important to sustain multiple antioxidant defense systems in cancer cells, thus preventing the activation of ROS-mediated death pathways[5]. NADP(H) is further important for cellular anabolic processes due to its role as electron surce for reductive synthesis reactions, such as non-essential amino acids, nucleotides and streroids synthesis[6].

The Warburg Effect: Concept and regulation

One of the main building pieces of evidence of deregulated cancer metabolism was described by Otto Warburg in the early 1920s. Under aerobic conditions, normal cells fully oxidize glucose via respiration in the mitochondria, producing CO_2 as end product. This highly efficient process for energy production is known as oxidative phosphorylation (OXPHOS) and offers a high yield of ATP molecules[7]. Instead, the "Warburg effect", describes the ability of cancer cells to use glycolysis to produce ATP and macromolecules, even under aerobic (non-hypoxic) conditions, resulting in the production of lactate from pyruvate, by lactate dehydrogenase (LDH)[8,9]. According to Warburg, this metabolic trait occurs due to a mitochondrial disfunction, that are unable to carry out OXPHOS. However, even if the Warburg phenotype constitutes a metabolic signature of 70-80% of human cancers, nowadays that are clear evidence that mitochondria are not defective in most of them. Instead, the "Warburg effect" is driven by major mechanisms that include the induction of the hypoxia inducible factor 1 (HIF-1), the alteration of growth factor signaling (PI3K/AKT), oncogene activation (MYC) and loss of function of onco-suppressors (P53)[10–13] (Figure 2).

HIF-1 activation up-regulate oxygen independent energy production pathways by increasing the expression of glycolytic enzymes like hexokinase (HK) and pyruvate dehydrogenase kinase 1 (PDK1); of glucose transporter proteins (GLUTs) and consequently the glucose-derived lactate production[14,15]. Like HIF-1, also the phosphoinositide 3-kinase (PI3K)/AKT pathway has diverse downstream

effectors in cellular metabolism. Upon activation by insulin, growth factors or cytokines, it regulates nutrient transporters and metabolic enzymes[14,16].

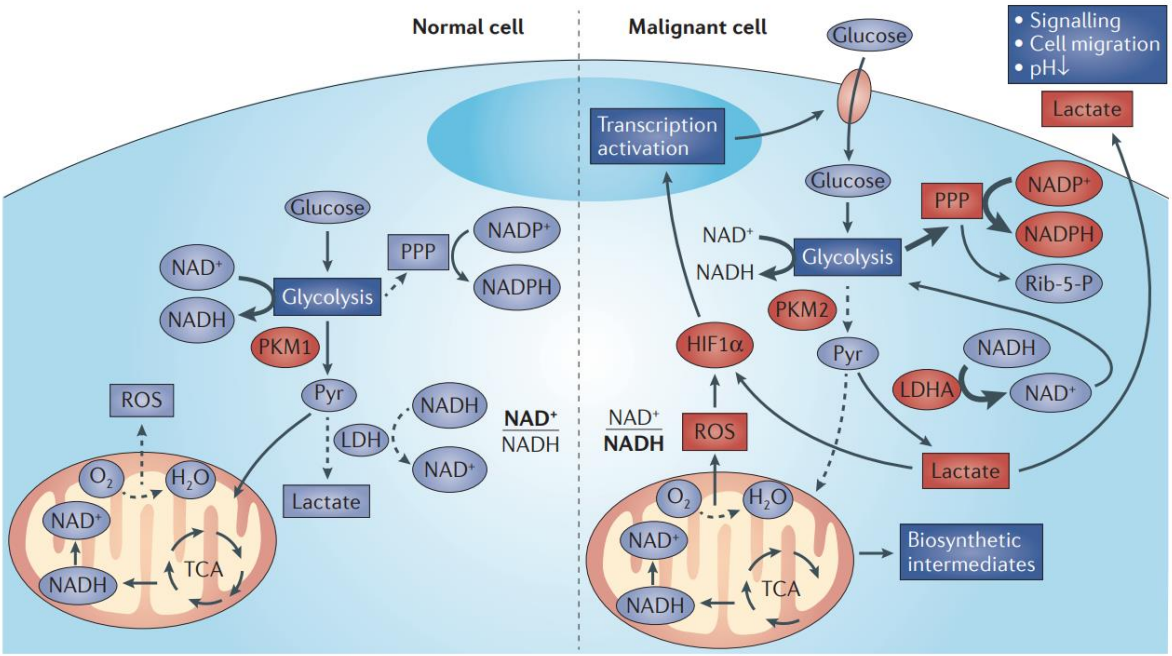

Figure 2 The Warburg effect. Schematic representation of the metabolic differences between normal (left side) and malignant/tumor cells (right side). In normal cells, glucose generates pyruvate that enters the TCA and is used for mitochondrial ATP production with regeneration of NADH to NAD^+. In malignant cells, HIF1α-dependent transcription activation, lead to the upregulation of glucose transporters, glycolytic flux, and pentose phosphate pathway (PPP) intermediates. Pyruvate is converted to lactate by LDHA, regenerating NAD^+ in the cytoplasm (Figure adapted from [88]**)**.

Of note, AKT promote GLUT1 and GLUT4-mediated glucose uptake[17,18], as well as phosphorylation and activation of glycolytic enzymes like HK2 and phosphofructokinase 1 (PFK1)[19,20]. Importantly, AKT induce also the activity of enzymes in the oxidative pentose phosphate pathway (PPP) through the SREBP axis, contributing for the reduced nicotinamide adenine dinucleotide phosphate (NADPH) pool in the cytoplasm and for the redox balance[21]. Instead, the loss of expression of the tumor suppressor *p53* results in a switch towards aerobic glycolysis, while the *MYC* oncogene directly bind and activate HK2 and lactate dehydrogenase A (LDHA)[22]. Overall, the "Warburg effect" confers cells an accelerated glycolytic flux and ATP synthesis with subsequent accumulation of

glycolytic intermediates for biomass synthesis, that is essential for cancer growth and progression[14,15].

Additionally, the NAD^+/NADH ratio also differs from normal to cancer cells. In normal cells, pyruvate generated from glycolysis is preferentially oxidized in the mitochondria, via the TCA cycle, balancing the NAD^+/NADH in favor of NAD^+. Instead, the increasing levels of cytoplasmatic LDHA allow the regeneration of NAD^+ from NADH without taking part in the mitochondrial ETC, rendering aerobic glycolysis efficient, and decreasing the NAD^+/NADH redox ratio. The inability of cells to regenerate NAD^+ pool would limit glycolysis by preventing the conversion of glyceraldehyde 3-phosphate to 1,3-bisphosphoglycerate by glyceraldehyde-3-phosphate dehydrogenase (GAPDH).

Lastly, it is relevant to mention the role of the lactate, which is not anymore seen only as a “metabolic waste-product”, but as an oncometabolite with relevant roles in the cellular energetic reprogramming (Figure 3).

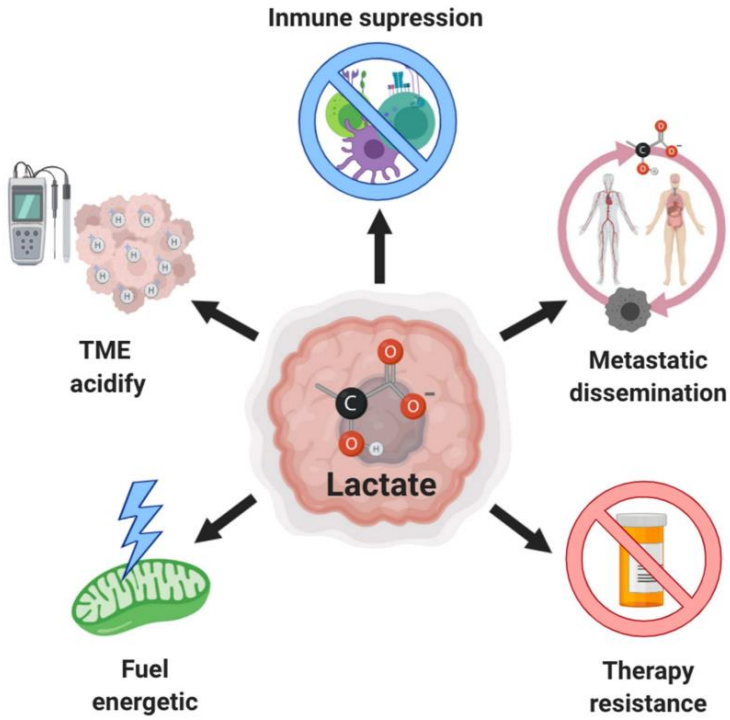

Figure 3 Lactate as an oncometabolite. Schematic view of the lactate role in cancer. This molecule can directly fuel TCA, and upon release from cancer cells, contribute to TME acidification, inhibition of the immune system, induce invasiveness, and metastasis and contribute to the acquirement of resistance to therapy (Figure adapted from [25]**).**

Being the final product of aerobic glycolysis, lactate is excessively produced and exported to the extracellular space, leading to an acidification of the tumor microenvironment (TME), which favors metastasis, angiogenesis, therapy resistance and immunosuppression[23–25]. HIF-1 and MYC induce aberrant expression of the glycolytic enzymes, including LDHA and thus lactate production, but also of the monocarboxylate transporters 1 and 4 (MCT1 and MCT4), that participate in the lactate import from and export to the extracellular milleau[15,26]. Moreover, lactate can be converted to pyruvate by the mitochondrial lactate dehydrogenase B (LDHB) and incorporated in the TCA cycle for energy production in normoxic cancer cells[27].

Pyruvate utilization: a bottleneck

Pyruvate remains at a central biochemical node connecting cytoplasmatic and mitochondrial energy production, as glucose-derived carbons can either be converted to lactate by LDHA, or imported into the mitochondria to enter the tricarboxylic acids (TCA) cycle[28]. In fact, several proteins that regulate pyruvate synthesis and consumption present difference expression or activity in normal versus cancer cells[29].

Pyruvate production in the cytoplasm for LDHA utilization is mainly promoted by the enzyme pyruvate kinase (PK) that irreversibly catalyzes phosphoenolpyruvate (PEP) to pyruvate. This enzyme present two different isoforms, M1 and M2, with distinct enzymatic activities, being PMK1 the most active one[30]. The most active M1 is found predominantly in non-cancerous tissues with high ATP demand[29]. Instead, the less active PKM2 isoform is exclusively expressed in tumor tissues and its overexpression leads to a glycolysis flux slowing down, allowing the accumulation of upstream glycolytic intermediates to be used for anabolic processes[31] (Figure 4).

Differently, pyruvate entrance in the mitochondria is mediated by the mitochondrial pyruvate carrier (MPC1 and MPC2). Pyruvate mitochondrial oxidation to acetyl-CoA occurs in the mitochondrial matrix and is mediated by pyruvate dehydrogenase (PDH) complex, that by its turn is regulated by PDH kinase 1 (PDK1)[29]. PDH activity is negatively regulated by PDK1 phosphorylation. PDK1 is frequently overexpressed in cancer, decreases pyruvate mitochondrial utilization,

TCA cycle intermediates and redox stress, and has been strongly implicated with oncogenesis[32,33].

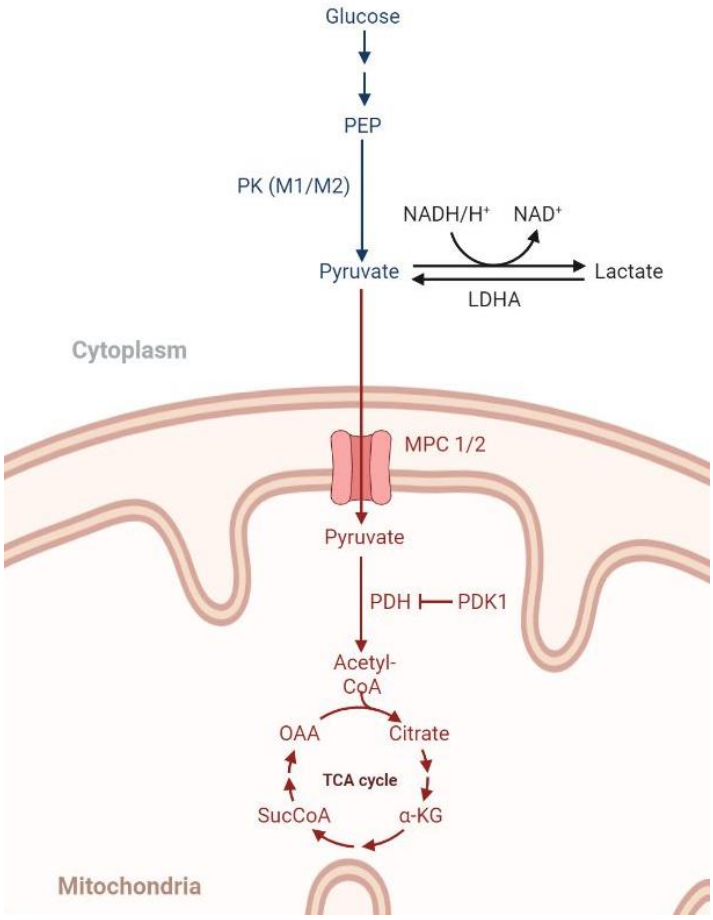

Figure 4 Pyruvate as a bottleneck. Schematic representation of pyruvate usage by cancer cells. Pyruvate is produced from glycolysis in a multistep reactions process, culminating in the oxidation of phosphoenolpyruvate (PEP) by pyruvate kinase (PK) M1 or M2 isoforms. At the cytoplasm, it can be oxidized by LDHA to produce lactate, with the concomitant regeneration of NAD^+ from NADH. Alternatively, MPC-mediated imported pyruvate can be integrated in the TCA cycle upon conversion to Acetyl-CoA by the pyruvate dehydrogenase complex (PDH), which is in turn inhibited by pyruvate dehydrogenase kinase 1 (PDK1).

Mitochondrial pyruvate carrier (MPC)

Pyruvate transport into the mitochondria was initially measured in 1974, but MPC was only formally identified in the last decade[34]. It was described as an inner mitochondrial membrane-located heterocomplex of two previously uncharacterized protein family members conserved from yeast to mammals[35,36]. More recently, it was classified as belonging to the SLC54 family of mitochondrial transport[37]. MPC is either lost or down regulated in variety of cancers (like colorectal cancer and renal cell carcinoma), and these conditions have been mainly associated with pro-

tumorigenic phenotype and poor clinical outcomes[38,39]. It was shown that MPC loss enhances mitochondrial metabolic flexibility, as it stimulates pathways that fuel carbon utilization by the TCA cycle, like glutaminolysis and fatty acids or amino acids oxidation[40,41].

MPC can be regulated both at transcriptional and post transcriptional levels. In prostate cancer, the direct binding of the transcriptional repressor chicken ovalbumin upstream promoter-transcription factor II (COUP-TFII) to promoter of the MPC1 gene reduced its expression[42]. Similar data was shown for glioblastoma cells *in vitro* and *in vivo*[43]. Peroxisome proliferator-activated receptor-gamma co-activator (PGC1-α) levels is reported to differently modulate MPC expression in cancer models. In kidney cell adenocarcinoma, PGC1-α silencing prevents its interaction with estrogen-related receptor alpha (ERR-α) and consequent recruitment to the ERR-α response element motif located in the proximal MPC1 promoter, leading to the downregulation of the MPC1 transcription[44]. Similar results were shown for breast cancer cell models[45]. Also in cholangiocarcinoma, the overexpression of PGC1-α induces an upregulation of the PDHE1A and MPC1 to increase the mitochondrial pyruvate influx[46]. At the post-transcriptional level, Sirt3-mediated acetylation of lysine 45 and 46 in MPC1 has been associated with decreased MPC activity in colon cancer, upon high glucose exposure[47]. Regarding MPC2, so far, it was only described lysine 19 and 26 acetylation as a negative regulation of the transporter activity in the diabetic hearth[48].

The first identified and characterized inhibitor of the mitochondrial pyruvate transport was α-cyano-4-hydroxycinnamate (CHC), that was able to block pyruvate transport in a non-competitive fashion, without disrupting the mitochondria[49]. After, the CHC analogue UK5099 (α-cyano-β-(1-phenylindol-3-yl)-acrylate) was developed to specifically modify a thiol group of the transporter, thus inhibiting its activity[50]. In 2005, while developing compounds to be used as potential antidiabetic drugs, Hildyard *et al.* discovered two novel thiazolidine compounds, GW604714X and GW450863X, and described them as potent inhibitors of MPC[51]. More recently, also thiazolidinediones (like rosiglitazone), a class of insulin sensitizers were identified as acute, specific inhibitors of MPC in a variety of cell types[52].

Of note, MPC inhibitor's therapeutic use could be envisioned under certain circumstances. For instance, several cancer cell lines (squamous cell carcinoma , cervix and breast cancer cells) derived spheroids showed local reoxygenation upon mitochondrial pyruvate transport inhibition with 7ACC2, which further sensitize tumor xenografts to radiotherapy[53]. Combination therapy of MPC inhibitors and glutamate dehydrogenase (GDH) inhibitors were shown to be very effective in preclinical models of liver cancer, as MPC inhibition-dependent GDH activation increase cellular dependence on glutamine metabolism[54]. Instead, MPC overexpression in colon cancer cells is able to promote ROS production and increase IFNγ-induced apoptosis[55].

Mitochondrial plasticity in cancer

Glycolytic/OXPHOS cancer phenotypes

Aligned with Warburg's initial observation, aerobic respiration can result from mitochondrial disfunctions in a small set of cancers. For example, in gliomas and acute myeloid leukemia (AML), mutations in the isocitrate dehydrogenase 1 and 2 (IDH1 and IDH2) lead to the production of the oncometabolite 2-hydroxyglutarate (2-HG) and inhibition of the IDH decarboxylase activity of conversion of isocitrate to α-ketoglutarate[56,57]. Similarly, mutations in other Krebs cycle genes like succinate dehydrogenase (SDH), in hepatocellular carcinoma, and fumarate hydratase (FH), in renal cell carcinoma, results in impairment of the OXPHOS and a metabolic shift towards aerobic glycolysis[58,59].

However, increasing evidence shows a critical role for functional mitochondria in tumor progression, metastasis and therapy resistance, in hybrid glycolytic/OXPHOS cancer phenotypes[11,60,61]. In fact, accordingly with Yu *et al.*, tumor tissues can be distinguished in at least three main metabolic phenotypes: glycolytic, OXPHOS, and hybrid glycolytic/OXPHOS cells, that present the highest level of metabolic flexibility (Figure 5)[62].

Mitochondria use a range of metabolic sources, such as glucose, fatty acids and glutamine, whose oxidation products replenish TCA cycle and enable not only the maintenance of the ETC and consequently ATP production, but also provide building blocks for macromolecules synthesis[63]. Also some amino acids like

alanine, proline, aspartate and glutamate participate in anaplerotic pathways to fuel mitochondrial metabolism[64].

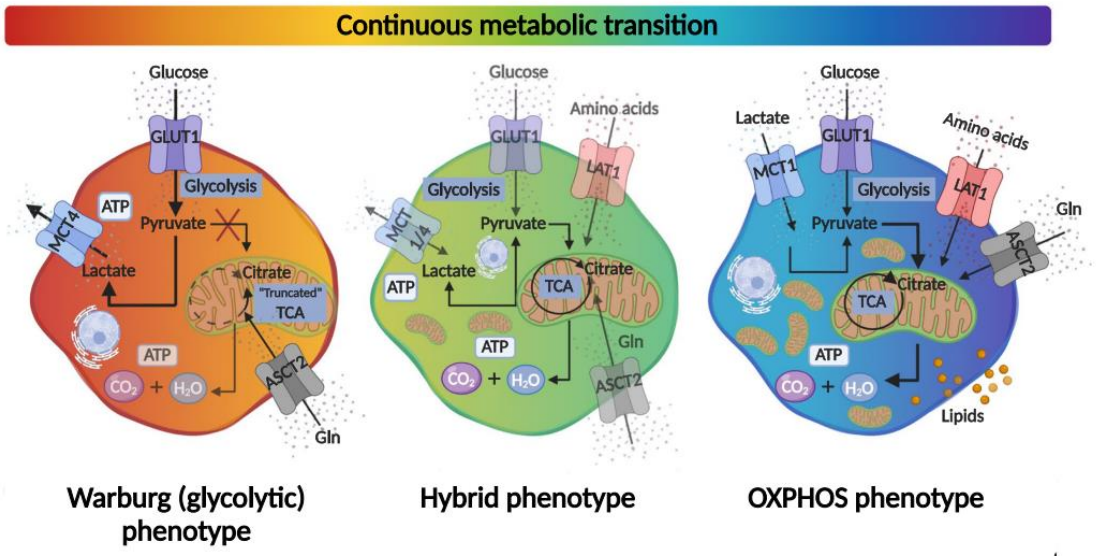

Figure 5 Cancer cells metabolic phenotypes. Schematic representation of the Warburg effect (left), with lactate production from pyruvate and released to the extracellular space. Glutamine can be used as alternative carbon source for the mitochondria. Hybrid glycolytic/OXPHOS phenotype (middle) with pyruvate sustaining both lactate production and the TCA. OXPHOS phenotype (right), with pyruvate being produced through glycolysis or the conversion from extracellular lactate, and consequently sustaining TCA (Figure adapted from [62])

In fact, it is the existence of multiple circuitries centered on the mitochondria, that ensure such a metabolic adaptation and a switch of substrate utilization[65]. Several cancer types like ovarian and pancreatic cancers, under hypoxic conditions and aerobic respiration activation were reported to present an augmented glutaminolysis[66,67]. Instead, reliance on the fatty acids oxidation (FAO) was observed in a model of triple negative breast cancer (TNBC) despite its dependence on glycolysis[68].

Beyond bioenergetics: mitochondrial dynamics

Mitochondria are essential organelles sensing the energetic stress, as fluctuations on blood glucose and lipids, and promoting the adaptation to energy-deprived environments. Beyond mitochondrial bioenergetics, several other aspects of

mitochondrial biology support malignant transformation, particularly the modulation mitochondrial mass and mitochondrial dynamics[69].

The mitochondrial mass is determined by the balance between two different processes: mitochondrial biogenesis, that contributes to an increase of mitochondrial mass and mitochondria turnover, through the selective autophagic mitochondrial pathway (mitophagy)[70].

PGC1-α interacts with several factors to maintain energy homeostasis, as NRF-1/2, PPARα/β/δ, and ERRα,β,γ, and is the main regulator of mitochondrial biogenesis[71–74]. However, this transcription factor presents an ambiguous role on tumorigenesis[75]. PGC1-α levels are usually positively correlated with tumor reliance on mitochondrial respiration and mitochondrial-regulated processes, like ROS detoxification, glutamine-derived lipogenesis, and fatty acid oxidation (Figure 6)[75].

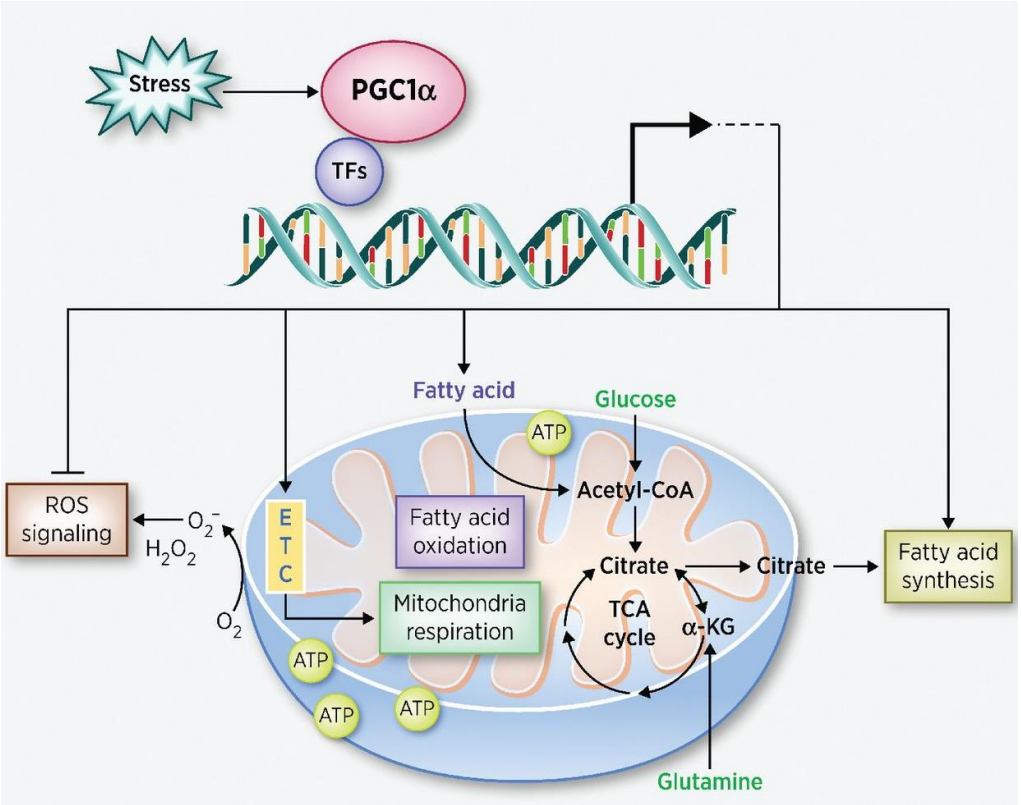

Figure 6 Biological functions of PGC1-α in cancer cells. Upon stress signaling, PGC1-α exerts it's transcriptional activity, promoting mitochondrial biogenesis and respirations, fatty acid and glutamine metabolism, and preventing ROS accumulation, facilitating cancer metabolic adaptation[75].

However, for some type of tumors, like in colorectal and ovarian cancer, it is considered a tumor suppressor as it induces Bax-mediated cell death[76,77]. Also in clear clean renal cell carcinoma (ccRCC) and breast cancer, low PGC1-α expression is associated with poor survival[78,79].

c-Myc is also a strong regulator of mitochondrial biogenesis, as studies with Myc gain/loss of function are associated with increased/reduced mitochondrial mass[8081]. It induces the expression of PGC1-α, but also of the mitochondrial transcriptional factor A (TFAM), that is essential for mitochondrial DNA replication and transcription[81].

Unlike mitochondrial biogenesis, mitophagy prompts the clearance of damaged mitochondria, and thus decrease of mitochondrial mass. This process is mainly triggered via the PTEN-induced putative kinase 1 (PINK1) pathway, but alternative autophagy induction is mediated by HIF-1α target genes like BCL2[70]. Similarly to its antagonist process, mitophagy can be pro- or anti-tumorigenic based on the tissue context and tumor stage[82].

Mitochondria dynamics is also dependent on the balance between fission and fusion that determines gross mitochondrial morphology[70]. Fission – division of the mitochondria- is mediated by dynamin-related protein 1 (Drp1) that interacts with outer mitochondria membrane (OMM) proteins, to cause a GTPase-dependent mitochondrial membrane constriction. Instead, fusion – combination of two mitochondria into an individual elongated mitochondrion - is mediated by mitofusions, Mfn1 and Mfn2, along with optic atrophy-1 (Opa1). Continuous cycles of fission/fusion allow cells to maintain a healthy pool of mitochondria, while the unbalance of these processes lead to fragmented or hyperfused pools of mitochondria[83] While hyperfused mitochondrial networks are described to present enhanced OxPhos ability and lower mitochondrial trafficking, cells with fragmented mitochondria are more glycolytic and less permissive for mitochondrial trafficking[84–86].

NAD(H) metabolome: NAD^+ biosynthesis and consumption

The pyridine nucleotides nicotine adenine dinucleotide (NAD^+) and its reduced form (NADH) play a central role in regulating biologic processes and cellular homeostasis. As major components of bioenergetic and signaling pathways,

NAD(H) regulate important cellular processes as transcription, DNA repair, cell cycle progression, circadian rhythms, apoptosis and metabolic regulation[87,88]. Recently, it was described a role of NAD^+ in DNA ligation and RNA capping, by serving as a nucleotide analogue[89,90]. Of note, NAD^+ can be converted to its phosphorylated form (NADP), that by its turn is reduced to NADPH and participates in fatty acid synthesis and maintenance of the redox balance[91].

At the metabolic level, NAD(H) works as a coenzyme, reversibly transferring hydrogen in several redox reactions of glycolysis, TCA cycle and oxidative phosphorylation[92]. During glycolysis, the enzyme GAPDH catalyzes the conversion of glyceraldehyde 3-phosphate (G-3-P) to 1,3-bisphosphoglycerate (1,3-BPG) using NAD^+ as cofactor and converting it to NADH[93]. Electrons from NADH enter the mitochondria ETC through the malate-aspartate or the glycerol-3-phosphate shuttles, as the inner mitochondrial membrane have always been considered impermeable to NAD(H)[94,95]. More recently, the mitochondrial protein SLC25A51 (also known as MCART1) was identified as a NAD^+ transporter in mammals, able to restore its levels in the organelle[96]. Alternatively, NADH is regenerated to NAD^+ by LDHA, thereby maintaining the cytoplasmatic NAD^+/NADH pool and active aerobic glysolysis[97]. In the mitochondria, NAD^+ accepts electrons from TCA cycle intermediates being converted to NADH, that acts as an electron donor molecule to complex I (NADH: ubiquinone oxidoreductase) of the ETC chain and drives oxidative phosphorylation, ultimately leading to ATP synthesis[91].

NAD^+ serves as a substrate for several families of mammalian enzymes including poly-ADP-ribose polymerases (PARPs), sirtuins and ectoenzymes. PARPs are a family of 17 proteins that catalyzes the transfer of ADP-ribose unites from NAD^+-onto target proteins, to maintain cellular transcriptional regulation, apoptosis and DNA damage response[98–100]. Importantly, PARP-1 expression and activity are found upregulated in several cancer, including ovarian cancer, colorectal cancer and leukemia, which pave the way for PARP inhibitors' clinical usage for cancer treatment[98,101,102].

Sirtuins are a family of protein deacetylases and adenosine diphosphate (ADP)-Ribosyltransferases belonging to the class III histone deacetylase family, which requires NAD^+ for its function[103]. Similarly to PARPS, sirtuins also modulate pivotal

cellular processes involved in cancer initiation and progression like DNA repair, transcriptional regulation and metabolism[104,105].

The cyclic ADP-ribose (cADPRs) family of ectoenzymes, including CD38 and CD73, hydrolyze NAD^+ to produce cADPRs, which are involved in Ca^{2+} mobilization, regulation of the cell cycle and insulin signalling[106,107].

Of note, even if these enzymes participate in different NAD^+-dependent reactions, they all involve the release of nicotinamide (Nam)[88]. The fact that signaling pathways, unlike redox reactions, continuously consume NAD^+, prompted the interest on the understanding of NAD^+ biosynthetic pathways (Figure 7).

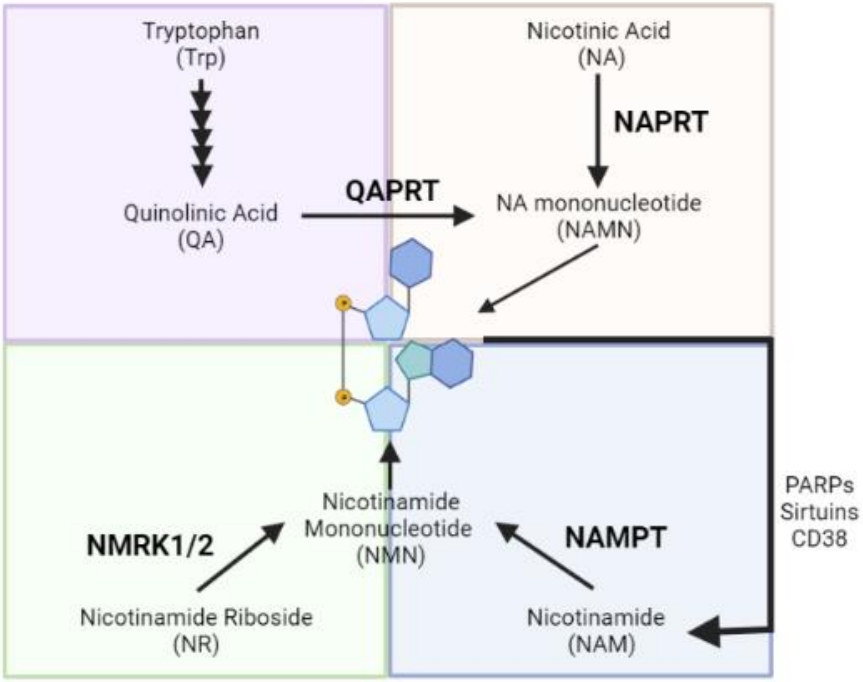

Figure 7 Overview of NAD(H) biosynthesis pathways. Tryptophan-derived quinolinic acid is used as substrate for NAMN synthesis. NAMN is also obtained by the NAPRT-mediated conversion of NA. Instead, NAMPT and NMRK1/2 synthetize NMN, respectively using NAM or NR as substrates. Formation of NAD^+ is the common step in all NAD+ biosynthetic routes. This molecule can be used by PARPs, sirtuins and ectoenzimes, like CD38, and regenerate NAM (adapted from[88]).

Several substrate-based pathways lead to NAD^+ synthesis. In the *de novo* NAD^+ synthesis, the amino acid tryptophan is converted to nicotinic acid mononucleotide (NAMN) through a series of reactions ending with the formation of quinolinic acid (QA), the substrate of QA phosphoribosyl transferase (QAPRT). NAMN can be also produced through the Press-Heindler pathway, with nicotinic acid (NA) being used as substate for nicotinic acid phosphoribosyl transferase (NAPRT). NAMN is

further converted to NAD^+ by NMN adenyl transferases (NMNAT) and NAD synthetase (NADSYN). Instead, the NAD^+ synthesis salvage pathway relies on nicotinamide phosphoribosyl transferase (NAMPT), that catalyzes the conversion of NAM to nicotinamide mononucleotide (MNM) and is the rate-limiting enzyme of NAD^+ synthesis. NAM levels are sustained by dietary input, as well as by the regeneration through NAD^+-consuming enzymes like PARPs, sirtuins and CD38/157. NMN is also the product of the conversion of nicotinamide riboside (NR) by nicotinamide riboside kinase (NMRK) and is the substrate of NMNAT for NAD^+ synthesis.

Targeting NAD^+ synthesis in cancer cells

The requirement of NAD^+ for several reactions that sustain metabolic processes and signaling, highlights its importance for the maintenance of cellular homeostasis. It is then conceivable that the metabolic rearrangement orchestrated throughout tumorigenesis may be counteracted by limiting NAD^+ availability, through the inhibition of the enzymes involved in its biosynthesis.

Recent studies showed that the major determinant of the cancer cells' dependence on the NAD^+ biosynthetic pathway is the tissue context: if tumors arise from normal tissue types that highly express NAPRT, this will be the main route for NAD^+ production. Instead, if NAPRT is not highly expressed in the normal tissue, tumors will be dependent on NAD^+ salvage pathways[108]. To date, very few NAPRT inhibitors have been reported, and 2-hydroxynicotinic acid (2-HNA) and several non-steroidal anti-inflammatory drugs (NSAIDs) were the widely used molecules to study the effects of NAPRT inhibition[109,110]. More recently, two additional chemical scaffolds that function as NAPRT inhibitors were identified through an *in silico* screening[111].

By the other side, potent NAMPT inhibitors have been developed throughout the years, and revealed as promising anti-cancer drugs[112].

NAMPT enzyme

NAMPT (also known as pre-B cell colony enhancing factor – PBEF – or visfatin) was firstly described by Preiss and Handler in 1957, as a distinctive enzyme that catalyze NAD^+ synthesis[113]. This phosphoribosyl transferase is expressed in

several organs and cells, and its homozygous knockout in mice is embryonically lethal, confirming it's crucial role in cellular physiology[114]. Nowadays, it is reported that the enzyme present both intracellular (iNAMPT) and extracellular (eNAMPT) forms (Figure 8)[115].

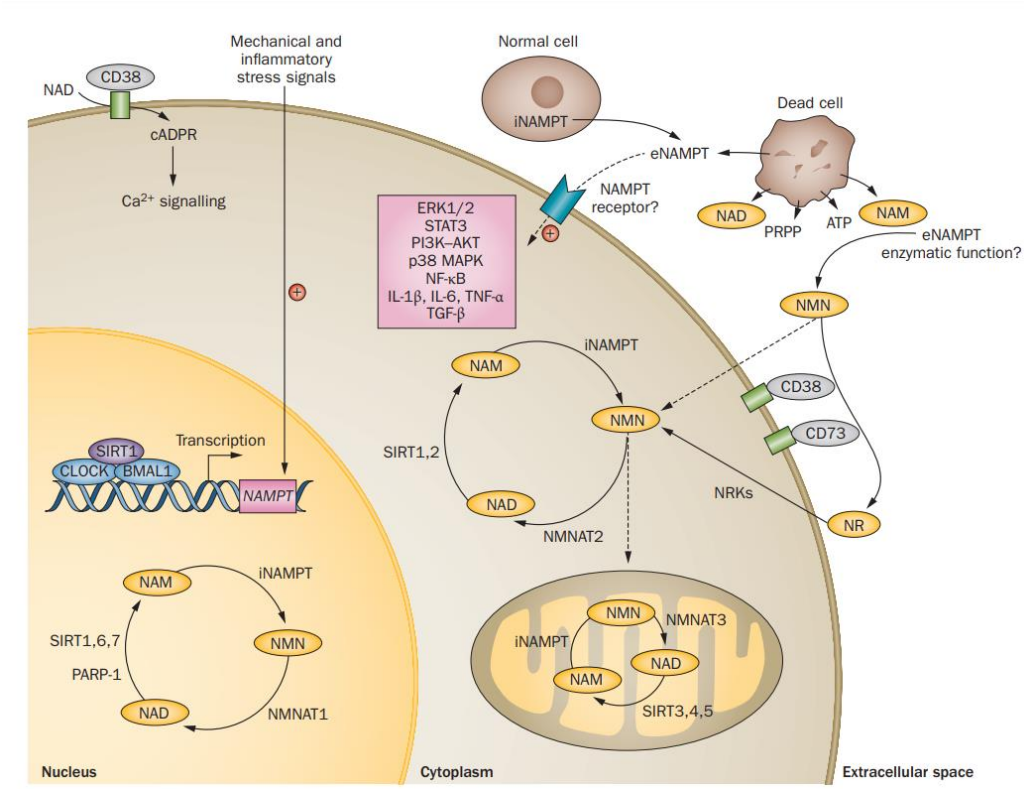

Figure 8 Physiological roles of NAMPT. eNAMPT act as anti- or pro-inflammatory cytokine, but its receptor is not yet identified. iNAMPT maintains the intracellular levels of NAD^+ and participates in the recycling of NAM, the product of sirtuins and PARPs. NAMPT expression is regulated by the circadian regulators CLOCK and BMAL1[122].

Samal *et al*. first described eNAMPT in 1994, as an active extracellular protein secreted from pre-B cells, that promote colony formation in synergy with stem cell factor and interleukin-7 (IL-7)[116]. Nowadays, it is known that eNAMPT is actually produced by most cell types, and particularly cancer cells, even though the understanding of its structure, function and biological roles are still poorly understood[117]. In breast cancer, eNAMPT is described as a cytokine able to activate TGFβ signaling and induce epithelial-to-mesenchymal transition (EMT)[118]. Accordingly, in chronic lymphocytic leukemia (CLL), it showed a role as a modulator of the immune system in the tumor microenvironment, turning it immunosuppressive and tumor-promoting. Its function is however independent of

NAMPT catalytic activity[119]. Overall, eNAMPT is currently defined as a tumor-promoting cytokine, released upon cellular stress, nutritional cues and inflammation[117]. Interestingly, increased levels of eNAMPT were found in serum or blood of cancer patients, and its level is positively correlated with both tissue NAMPT ones and cancer progression[119–121].

By its turn, iNAMPT is expressed in nucleus, cytoplasm, and mitochondria of several cells[122] and catalyzes the synthesis of NAD^+ from nicotinamide, that can be used not only as an energy cofactor, but also as a signaling pleiotropic molecule. In fact, iNAMPT is the only enzyme of NAD^+-biosynthetic pathways able to recycle nicotinamide (produced in reactions mediated by NAD-dependent enzymes like sirtuins, PARPs and ectoenzymes), and thus it's considered the rate-limiting enzyme of this nucleotide biosynthesis[88,123]. Of note, NAMPT mediated NAD^+ synthesis is involved in the regulation of the circadian clock, as inhibition of NAMPT releases CLOCK:BMAL1 from sirtuin 1-mediated supression[124]. Additionally, NAMPT has also been associated with angiogenesis and inflammation[123,125].

Given the crucial role of this enzyme on the maintenance of cellular NAD^+ levels, and the higher NAD^+ requirement of cancer cells, it is not surprising that NAMPT has been found upregulated in several tumors[104,126,127]. Therefore, NAMPT targeting presents itself as a therapeutic anticancer strategy, potentially leading not only to impairment of cancer cell metabolism but also bring about pleiotropic antitumor effects, like undermining inflammation[88].

NAMPT inhibitors

The first NAMPT inhibitor was reported in 2003. FK866 (APO866) was identified as an apoptosis inducer with high specificity to NAMPT, in a NAD^+-depletion based screening in HepG2 (human liver carcinoma cells)[128]. Crystallography studies showed that FK866 directly compete with NAMPT substrate NAM for the binding to the catalytic pocket (Figure 9)[129,130]. Thus, FK866 is a specific, competitive, and potent (nanomolar range) inhibitor of NAMPT that displays cytotoxicity to a broad panel of cancer cells[131–133].

The pharmacological signature of FK866 is characterized by intracellular NAD depletion, that reduces GAPDH activity and consequently glycolytic rate, carbon

supply to the TCA cycle and ATP levels[134,135]. Additionally, FK866 impairs the mitochondrial membrane potential (MMP) and increase reactive oxygen species (ROS) production in several models of leukemia and solid tumors[136–138].

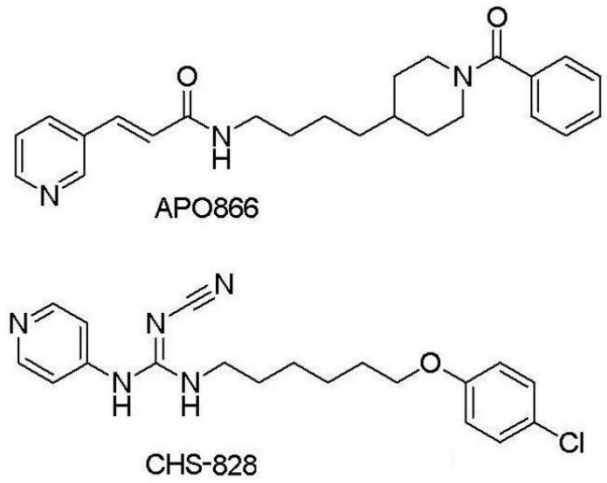

Figure 9 Chemical structures of firstly described NAMPT inhibitors. Structures of APO866/FK866 (above) and CHS-828 (below), revealing their chemical distinction[115]

Still, FK88-induced mechanism of cell death is still under debate in the literature as it seems to be tumor-dependent. In multiple myeloma cells, FK866 is described to decrease NAD^+ levels and consequently trigger autophagy but not apoptosis[139]. Similarly results were obtained for models of neuroblastoma, where NAMPT inhibition led to the formation of LC3-positive vesicles that fused with the lysosomes[140,141]. Instead, in adult T-cell leukemia/lymphoma (ATL) and CLL , apoptosis is the cellular death pathway activated in response to NAD^+ depletion through FK866 treatment[136,142]. Also in TNBC, NAD^+ depletion triggers adenine levels reduction that prime cells for apoptosis[143].

In-vitro FK866 cytotoxic profiles in cancer cells encouraged its usage in phase I clinical trials, where it revealed to be well-tolerated by patients with advanced solid tumor malignancies refractory to standard therapies[144]. However, owing to its short half-time in circulation, anti-tumor benefits were barely observed. The requirement of prolonged treatment regiments raised several side effects as lympho- and thrombocytopenia. Accordingly, FK866 and other NAMPT inhibitors like CHS-828 (GMX1778) (Figure 9) and its prodrug GMX177, did not demonstrate sufficient tumor-selectivity to achieve clinical success as single agents[112,145,146].

Interestingly, combining FK866 with other drugs targeting metabolism may enhance therapeutic efficacy of NAMPT inhibitors. It is reported that FK866, by depleting cellular NAD/NADH, increases metformin sensitivity in pancreatic cancer cells, resulting in a reduction of mitochondrial complex I activity and activation of the p53 pathway and oxidative stress[147]. Also in prostate tumor spheroids, FK866 treatment increases doxorubicin retention and cytotoxicity, by interfering with the cellular energy metabolism and the function of efflux pumps[132]. In glioblastoma, cisplatin and etoposide effect is potentiated by cotreatment with subtoxic doses of FK866, that increase their effect on DNA damage[140]. In leukemia cells, NAMPT inhibition is reported to be synergistic with histone deacetylase (HDAC) inhibitors and with the tumor necrosis factor-related apoptosis-inducing ligand (TRAIL)[148,149].
Strategies to deliver well-tolerated payloads of NAMPT inhibitors with reduced secondary effects are also being developed. Currently, antibody-drug conjugates (ADC) are being synthetized using biological active FK866 derivatives with chemical functionality to allow the synthesis of enzyme-cleavable drug linkers[150].
Very recently, another NAMPT inhibitor was identified through a chemical library screening to search for novel agents to selectively target hematological malignancies. OT-82 is a small molecule with a pyrazole group, with low-nanomolar range IC_{50} for hematological malignant cancer cells. It presented no cardiac, neurological or retinal toxicities in mice and non-human primates. A new clinical trial (NCT03921879) is currently recruiting patients to test safety of OT-82 usage for relapsed and refractory lymphoma[112,151].
Additionally, efforts are being made to target eNAMPT. For example, Oita *et al*. used NAMPT-neutralizing antibodies, to prevent NF-κB signaling activation via TLR4 and increase sensitivity of lung endothelial cells to TNF-α–induced apoptosis[152].

Drug resistance

Chemotherapy is currently one of the main cancer treatments, as it improves prognosis and overall survival of cancer patients. However, small anti-cancer drugs are rarely curative, as tumor diversity and heterogeneity favors adaptation to the therapeutic approach and thus the insurgence of chemoresistance[153].

There are several mechanisms supporting drug resistance. The increased efflux of drugs, primarily mediated by the overexpression of efflux pumps from members of the ABC transporter superfamily. These permeability glycoproteins (P-gp) decrease intracellular drug accumulation, and are considered one of the major reasons for chemoresistance[154–156]. The combination of the P-gp inhibitors Verapamil or cyclosporin A (CsA), with other cytotoxic drugs like doxorubicin and mitoxantrone, respectively, have actually been proposed to overcome multidrug resistance[157,158]. Regularly used chemotherapeutics (like 5-FU or cisplatin) act by inducing DNA damage on cancer cells and consequently activation of death pathways, but the repairment of these lesions by a number of DNA repair pathways promotes survival[159]. The utilization of targeted therapies rather than conventional anti-proliferative chemotherapeutics is also prone to the development of chemoresistance, as cells can induce the alteration of the drug target, either by point mutations or changes in protein expression levels [160]. In the recent years, importance has been given to many other escaping mechanisms, like evasion of senescence and influence of the tumor microenvironment[160].

Resistance to NAMPT inhibitors has been observed in several cancer cellular models, upon prolonged exposure to the small molecules. Acquired resistance to the NAMPT inhibitor GNE-618 was observed *in vitro* and *in vivo* due to the presence of point mutations in the *NAMPT* gene sequence: mutation of Ser165 resulted in an α-helix unwinding and prevention of the NAMPT substrate 5-phosphoribosyl-1-pyrophosphate (PRPP) binding; while mutations on Gly217 prevent the binding of GNE-618[161]. Ogino *et al.* showed that human colon cancer cell line HCT116 resistant to FK866 ($HCT116R^{FK866}$), exhibit cross-resistance to other NAMPT inhibitors like CHS-828, GNE-617, and STF-118804. In this model, NAMPT mutation H191R prevents its interaction with partner proteins of the POTE ankyrin family member, and thus acquirement of resistance[162]. Additionally,

HCT116R^{FK866} presented an increased expression of the drug efflux pumps/multidrug resistant proteins (MDR), whose inhibition (verapamil treatment) led to the re-sensitization to FK866[163].

Instead, studies with human fibrosarcoma cell line refractory to GMX1778 treatment, revealed a point mutation on NAMPT (Y18C) and an increased dependency of these cells of QAPRT, a key enzyme of the NAD^+ synthesis[164]. Similar results were observed in a model of T cell acute lymphoblastic leukemia (CCRF-CEM cell model), where QAPRT overexpression allows the exploitation of amino acids catabolism as a source for NAD^+ synthesis. Both in this model and in breast cancer cells resistant to FK866, the NAMPT coding sequence was not mutated, but a shift towards a glycolytic metabolism and dependence on LDHA was observed[133].

Finally, it was recently demonstrated that tumors presenting NAMPT but not NAPRT dependence are subject to resistant by NMRK1-dependent synthesis of NAD^+, which would explain the failure of NAMPT inhibitors[108].

YAP and the Hippo pathway

Cell and tissue homeostasis maintenance is widely dependent on the regulation and balance of key processes like cell proliferation and cell death, while disruption of such mechanisms often drives pathologic conditions[165].

The Hippo pathway, named after the "big-headed" phenotype of *drosophila melanogaster* mutants, regulates organ size by balancing cell proliferation and survival signaling[166]. In fact, these mutants were isolated in genetic screening for genes regulating organ size, and the phenotype attributed to mutations on *warts* (*wts* or *large tumor suppressors*, *lats*), *salvador* (*sav* or *sharpei*, *shrp9*) and *hippo* (*hpo* or *Drosophila mammalian Ste-20 kinase*, *dMst*)[167,168]. It was observed a tissue overgrowth in somatic clones with loss of *sav*, *hpo* or *wts,* with concomitant cell-autonomous increase of DIAP-1 (Drosophila inhibitor of apoptosis gene product) and Cyclin E, a cell cycle regulator[169]. The Hippo pathway gained particular attention upon *Yorkie* (*Yki*) identification in a yeast two-hybrid screen for *wts* binding protein[170]. Yki is the Drosophila homologous version of the mammalian Yes-associated protein (YAP), previously identified on 1994, and characterized as a proline-rich phosphoprotein able to bind to the Yes proto-oncogene product[171]. Thus, YAP and its homolog, the transcriptional co-activator with PDZ-binding motif (TAZ) are the major downstream effectors of the Hippo pathway in mammals[172]. Of note, YAP presents a N-terminal TEAD-binding domain (TBD), as well as two WW domains and a C-terminal transactivation domain (Figure 10) [173].

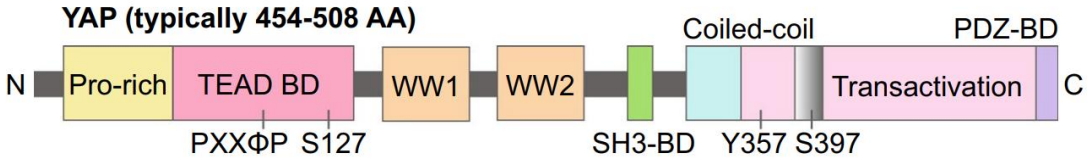

Figure 10 Overview of YAP domain. From N- to C- terminus, YAP presents a proline rich domain, a TEAD-binding domain, WW1 and WW2 domains, a coiled coil domain, a transactivation domain, and a PDZ-binding domain (Figure adapted from [173]).

As it lacks a DNA-binding motif, YAP-dependent gene transcription is regulated through its binding to transcription factors such as TEAD1-4, p73 and ZEB1[173–176]. The translocation of YAP from the cytoplasm to the nucleus, where it can activate

the expression of target genes, is a relevant step of the regulation of YAP activity[177]. YAP translocation into the nucleus is mainly accomplished through its phosphorylation in conserved HXRXXS motifs, including serine 127 (S127) and serine 397 (S397) sites, mediated by the Hippo pathway signaling[178,179]. Shortly, when the Hippo pathway is active (on), the mammalian STE20-like protein kinase 1 (MST1) or MST2 phosphorylate Salvador homolog 1 (SAV1). Their combined action phosphorylates and activates both the MOB kinase activator 1A (MOB1A), MOB1B, and the large tumor suppressor homolog 1 (LATS1) kinase and LATS2 kinase. Following the signaling cascade, the latest phosphorylates YAP and TAZ, that remains sequestered in the cytoplasm through the binding with the 14-3-3 protein. As a consequence, phosphorylated YAP/TAZ is primed to proteasomal degradation and unable to exert its transcriptional activity (Figure 11A).

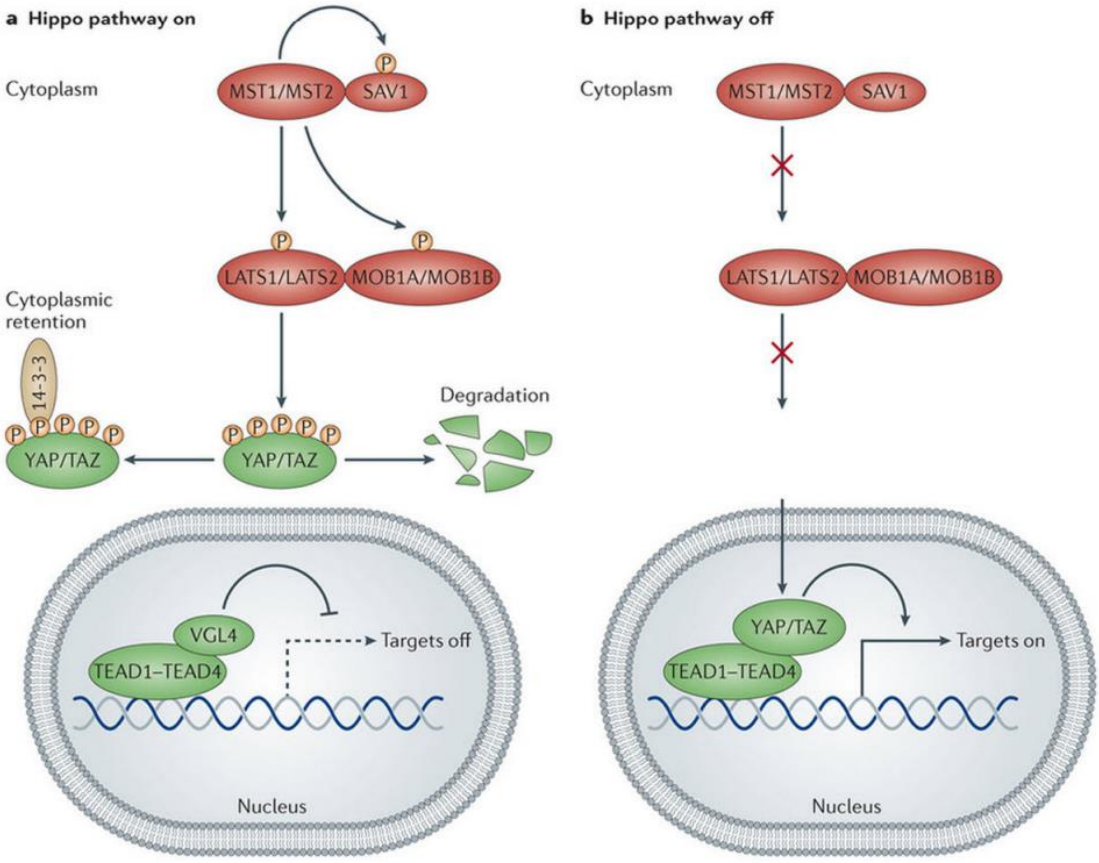

Figure 11 Schematic representation of the Hippo pathway. (A) When the Hippo pathways is ON, YAP is phosphorylated by a kinase signaling cascade including MST1/2, LATS1/2 and MOB1A/B. Phosphorylated YAP remains in the cytoplasm and it's degraded. Instead, when (B) the Hippo pathway is OFF, YAP remains not phosphorylated and migrates to the nucleus, binds to TEAD1-4 or other transcription factors, and activates the expression of its target genes[180].

Instead, when the Hippo pathway is off, the kinase-dependent signaling cascade is inactive, and the non-phosphorylated YAP/TAZ accumulates in the nucleus, where it forms a complex with TEAD1-4 proteins or other transcription factors (p73 or ZEB1, as mentioned above) and promotes the expression of target genes, including the connective tissue growth factor CTGF and CYR61 (Figure 11B)[180].

The activation of the Hippo pathway is reported to be regulated by the microenvironment and via extracellular signaling through soluble extracellular factors, cell-cell adhesions, mechanotransduction, and energy or endoplasmic reticulum stress[172,181,182]. In fact, up to date more than twenty regulators that intersect the core Hippo pathway at different levels have been identified, and grouped in four branches: the Crumbs homolog (CRB) complex; regulators that act upstream of the MST kinases; the actin cytoskeleton; and the adherent junction[180].

Dual role of YAP in cancer

YAP as oncogene

Since initial studies in *Drosophila* where loss of the Hippo pathway activity was leading to overgrowth phenotypes, this pathway have been thought to act as tumor suppressor[168]. Instead, YAP and its homolog TAZ which are activated upon Hippo-signaling cascade deactivation, were initially classified as oncogenes[183]. YAP/TAZ are described to regulate several functions that contribute to cancer development and progression like proliferation, epithelial to mesenchymal transition (EMT), cell migration, cell survival, drug resistance and stemness[180]. In fact, mice deficient of the Hippo kinases like MST1 and LATS1 showed tissue overgrowth and tumorigenesis in the liver, skin, ovaries and intestine[184,185]. In cholangiocarcinoma (CCA), high levels of nuclear YAP are correlated with poor prognosis, while its silencing increase chemosensitivity and inhibit metastasis *in vivo* and *in vitro*[186]. Similar results were observed for oral squamous cell carcinoma (OSCC), where YAP accumulation drives proliferation, migration and survival *in vitro*[187]*.* In lung adenocarcinoma, YAP activation and consequent expression of the antiapoptotic oncoprotein Survivin promotes the malignant progression of the serine/threonine kinase LKB1-deficient tumors[188]. Besides upregulation of antiapoptotic proteins, YAP drives the transcription of cell cycle-

promoting genes as CCND1 and FOXM1, resulting in malignant mesothelioma cell proliferation[189]. Resistance to the RAF- and MEK-targeting drugs vemurafenib and trametinib, respectively, was also attributed to YAP in BRAF-mutated tumors, were its increase expression is a biomarker of worse initial prognosis for tumors harboring BRAF V600E[190].

YAP as tumor suppressor gene

Despite the clear role of YAP/TAZ in promoting tumorigenesis, increasing number of studies report clinical evidence suggesting their context specific role as tumor suppressors. For example, YAP and TAZ can mediate β-catenin degradation in the absence of WNT, dampening the WNT signaling, that play important roles in cell-cell communication, cell fate, proliferation and stemness. Similar effects were observed for the YAP/TAZ-mediated β-catenin cytoplasmatic retention[191,192]. Apoptosis is also a YAP-regulated process, as in some cancer cell lines like H1299, HCT116, and MCF7, YAP was reported to promote the expression of apoptotic genes in response to DNA damage[193,194]. Also in MCF7, the increased expression of the proapoptotic gene *puma* is promoted by the RASSF1A-enhanced interaction between YAP an p73[195]. Furthermore, in models of hematologic malignancies, including multiple myeloma, lymphoma and leukemia, the pervasive DNA damage activates a proapoptotic network, supported by low YAP and consequently nuclear ABL1-induced apoptosis levels[196].

On non-small lung cancer, YAP function as tumor suppressor is mediated by the downregulation of the antioxidant enzyme GPX2 and consequent accumulation of .ROS[197]. Recently, it was also shown that prostate cancer cell lines presented an increased metastatic potential upon YAP knockdown, due to an activation of the EMT pathway, further suggesting a YAP tumor suppressive role[198].

YAP and energy metabolism

Cancer cells high proliferative rate translates into an increased metabolic demand, sustained by the enhancing of energy and biomass synthesis. Given the role of YAP and TAZ in promoting cellular growth programs, several studies report their involvement in metabolic regulation. By the other side, a plethora of metabolic cues are also reported to regulate YAP/TAZ activity (Figure 12)[182].

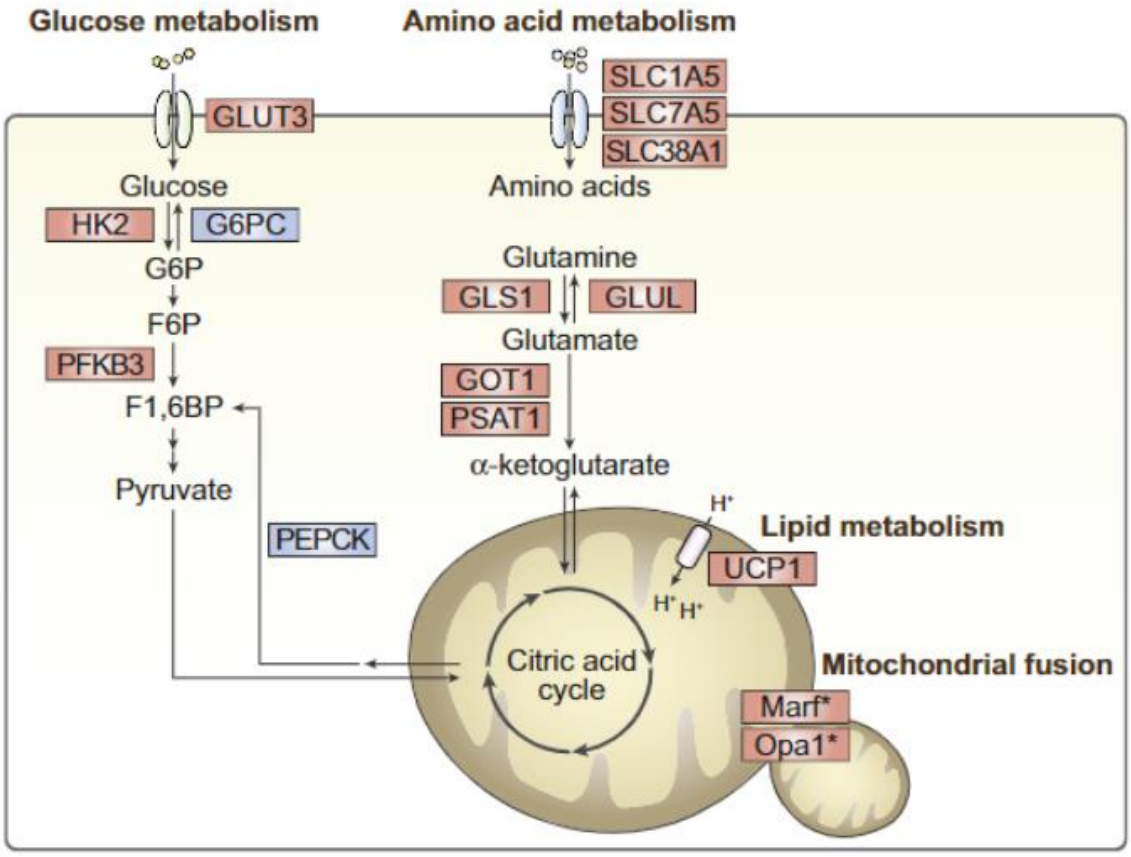

Figure 12 YAP/TAZ regulate metabolic processes. YAP/TAZ enhance glucose , amino acid and lipid metabolism, as well as mitochondrial fusion[182]. Genes transcriptionally regulated by YAP are in red boxes.

In alignment with the higher glycolytic dependence of cancer cells for proliferation, YAP/TAZ are described to enhance glycolysis through the upregulation of key glycolytic genes like GLUT3, HK1,HK2, PFKFB4, PFKP, GAPDH, PGK1, PGAM1, LDHA, PDHA and PDHB[199]. Instead, it was shown that under low glucose conditions or inhibited glycolysis, YAP is inactive, while presented the opposite behavior in response to increased glucose levels.

In fact, glucose deprivation alters the AMP to ATP ratio, which is sensed by the AMP-activated protein kinase (AMPK), that by its turn induces LATS1-dependent YAP phosphorylation and inactivation[200,201]. AMPK can mediate YAP inactivation by angiomotin-like 1 (AMOTL1)-mediated LATS1 phosphorylation and activation[202]. In conditions of high glucose levels, YAP/TAZ are O-GlcNAcylated at serine 109 by the O-GlcNAc transferase (OGT), which prompts its nuclear translocation and the transcriptional activation of target genes[203,204].

YAP/TAZ is also critical for fatty acids metabolism. A recent study suggests that YAP overexpression increases fatty acid oxidation on a melanoma mouse model, which is critical for lymph node metastasis[205]. YAP was also reported to interact with the nuclear forms of the sterol regulatory element-binding proteins (SREBPs), that control fatty acid and cholesterol biosynthesis, enhancing their transcriptional activity[206]. Instead, the palmitic acid was shown to induce both YAP inhibition or activation, respectively, through its modulation via the cGAS-STING-IRF3-MST1 pathway, or via palmitoylation of TEAD[207,208].

Regarding amino acid metabolism, YAP/TAZ modulate the expression of glutamine-metabolizing enzymes. For example, in breast cancer cells, YAP/TAZ stimulates the overexpression of glutamic–oxaloacetic transaminase (GOT1) and phosphoserine aminotransferase (PSAT1), and consequently the conversion of glutamate to AKG, thus increasing the dependence on exogenous glutamine[209]. Moreover, the uptake of amino acids is also affected by YAP and TAZ, as they stimulate the transcription of SLC1A5, SLC7A5, and SLC38A1, higher-affinity amino acid transporters[210,211].

Finally, YAP/TAZ can modulate mitochondrial biogenesis and size. It was observed larger mitochondria in cells overexpressing YAP, due to accelerated fusion mechanisms[212]. Instead, forced mitochondria fission has been associated with inhibition of YAP and TAZ[213].

The overall aim of this PhD is to decipher mechanisms of resistance to the NAD(H) inhibitor FK866 in cancer cells. The results obtained and reported are presented as two linked projects.

In the **First Project**, we aimed to characterize the metabolic rewiring of FK866-resistant cells in comparison with their sensitive counterparts in a cellular model of triple negative breast cancer.

In the **Second Project,** we unravelled the role of the co-transcriptional factor YAP as a mediator of FK866 sensitivity in the same cellular model.

FIRST PROJECT

“Mitochondrial rewiring drives metabolic adaptation to NAD(H) shortage in triple negative breast cancer cells”

BACKGROUND

Reprogramming of energy metabolism has been considered a hallmark of cancer, as neoplastic diseases are characterized by a deregulated control of cell growth and division, that require adjustments of energy metabolism[214]. The metabolic rewiring of cancer cells is often sustained by an increased glycolysis, in the presence of oxygen, known as the Warburg effect, that allows both ATP and biomass production due to an increased glucose uptake[215]. However, aerobic glycolysis does not always depend on dysfunctional or impaired mitochondria functioning, but instead mitochondrial metabolism and ETC function are required for tumor growth in nutrient-deprived conditions[13,216,217]. In fact, mitochondria plasticity allows not only a switch of substrate utilization, with reliance on glutaminolysis and fatty acid oxidation observed in a myriad of tumors, but also alterations of mitochondrial mass and number, to sustain higher mitochondrial respiratory capacity[65].

Nicotinamide adenine dinucleotide (NAD^+) is fundamental for energy metabolism, as it is a cofactor for enzymes involved in glycolysis, fatty acid oxidation and the tricarboxylic acids (TCA) cycle[218–220]. Additionally, NAD^+ plays a critical role as substrate for NAD^+-consuming enzymes like sirtuins, poly-ADP-ribose polymerases (PARPs) and CD38/157, that among others, sustain DNA repair, genomic integrity and regulation of transcription and signalling[221–223]. Among the enzymes involved in the synthesis pathways, NAMPT, that catalyzes the conversion of NAM to NMN, is considered the rate-limiting enzyme of the NAD^+ "salvage" pathway[224–226].

Due to its central role in NAD^+ synthesis and bioenergetics, NAMPT has been found to be upregulated in many solid tumors, revealing the significance of the development of NAMPT inhibitors for cancer treatment[127,227–229]. Moreover, NAMPT inhibitors like FK866 (APO866) have been extensively used in preclinical cancer research to mimic cellular NAD(H) shortage, characteristic of the high energetic demand of rapidly proliferating cancer cells[230].

AIMS

My PhD project was performed within the scope of the H2020 Marie Skłodowska-Curie ITN program INTEGRATA, an European Training Network (ETN) aiming to promote a strong interaction between academia and industrial sectors to integrate chemical and biological approaches to target NAD production and signaling in cancer. Specifically, we aimed to unravel the molecular mechanism leading to acquired pharmacoresistance to the NAMPT inhibitor FK866 in cancer cell models, which can prevent the success of NAMPT inhibitors for clinical application.

Moreover, previous work from our lab showed that cancer cells' acquirement of resistance to NAMPT inhibition, in absence of target gene mutation or acquirement of multi drug resistance mechanisms, invariably induces dependency of LDHA, but does not shift towards aerobic glycolysis[231].

Thus, the main goal of the project is to characterize potential vulnerabilities of FK866-resistant cancer cell models. We aimed to:

(1) Implement an HTS drug screening to deconvolute the vulnerabilities by a chemical-biology approach.

(2) Deeper characterize the metabolic adaptation by:

(A) Understanding the potential role of the NAD^+-biosynthetic enzymes on counteracting FK866-induced NAD(H) shortage;

(B) Dissect the role of mitochondria in sustaining NAD(H) levels and ATP production in FK866-resistant cancer cell lines.

MATERIALS AND METHODS

Cell lines culture conditions

MDA-MB-231 (MDA p.) human breast cancer cell line was obtained from American Type Culture Collection (ATCC). From these cells, it was developed the FK866-resistant cell line (MDA r.) by increased exposure to FK866 during a 3 month period of time, as previously described[133]. Cell lines were cultured in DMEM (Gibco), and supplemented with 10% fetal bovine serum (FBS), 2mM L-glutamine, and 100U/mL penicillin-streptomycin (all from Lonza). The culture media of MDA r. and was additionally supplemented with 100nM of FK866. Cells were maintained at 37ºC under humidified conditions with 5% CO_2.

Prestwick High-Throughput Screening (HTS)

The primary screening was conducted on MDA p. and MDA r., using the Prestwick chemical library (from Prestwick Chemical Libraries), composed of 1200 off-patent FDA and EMA-approved compounds. Cells were seeded using the Tecan EVO200 liquid handler, in Cellcarier 384 white plates (PerkinElmer) for luminescence measurement. After 24 hours of attachment, cells were treated with 1uM of the each compound using the Echo 650 liquid handler (Beckman). Each drug was tested in two replicates, in independent plates. Vehicle treated controls (DMSO %) and positive controls treated with doxorubicin (Sigma, D1515) at the concentration of 10 µM were added in the first and last two columns of the 384 plates. After 48 hours of incubation, cells were assayed for viability by measuring ATP with CellTiterGlo kit (Promega) following the manufacturer's instructions. Cytotoxicity was quantified by the percentage of reduction of cells after treatment (percentage of control, POC). For the confirmatory dose-response screening, chlortalidone was assayed at 6 different concentrations (100nM to 100uM) in both MDA p. and MDA r. cells, with or without FK866 co-treatment at 10nM and 100nM, using the same protocol. The dose-response curves were analyzed with GraphPad Prism with a non-linear regression curve fit.

Drug treatments and in vitro cell viability

MDA p. and MDA r. cells were treated with FK866 (sc-205325, Santa Cruz Biotechnology), CHS-828 (200484-11-3, Cayman Chemical), verapamil (V4629, Sigma), antimycin A (A8674, Sigma), 5-FU (F6627, Sigma), cisplatin (PHR1624, Sigma), UK5099 (5048170002, Sigma) and rosiglitazone (R2408, Sigma), for 48h. In vitro drug sensitivity was assessed through two different assays: the OzBlue Cell Viability kit (OzBiosciences) and the surforhodamide B (SRB) assay. Fluorescent signal from the OzBlue cell viability assay was measured after 2 hours of incubation, according to the manufacturer instructions. For the SRB assay, after the 48h treatment, cells were fixed with 10% trichloroacetic acid for 30 minutes at 4ºC. Thereafter, plates were washed in Milli-Q water, hair-dried and stained for 10 minutes with 0.4% sulforodamine B (SRB) in 1% glacial acetic acid. After rinsing in 1% glacial acetic acid for three times, and air-dried again, SRB was dissolved in 10mM Tris Base, and absorbance was measured at 560nm at the Tecan plate reader.

Cell proliferation assay

For proliferation assays, 30 K cells were seeded and counted every 24 hours using 0.2% trypan blue exclusion to determine the number of viable cells. Doubling time was calculated at the exponential growth phase, between 48 and 73 hours of seeding.

Determination of NAD(H) and ATP/AMP levels

For intracellular NAD(H) content determination, cells were lysed in 0.6 M perchloric acid (PCA) (for NAD+) or in 0.1M NaOH (for NADH) at 4°C. Cell extracts were centrifuged for 3 min at 16,000g and the supernatants were collected for the determination of NAD(H) content, as described31. NAD(H)values were normalized to protein content, determined through the Bradford assay.

To evaluate the ATP/AMP ratio as a marker of cellular energy status, intracellular ATP and AMP content was assayed spectrophotometrically at 340 nm. ATP was measured in a medium containing 0.02 ml of neutralized perchloric extract, 50 mM Tris-HCl pH 8.0, 1 mM NADP, 0.5 mM MgCl2, 5 mM glucose, and 4 µg of purified

hexokinase/glucose-6-phosphate dehydrogenase in 1 ml final volume, before and after the addition of the hexokinase/glucose-6-phosphate dehydrogenase. For AMP assay, 0.02 ml of neutralized perchloric extract was added to an assay medium containing 50 mM Tris-HCl, pH 8.0, 0.2 mM NADH, 0.5 mM MgCl2, 1 mM phosphoenolpyruvate, 0.2 mM ATP, 5 µg of purified pyruvate kinase/lactate dehydrogenase mixture, and 2 µg of purified adenylate kinase32. ATP and AMP concentrations were normalized to protein content, determined through the Bradford assay.

For measurements of total ATP levels, the CellTiter-Glo Luminescent Cell Viability Assay (G7571, Promega) was used, following the manufacturer's protocol. Protein content of the cell lysate was measured by the Bradford method and used for normalization of the luminescent values.

Protein extraction and western blot analysis

Samples were lysed for 10 min on ice with RIPA lysis buffer supplemented with Protease Inhibitor Cocktail (ThermoScientific), followed by sonication and clarification. SDS-polyacrylamide gel loaded with equal amounts of proteins was used for protein separation, followed by the transference to a PVDF membrane. The primary antibodies used were: NAMPT/Visfatin (A300-779A, Bethyl Laboratories), NAPRT (ab211529, Abcam), QAPRT (TA501520, OriGene), NMRK1 (sc-398852, SantaCruz Biotecnhologies), MPC1 (PA5116938, Cell Signalling), MPC2 (ab236584, Abcam), PDH1Ea (sc-377092, SantaCruz Biotechnologies), TOMM20 (HPA011562, Sigma), Actin (BK4970S CST) and Calnexin (ab133615, Abcam). Actin and Calnexin were used as protein loading controls. The anti-mouse and anti-rabbit secondary antibodies (111-035-003) used were obtained from Jackson Immunoresearch Laboratories. Signal was revealed with chemiluminescence detection kit reagents (Amersham ECL Select, GE Healthcare) at ChemiDoc (BioRad). The relative density of protein bands was analyzed using the ImageJ software and represented as the fold change of the corresponding control. A representative western blot of three independent biological experiments is shown.

RNA extraction and real-time qPCR

TriZOL reagent (Invitrogen) was used for total RNA extraction, according to the manufacturer's instructions. cDNA synthesis was carried out with RevertAid RT Reverse Transcription Kit (K1691, ThermoScientific) following manufacturer's instructions. Real-time quantitative PCR (RT-qPCR) analyses were performed in triplicate using the ExcelTaq™ 2X qPCR Master Mix (SMOBIO) on a CFX96 Real-Time PCR Detection System (Bio-Rad). The sequences of the primers employed in the study are present in **Table 1**. ΔCq method was used for samples' mRNA quantification, with RPLP0 or actin as housekeeping genes.

Gene	Primers
NAMPT/Visfatin	FW: TTATGGAACGAAAGATCCTG
	RV: AAAAGCATCTTTTTCATGGTC
NAPRT	FW:CTATGCCTTGGCTTTTCCCC
	RV:GAAGACCTTGCGGATCTCCT
QAPRT	FW:CCCTCTGGGTCACACATCTT
	RV:GTGCTCATTATCACCGCAGA
NMRK1	FW:TGTGTTTGGGAGGACTCGAA
	RV:CACTGCAATTTGGGAGGTGT
MPC1	FW:CAGTGGGCGGATGACATTTG
	RV:GCGTGGCATGCAAACAGAAG
MPC2	FW:ACCTACCACCGGCTCCTCGAT
	RV:CCAGCACACACCAACCCCCATT
PGC1α	FW: CAAAGGATGCGCTCTCGTTCA
	RV: GGTGTCTGTAGTGGCTTGACT
TFAM	FW: CCGAGGTGGTTTTCATCTGT
	RV: AGTCTTCAGCTTTTCCTGCG
Sirt1	FW: CAGTGTCATGGTTCCTTTGC
	RV: AAGACATCGAGGAAGTACCTG
RPLP0	FW:CATTCTCGCTTCCTGGAG
	RV:CTTGACCTTTTCAGCAAGTGG
Actin	FW: CTGGAACGGTGAAGGTGACA
	RV: GGGACTTCCTGTAACAATGCA

Table 1: List of primers used to evaluate the expression of genes of interest by RT-qPCR analysis.

shRNA and siRNA transfection

HEK293T cells were used to produce lentiviral vector particles (LVP). Cells were co-transfected with a Δ891 and a VSV-G encoding vector along with the shNMRK1 plasmid. PLKO vector was used as the transfer plasmid. Viral supernatants were collected, filtrated, and quantified 72 hours post-transfection. Selection with puromycin (1ug/mL) was performed on MDA r. stably infceted with shNMRK1.

Downregulation of MPC1 and/or MPC2 in MDA p. was performed with transient transfection of siMPC1 (sc-95332, Santa Cruz Biotechnology) and/or siMPC2 (sc-78813, Santa Cruz Biotechnology) using INTERFERin in vitro siRNA transfection reagent (Polyplus), according to the manufacturer's instructions.

Glycolysis Rate and Mitochondrial Respiration

The glycolytic rate, spare respiratory capacity and the mitochondrial respiration were assessed in both MDA p. and MDA r., respectively with the Seahorse Glycolysis Rate assay kit (103344-100, Agilent) and with the Seahorse MitoStress kit (103015-100, Agilent), following the manufacturer's instructions. Shortly, cells were seeded in the seahorse assay plates for 48h in Seahorse DMEM supplemented with 10mM glucose, 2mM glutamine, 1mM pyruvate (all from Agilent). The day before the assay, a cartridge was hydrated using Seahorse calibrant XF (Agilent) and incubated overnight at 37ºC in a CO_2 deprived atmosphere. The oxygen consumption rate (OCR) and the extracellular acidification rate (ECAR) were determined on a XF^e96 Seahorse Bioanalyzer (Agilent). The final concentration of injected compounds was: 1µM oligomycin; 2µM FCCP (carbonyl cyanide-4(trifluoromethoxy) phenylhydrazone); 2µM UK5099; 5µM of each rotenone and antimycin A; 10mM glucose; and 50mM 2-DG (2-deoxy-glucose). OCR and ECAR were normalized to the samples' protein content using the Bradford reagent.

In other experiments, to assess the contribution of the pathways leaded by respiratory complex I or II, the OCR was measured with an amperometric electrode (Unisense Microrespiration, Unisense A/S, Denmark) in a closed chamber, at 25°C. For each experiment, 2 x 10^5 cells were resuspended in

phosphate buffer saline (PBS) and permeabilized with 0.03 mg/ml digitonin for 1 min. To activate the pathway composed by respiratory complexes I, III, and IV, 10 mM pyruvate plus 5 mM malate were added. To induce the pathway formed by complexes II, III, and IV 20 mM succinate plus 100 µM rotenone (the specific inhibitor of complex I) were employed [232].

DNA extraction and mitochondrial mass determination

DNA was extracted from MDA p. and MDA r. to determine mitochondrial mass by estimating the mitochondrial DNA (mtDNA) to nuclear DNA (nuclearDNA) ratio. Cells were lysed in 100uL of lysis buffer (100 mM Tris-HCl pH 8, 200 mM NaCl, 5 mM EDTA, 0.2% SDS, 0.2 mg/mL proteinase K freshly added) for 2h at 56ºC. Debris removal was obtained by centrifugation at 14000rpm for 10min at room temperature, followed by DNA precipitation with 500uL of isopropanol. After centrifugation at 14000rpm for 5min at room temperature, the pellet was washed with 70% ethanol. Subsequently, samples were centrifuged at 14,000 rpm for 5 min at room temperature, the supernatant was discarded, and the DNA pellet was dried at room temperature. Finally, the DNA pellet was resuspended in 50µl DNase-free water and one hundred nanograms was used for further analysis. RT-qPCR was performed in triplicate using the ExcelTaq™ 2X qPCR Master Mix (SMOBIO) on a CFX96 Real-Time PCR Detection System (Bio-Rad). The nuclear-encoded gene, human B2M, and the mitochondrial-encoded gene, human tRNALeu were used to calculate the relative mtDNA:nuclearDNA ratio using the $2^{-\Delta\Delta Ct}$ method. The sequences of the used primers were: B2M FW: TGCTGTCTCCATGTTTGATGTATCT, B2M RV: TCTCTGCTCCCCACCTCTAAGT, tRNALeu FW: CACCCAAGAACAGGGTTTGT, and tRNALeu RV: TGGCCATGGGTATGTTGTTA.

Mitochondrial substrate dependencies

Mitochondrial substrate utilization was assessed with Biolog MitoPlates S-1 (Biolog, Hayward, CA, USA, #14105), as suggested by the manufacturer. Briefly, MitoPlates were incubated in Omnilog® at 37ºC for 1h with Biolog Mitochondria Assay Solution (MAS) containing Biolog redox dye MC and saponin (Sigma-

Aldrich, 84510, 20ug/uL) to allow substrate rehydration and cell permeabilization, respectively. Viable cell number was previously determined by trypan blue exclusion and resuspended in Biolog MAS, after washing with PBS 1x. Cells were added to the MitoPlates and the kinetic reading of the rate of purple color formation was measured in Omnilog® system (OD_{590nm}) for 4h. The background was corrected for the blank sample (no substrate).

Respiratory complexes activity

To determine the activity of respiratory complexes I, II, III and IV, 50µg of total protein homogenate was used[233]. The reactions were followed for 5 min, with 1 min-interval collecting data, and absorbance values were measured in a spectrophotometer. Complex I (NADH-ubiquinone reductase) activity was assayed in a medium containing 50mM Tris–HCl pH 7.4, 50mM KCl, 5mM $MgCl_2$, 1mM EGTA, 0.6mM NADH, 0.8mM ferricyanide, and 50µM antimycin A. The reduction of ferrocyanide in the presence of NADH was followed at 420 nm (ε = $1mM^{-1}{\cdot}cm^{-1}$). Similarly, Complex II (succinate dehydrogenase) activity was assayed in similar conditions but using 20mM succinate instead of NADH. Complex III (cytochrome c reductase) activity was assayed in a 50mM Tris buffer pH7.4, 5mM KCl, 2mM $MgCl_2$, 0.5M NaCN, 0.03% oxidized Cyt C, 0.6mM NADH, and 10mM succinate. The reduction of cytochrome c in the presence of NADH was followed at 550nm (ε = $19.1mM^{-1}{\cdot}cm^{-1}$). For Complex IV (cytochrome c oxidase) activity assessment, the oxidation of reduced cytochrome c was followed at 550nm (ε = 19.1 $mM^{-1}{\cdot}cm^{-1}$), in a 50mM Tris buffer pH7.4, 5mM KCl, 2mM $MgCl_2$, containing 0.03% reduced cytochrome c.

ATP synthesis through Fo-F1 ATP Synthase

To evaluate the ATP synthesis through the F_o-F_1 ATP synthase activity, cells were incubated for 10 min at 37 °C in a medium containing: 100mM Tris-HCl pH 7.4, 100mM KCl, 1mM EGTA, 2.5mM EDTA, 5mM $MgCl_2$, 0.2mM di(adenosine-5) penta-phosphate, 0.6mM ouabain, ampicillin (25 µg/ml), 5mM KH_2PO_4, and 10mM pyruvate plus 5mM malate, used as respiratory substrates. ATP synthesis started after the addition of 0.2mM ADP and was monitored for 2 minutes in a

luminometer (Glomax 20/20, Promega) by the luciferin/luciferase chemiluminescent method (luciferin/luciferase ATP bioluminescence assay kit CLSII, Roche, Basel, Switzerland). An ATP standard solution between 10^{-10} and 10^{-7} M was used for calibration. To assess the specificity of the method for ATP-synthase assay, ATP synthesis was also evaluated in the presence of 10 µM Oligomycin, a specific inhibitor of ATP synthases F_o moiety[234].

Determination of the mitochondrial membrane potential (MMP, $\Delta\psi_m$)

The lipophilic cationic probe TMRE (ab113852, Abcam) was used to determine the mitochondrial membrane potential ($\Delta\psi_m$). TMRE rapidly equilibrated between cellular compartments due to differential membrane potential, and a decrease in fluorescence indicated reduced $\Delta\psi_m$. Upon 48h treatment with FK866 and/or UK5099, cells were rising with PBS and TMRE (800 nM) was added directly to the assay wells. After 45 minutes' incubation at 37°C, the fluorescent signal was assessed in a microplate at the Spark (Tecan) plate reader, with excitation at 544 nm and emission at 590 nm. The uncoupling agent FCCP (20 µM) was used as negative control.

Statistical analysis

Data was expressed as mean ± standard error of mean (SEM) of three independent biological experiments conducted in technical triplicates, unless indicated otherwise. Statistical significance between control and test groups was determined using Student's t-test or one-way ANOVA, considering values of $*p < 0.05$, $**p < 0.01$, and $***p < 0.001$ as significant. Data were plotted by Graph prism 6 software.

RESULTS

Results in the thesis body reflect my personal contribution to the work and experiments performed by collaborators are properly acknowledged.

Development of FK866-resistant cell lines

To study the mechanisms of acquirement of resistance to NAMPT inhibition, FK866-resistant MDA-MB-231 cells (MDA r.) were obtained by exposing the MDA-MB-231 parental cells (MDA p.) to increasing concentrations of FK866, for over a 3-month period of time[133]. Both parental and resistant cell lines present the same proliferative rate, respectively with doubling times of 37,14 ± 1,56 and 33,04 ± 2,32 hours in the growth exponential phase (Figure 13A).

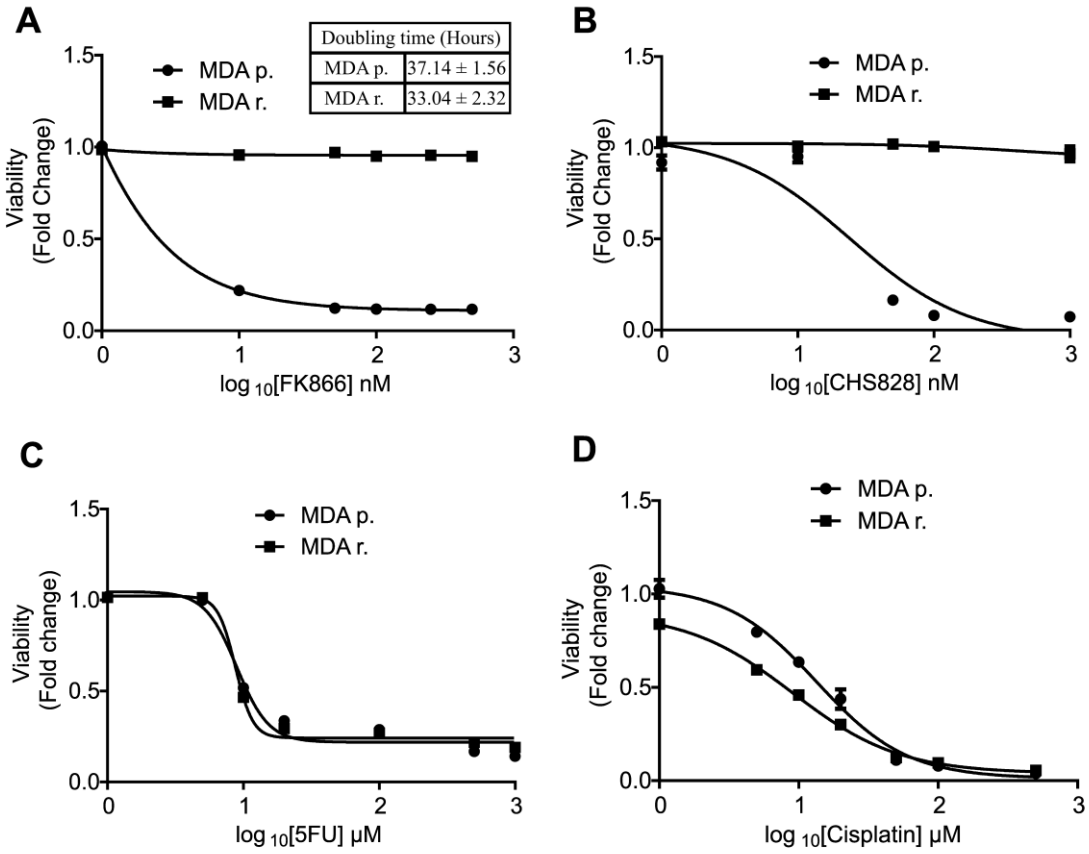

Figure 13 Resistance to FK866 is NAMPT-specific. Comparison of sensitivity of MDA-MB-231 cell lines to NAMPT inhibitors and chemotherapeutics. Sensitivity of MDA p. and MDA r. cells to the small molecules FK866 (A) and CH828 (B) assessed by OzBlue assay after 48h of exposure to 0.1-500 nM of the compounds. Cross-resistance of MDA p. and MDA r. to the chemotherapeutics 5-Fluoruracil (5FU)(C), and cisplatin (D) in the same conditions. Viability assessed through OzBlue assay. All the experiments were performed in triplicate. MDA r. were developed before the beginning of my PhD project by Dr. Thongon[133].

The sensitivity to FK866 treatment was assessed through OzBlue cell viability assay after 48h of exposure to the NAMPT inhibitor. The complete insensitiveness of MDA r. to FK866 did not allow the calculation of the EC_{50}, while for MDA p. it was calculated as 4.7nM (Figure 13A). Sensitivity to other NAMPT inhibitors as CHS-828 was also tested, and both cell lines present similar sensitivity to CH-828 exposure as to FK866 (Figure 13B). The cross-resistance of MDA r. to CH-828 was not observed for other common chemotherapeutic drugs like 5-fluoruracil (5FU) and cisplatin (Figure 13C-**D**), confirming a NAMPT-dependent resistance mechanism.

Canonical mechanisms of pharmacoresistance: efflux pumps

The expression of ABC transporters prevents drug accumulation in chemoresistance cells by improving drug efflux[155]. The treatment with inhibitors of drug efflux pumps, like verapamil or CsA, failed to sensitize MDA r. to FK866, excluding a role for the multi-drug resistance mechanisms in the acquirement of resistance to FK866 in this cell model (Figure 14).

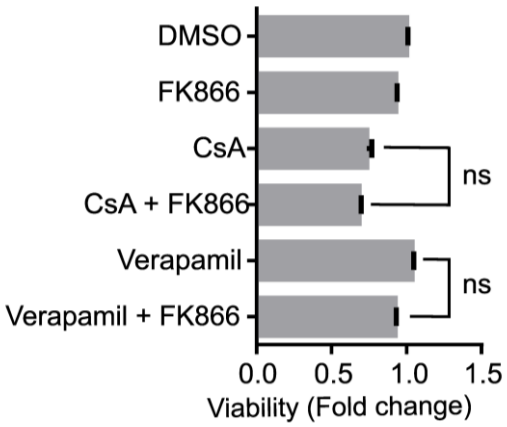

Figure 14 Efflux pumps do not contribute to FK866-acquired resistance. MDA r. sensitization to FK866 upon 48h of concomitant treatment with the efflux pumps inhibitors verapamil and cyclosporine A (CsA). Viability assessed by OzBlue assay. Final concentrations: FK866 - 20nM ; CsA - 5µM ; Verapamil - 5µM. The experiments were performed in triplicate. Repeated measures one-way ANOVA was used to calculate statistical significance (ns- non significant) between DMSO and experimental conditions.

Since the development of drug resistance to NAMPT inhibitors is commonly conferred by gene mutation[161,162,164], *NAMPT* coding sequence was sequenced. No mutations were found (**Data not shown**) in the resistant cell line. Therefore,

MDA r. developed alternative mechanisms, other than target mutation or activation of multi drug efflux pumps to acquire FK866 pharmacoresistance.

Drug screening does not reveal targetable vulnerabilities of MDA r.

Drug repurposing is often an effective way to both increase the range of available treatment options for several diseases , and provide clues regarding the molecular basis underlying the pathological phenotype[235,236]. Successful HTS to identify true active compounds depends on the adequate choice of the outcome results (assay to be performed) as well as on the choice of the relevant controls. The concept of z-factor/z-prime (Z') was firstly proposed by Zhang et. al in 1999, and provides a statistical evaluation of the assay signal dynamic range, and consequently of the differentiation between active (hits) and inactive compounds[237].

To explore potential vulnerabilities of MDA r., acquired during the adaptation to FK866 exposure, in comparison with their sensitive counterparts, a chemical high throughput screening (HTS) using the Prestwick Chemical Library was performed. The Prestwick Chemical Library is composed of around 1200 FDA-approved off-patent small molecules, targeting several cellular pathways for a plethora of therapeutic applications.

As FK866 treatment deprives cells of NAD(H) and consequently ATP, we decided to use an ATP-based cell viability (Cell-Titter Glo - CTG) to assess the effect of the library compounds on MDA p. and MDA r.. This luminescence-based assay measures the ATP presence on metabolic active cells, and is ideal for HTS as the single reagent CellTiter-Glo® Reagent can be added directly to serum-supplemented medium.

During screening optimization processes, different cell seeding concentrations were tested, to have an approximately 90% confluent population of cells on the day of the assay. Ideal cell seeding was determined as 600 cells/well. The DNA-interfering agent doxorubicin was used as a positive control of the screening, as it presents the same toxicity for MDA p. and MDA r. (Figure 15). A preliminary Z' assessment was performed after 48 hours of cell lines exposure to doxorubicin, followed by CTG measurement and Hoechst determination. For the CTG assessment, the Z' was calculated as 0,39 for MDA p. and 0,52 for MDA r., which

indicate a significant screening robustness and accuracy to detect hit compounds. Also, FK866 was used as a positive control for MDA p. but not for MDA r..

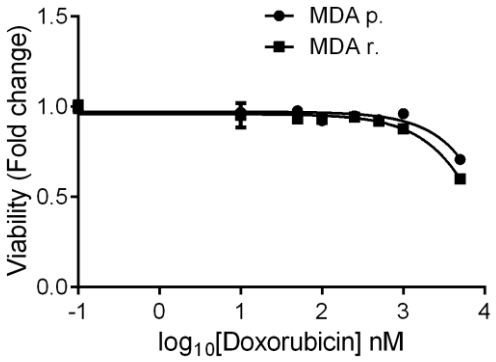

Figure 15 DRC of doxorubicin in MDA p. And MDA r. Sensitivity of MDA p. and MDA r. cells to the small molecule doxorubicin assessed by OzBlue assay after 48h of exposure to 0.1-1000 nM of the compound.

For the screening, MDA p. and MDA r. cells were treated for 48 hours with 1 µM of each compound present in the library. Technical duplicates in different mirrored plates were performed, and the Pearson correlation was determined. This statistical value reflects the linear correlation between two data sets. As Pearson correlation coefficient was determined as 0.871. the data obtained are linearly correlated (Figure 16).

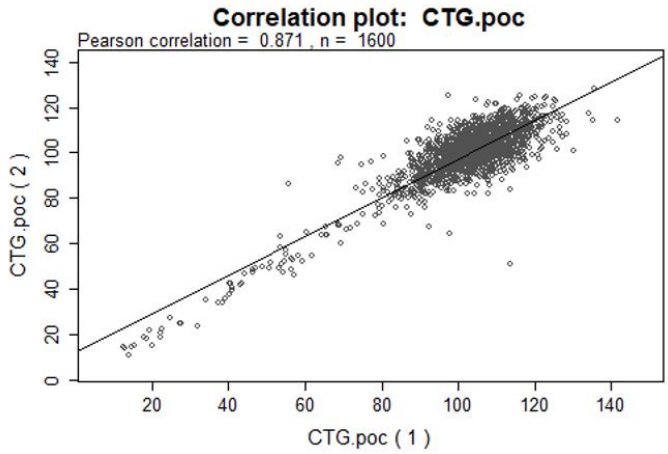

Figure 16 Screening quality control. Correlation plot between the values of cell titter glo (CTG) compared with the DMSO control condition, represented as percentage of the control, POC. The linearity between the CTG.POC of both replicates, was calculated using the Pearson correlation. Results for both MDA p. And MDA r. Are shown in the graph. Screening data was obtained with the support of CIBIO HTS facility.

The Z' of doxorubicin for the different plates used for the CTG assay ranged from 0,47 to 0,77 for MDA p. and 0,32 to 0,84 to MDA r.. Thus, the screening was considered suitable to detect hits[237].

To identify hits, a threshold of 70% of the CTG values in comparison with the DMSO control was selected. From all the 120 compounds in this condition, only the drug chlortalidone presented higher cytotoxicity to MDA r. than to MDA p (69,4 % vs 92,45%) (Figure 17).

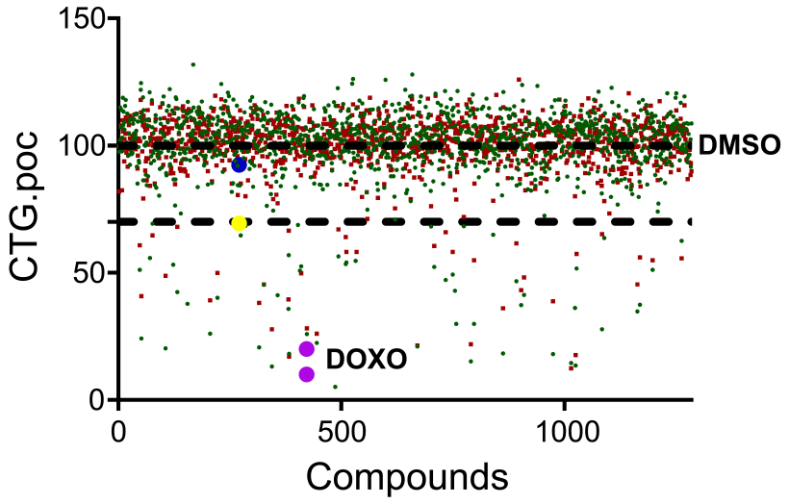

Figure 17 Screening results. CTG.POC values for MDA p. (green) and MDA r. (red) were obtained upon treatment with the ~1200 compounds of Prestwick Library, as well as for the DMSO (upper black dot lined) and Doxorubicin (DOXO – purple) controls. DMSO and DOXO values represented the average of the CTG.POC values for all the plates. The screening threshold was defined as 70% of the CTG.poc, and is represented by the bottom black dotted line. The effect of chlortalidone on the CTG.POC of MDA p. (blue d and MDA r. (yellow) are evidenced in the graph. Screening data was obtained with the support of CIBIO HTS facility.

Chlortalidone is a FDA-approved drug used for the treatment of hypertension. It inhibits the NA^+/Cl^- symporter in the distal convoluted tubule cells in the kidney, which prevents the water absorption in this organ, thus improving the blood pressure[238,239].

Validation screening was performed using the same protocol of the primary screening, and chlortalidone was assayed at concentrations ranging from 0.1 to 100 µM in both cell lines. The dose-response curves were also assessed in the presence of 10nM (for MDA p.) and 100nM of FK866 (for MDA r.) (Figure 18).

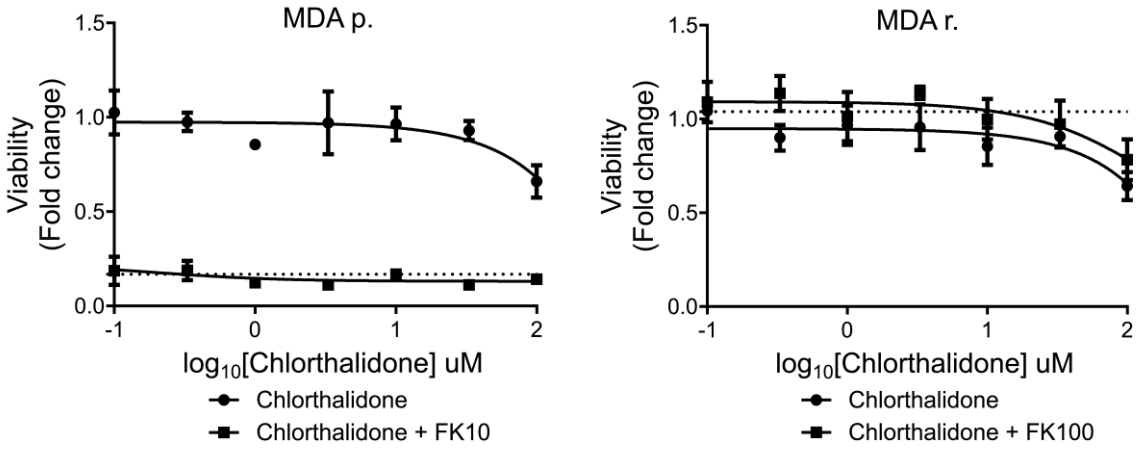

Figure 18 Hit validation. Screening's results were confirmed by performing a DRC of chlortalidone in both MDA p. (left) and MAD r. (right). Cells were treated with increasing ranges of chlorthalidone (0.1-100 µM), either as single-treatment or in combination with FK866. The effect of FK866 treatment (10nM for MDA p. and 100nM for MDA r.) is represented by the black dotted lined. Screening data was obtained with the support of CIBIO HTS facility.

However, data obtained from the validation screening did not confirm the primary screening results, as chlorthalidone as equally toxic to MDA p. and MDA r.. Moreover, no synergy was observed with the cotreatment of chlorthalidone and FK866, for both cell lines. Overall, we considered the screening unsuccessful to unravel MDA r. vulnerabilities.

Resistance to FK866 is not dependent on compensatory NAD+ biosynthesis pathways

One of the main pathways of mammalian intracellular NAD(H) biosynthesis is the salvage pathway from nicotinamide, sustained by NAMPT as the rate-limiting enzyme of the reaction. Additional NAD^+ biosynthesis pathways use nicotinic acid, tryptophan, and nicotinamide riboside, as substrates for NAPRT, QAPRT and NMRK, respectively (Figure 7).

Thus, given the role of these enzymes in the maintenance of intracellular NAD(H), we hypothesized that upon NAMPT inhibition through FK866, they could sustain intracellular NAD(H) levels by compensatory mechanisms of NAD^+ biosynthesis. We observed that the acquirement of resistance to FK866 leads to a downregulation of the target NAMPT. Similarly, also NAPRT expression levels were decreased, while NMRK1 was up-regulated. These results were consistent both at the protein and transcripts level (Figure 19 A-B).

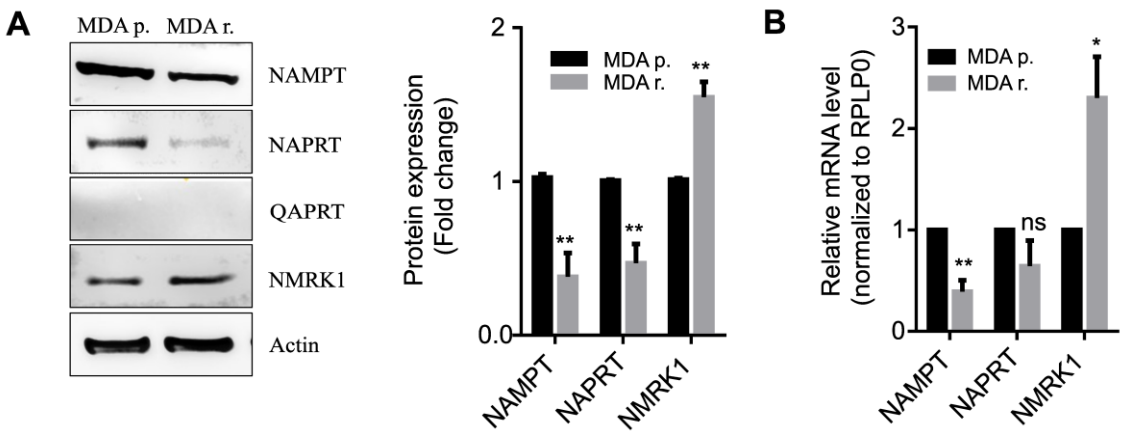

Figure 19 Expression of NAD⁺-biosynthetic enzymes. (A) Western blot showing endogenous levels of NAMPT, NAPRT, QAPRT and NMRK1, as well as it quantification, in MDA p. and MDA r.. Actin was used as a loading control. Representative image and quantification of 3 replicates are shown. (B) RT-qPCR to determine *NAMPT*, *NAPRT* and *NMRK1* expression in MDA p. and MDA r.. *RPLP0* was used as a house-keeping gene. All the experiments were performed in triplicate. Repeated measures one-way ANOVA was used to calculate statistical significance (ns-non-significant, *P<0.05, **P < 0.01, between control and experimental conditions.

Since both NMRK1 and NAMPT catalyze the production of the NAD^+ precursor Nicotinamide Mononucleotide (NMN), we hypothesized that NMRK1 up-regulation could compensate NAMPT down-regulation.

NMRK1 expression was analyzed during several steps of the acquirement of resistance to the NAMPT inhibitor, namely in cells exposed and resistant to the 2nM (MDA 2), 20nM (MDA 20) or 40nM (MDA 40) of FK866. We observed that NMRK1 expression increased in the initially FK866-exposed populations of cells and decreased slightly in final fully resistant population (MDA r.), although remaining higher than basal level (MDA p.) (Figure 20A). Based on these data, we generated an MDA r. cell line stably silenced for NMRK1 (Figure 20B). NMRK1 silenced cells did not significantly changed their proliferation ability. The doubling time for MDA r. shSCR was quantified as 31,82 ± 4,14 hours, while for MDA r. shNMRK1 it was 32,82 ± 4,14 hours (Figure 20C).

Further characterization of these cell lines revealed an unaltered cellular viability upon 48h of exposure to FK866 by OzBlue assay (Figure 20C). Total NAD(H) levels, NADH/NAD^+ ratio and ATP/AMP ratio were measured in the same conditions. Upon treatment, the total NAD(H) levels decreased in resistant cells independently of the NMRK1 silencing while the NADH/NAD^+ ratio increased. Instead, the ATP/AMP ratio followed the same fashion as the total NAD(H) levels (Figure 20D-F).

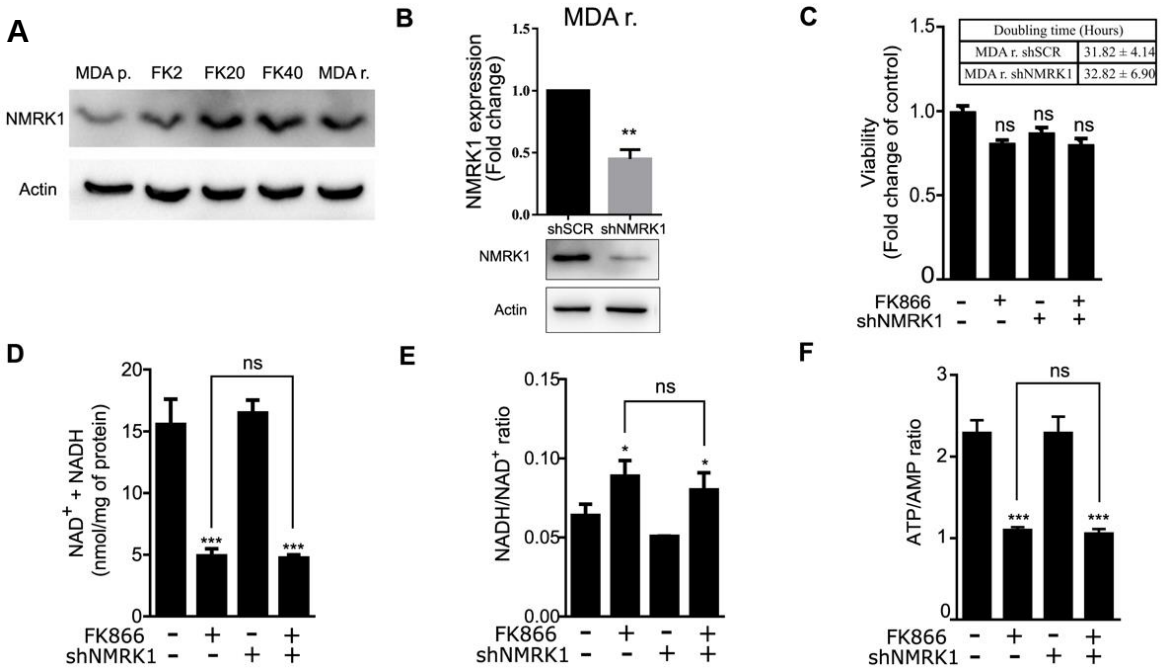

Figure 20 Resistance to FK866 is not dependent on compensatory NMRK1 expression.
(A) Western blot showing the NMRK1 levels in MDA p., MDA r. and three intermediate cell lines of the process of acquirement of resistance to FK866. FK2, FK20 and FK40 are respectively resistant to 2, 20 and 40nM of FK866 (B) Development of NMRK1 stable silenced MDA r. cell line. shNMRK1 did not sensitize MDA r. after 48h of FK866 treatment (20nM), through OzBlue assay, nor altered cell proliferation. (C) Total NAD(H) levels, (D) NADH/NAD^+ ratio and ATP/AMP ratio (F) were also not modulated by NMRK1 stable silencing. All the experiments were performed in triplicate. Repeated measures one-way ANOVA was used to calculate statistical significance (ns-non-significant) between control and experimental conditions. Experiments to determine NAD(H) levels and ATP/AMP ratio were performed in collaboration with Dr. Santina Bruzzone and Dr. Silvia Ravera, respectively.

Therefore, the silencing of NMRK1 did not sensitize MDA r. to FK866 in any of the assays tested, leading to the conclusion that compensatory NMRK1-mediated NAD^+ biosynthesis is not relevant for the fully resistant phenotype. However, a potential contribution of this enzyme activity for the initial steps of acquirement of resistance to NAMPT inhibition cannot be discarded.

Evaluation of glycolytic and mitochondrial functions in MDA r.

NAMPT inhibitors' mechanism of action leads to an overall decrease of intracellular NAD^+, which is an essential coenzyme for the glycolytic enzyme GAPDH. Similarly, this molecule is also involved in the TCA cycle reactions, and further converted to NADH to be used electron donor to Complex I. Thus, we performed real-time cell metabolic analysis using the Seahorse XF Analyzer to

directly measure the ECAR and the OCR, indicators of the two major energy-producing pathways: glycolysis and oxidative phosphorylation.

To understand if MDA r. presents a modulation of the glycolytic flux, we used the Seahorse Glycolytic Rate Assay, to determine the glycolytic proton efflux rate (glycoPER), an indirect measure of glycolysis. The conversion of glucose to pyruvate and the consequent extrusion of protons into the extracellular media gives a major contribution for the ECAR, quantified in this assay. Additionally, the OCR was used to subtract the mitochondrial-derived CO_2 contribution to the extracellular acidification.

Both basal glycolytic level at physiological rate and compensatory glycolysis were measured. Rotenone and antimycin A, complex I and III inhibitors, respectively, were injected, followed by the addition of 2-Deoxy-D-glucose (2DG). 2DG is a glucose analog and inhibitor of glycolysis first enzyme hexokinase that shuts down glucose oxidation and consequently the proton efflux, allowing to determine the contribution of other sources of extracellular acidification that are not attributed to glycolysis or OXPHOS. In this assay, we did not observe a significant difference of either basal or compensatory glycolysis between MDA p. and MDA r. (Figure 21).

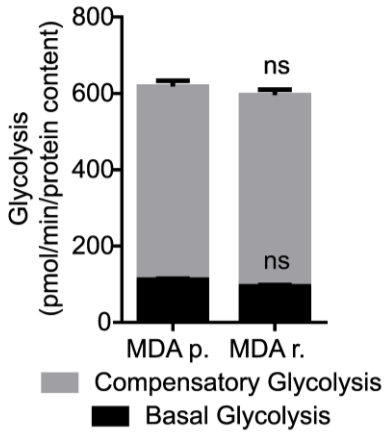

Figure 21 Metabolic evaluation of glycolytic rate. Glycolysis rate assay of MDA p. and MDA r. Was assessed to determine basal and compensatory glycolysis. The experiment was performed in triplicate, using the XFe96 Seahorse Bioanalyzer. Data was analyzed with Wave Software 2.6.3. Repeated measures one-way ANOVA was used to calculate statistical significance (ns-non significant) between MDA p. and MDA r..

We then assessed the mitochondrial function using the Seahorse MitoStress Assay, in which the OCR is measured after injection of modulators of cellular respiration. Initially, oligomycin, an ATP synthase inhibitor, was injected, leading to

a decrease of the electrons through the ETC and consequently of the mitochondrial respiration and OCR. Instead, FCPP present the opposite effect: being an uncoupling agent, it leads to proton leakage into the mitochondria, that is counteracted by an increase activity of complex I-IV, resulting on an increased OCR. FCCP injection is used to calculate the spare respiratory capacity, an indirect measure of the ability of cells to respond to increase metabolic demands.

It is important to titrate FCCP as its unspecific effects can lead to cell toxicity and paradoxical inhibition of mitochondrial OCR. MDA p. and MDA r. were titrated with increasing concentrations of the uncoupling agent, and an inflection point was observed at the concentration of 2µM for both the cell lines (Figure 22A-B). This value was used for further OCR experiments.

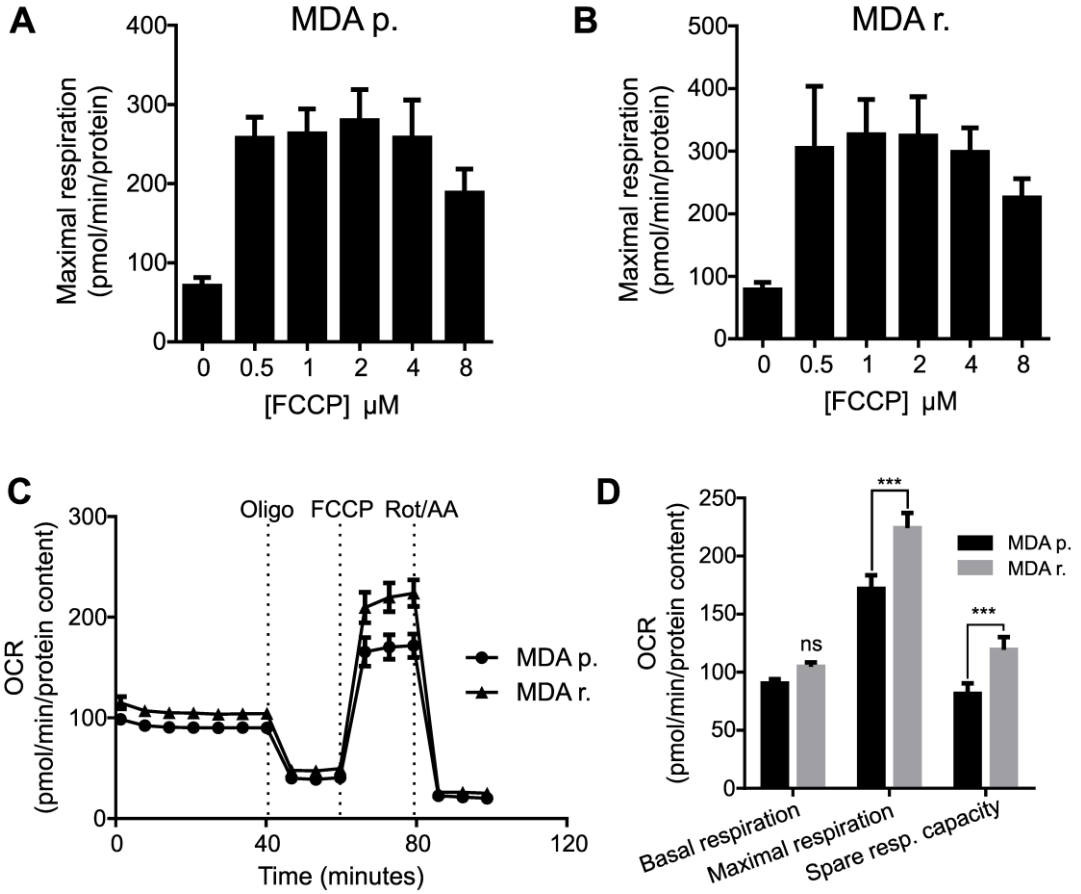

Figure 22 FK866 continuous exposure induces increase of spare respiratory capacity in MDA r.. Maximal respiration of MDA p. (A) and MDA r. (B) assessed by Seahorse XF Analyzer upon acute injection of the uncoupling agent FCCP at the indicated concentrations. (C) Representative MitoStress test to determine (D) basal respiration, maximal respiration and spare respiratory capacity of MDA p. and MDA r.. Abbreviations: Oligo - Oligomycin; FCCP -Carbonyl cyanide-p-trifluoromethoxyphenylhydrazone; Rot/AA - Rotenone and Antimycin A. FCCP titration experiment was performed only once, with 8 technical replicates. The MitoStress test was performed in triplicate. Repeated measures one-way ANOVA was used to calculate statistical significance (ns- non significant, *P<0.05, **P < 0.01, ***P < 0.001) between MDA p. and MDA r..

Lastly, rotenone and antimycin A are concomitantly injected to inhibit the mitochondrial dependent oxygen consumption. Representative Seahorse analysis for MDA p. and MDA r. are shown (Figure 22C). It is possible to observe that MDA r. present a significant higher maximum respiratory capacity than MDA p.. As both cell lines show approximately the same basal OCR values, the spare respiratory capacity (difference between maximum and basal respiration) is higher in MDA r., reflecting the induction of an adaptation of the mitochondrial function to the continuous exposure to FK866 (**Figure 22D**).

MDA r. presents a higher mitochondrial biogenesis and mass

The increased mitochondrial spare respiratory capacity in FK866-resistant cells pinpoint a potential role of mitochondrial rewiring during the acquirement of resistance to the small molecule, that we further decide to dig deeper into. In fact, several mitochondrial stress adaptations, like increased mitochondrial biogenesis, have been described to mediate drug resistance[240].

Interestingly, when comparing MDA r. to MDA p., we observed an increase in the tRNAleu/B2M ratio, which corresponds to mitochondrial and nuclear genes, respectively. Likewise, the mitDNA/nuclearDNA ratio was augmented after the acute treatment of MDA p. with 10nM of FK866 for 48h, suggesting that increased amount of mitochondrial DNA is an immediate mechanism of cell adaptation to NAMPT inhibition (Figure 23A).

In line with these findings, MDA r. showed enhanced expression of the nuclear gene encoding the translocase of outer mitochondrial membrane 20 (TOMM20), a proxy for mitochondrial mass[241] (Figure 23B). We also determined the expression of genes associated with mitochondrial enhanced metabolism. PGC-1α, an activator of mitochondrial biogenesis, was found 4-fold upregulated in MDA r. compared with MDA p., as well as TFAM (Figure 23C).

Collectively, these data indicate that acute FK866 treatment induces an immediate cell response leading to increased amount of mitochondrial to nuclear DNA ratio, that during long term FK866 administration results in increased mitochondrial mass and increased spare respiratory capacity.

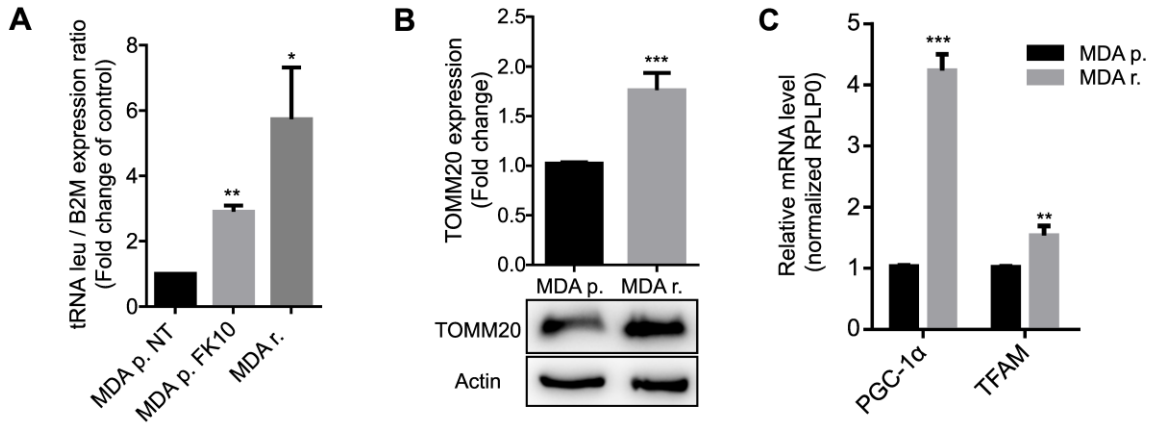

Figure 23 Mitochondrial function is improved in MDA r. (A) RT-qPCR to determine *tRNAleu* and *B2M* expression in MDA p. (non treated - NT - and treated for 48h with 10nM of FK866) and MDA r.. The ratio between these genes reflect the mitDNA/nDNA ratio (mitochondrial versus nuclear DNA). *RPLP0* was used as a house-keeping gene. (B) Western blot showing upregulation of TOMM20 in MDA r.. Representative image shown. (C) RT-qPCR to determine *PGC1-α* and *TFAM* expression in MDA p. and MDA r.. *RPLP0* was used as a house-keeping gene. All the experiments were performed in triplicate.. Repeated measures one-way ANOVA was used to calculate statistical significance (*P<0.05, **P < 0.01, ***P < 0.001) between MDA p. and MDA r..

MDA r. show a dependency on pyruvate as carbon source for the TCA cycle

Similarly to mitochondrial function modulation, rearrangement of mitochondrial bioenergetics is also observed in chemoresistance[240]. To dig deeper into the role of mitochondrial energetic hubs in the adaptation to FK866 exposure, we performed a mitochondrial substrate dependency assay with Mitoplate S-1. This assay measures the real time kinetics of electron flow rates upon oxidation of substrates that produce NADH or $FADH_2$. The rate of substrate oxidation is a measure of the reduction of a tetrazolium redox dye (MC) that acts as a terminal electron acceptor. For this experiment, MDA p. and MDA r. were permeabilized with saponin and incubated in a Mitoplate S-1 already containing the diverse mitochondrial substrates and the redox dye. The initial rate of substrate oxidation during the first three hours of the assay was used to identify mitochondrial metabolic dependencies.

Both cell lines presented an almost null background (no substrate) that was subtracted to every tested condition. The TCA cycle substrates α-keto-glutaric acid, succinic acid, fumaric acid and malic acid presented the highest levels of MC reduction, as they directly enter TCA cycle to produce NADH and $FADH_2$. These conditions are the positive control of the assay, assuring the successful cell

permeabilization without mitochondrial disruption. However, no differences were observed between the cell models tested. Of notice, MDA r. presented a decrease in fatty acids oxidation in comparison with MDA p, that is significant for the combination of palmitoyl-DL-carnitine and malic acid (Figure 24A). Instead, MDA r. shows a significant increase in pyruvic acid oxidation when in combination with lower doses of L-malic acid[242]. We also observed a tendency of pyruvic acid alone to increase the initial electron flow rate in MDA r. when compared with MDA p. (Figure 24A).

This result indicates a shift of mitochondrial substrate's dependencies, namely towards the utilization of pyruvate, upon FK866 long term exposure.

To confirm these observations, we performed a mitochondrial function assay using the Seahorse Mitostress kit, in the presence of UK5099, a MPC inhibitor, that will prevent the MPC mediated import of pyruvate into the mitochondria. This compound was acutely injected after the measurement of the cellular basal OCR levels, followed by the sequential addition of oligomycin, FCCP and rotenone/antimycin A. We observed that MDA p. cells are sensitive to MPC inhibition (Figure 24B) but MDA r. cells showed a stronger decrease of the maximal respiration in the cells exposed to UK5099 in comparison to the vehicle DMSO control, confirming the importance of the MPC-dependent pyruvate import for mitochondrial functioning (Figure 24C).

We hypothesized that an increase in pyruvate oxidation rate could be related with an increased expression of the pyruvate dehydrogenase complex or with an increase of the pyruvate import to the mitochondria. However, MDA r. cells did not show a modulation of the PDH1Ea subunit nor of the mitochondrial pyruvate carrier 1 and 2 (MPC1 and MPC2) when compared to MDA p. cells (Figure 25A-B).

Taken together, these data unravel the metabolic dependency of pyruvate as carbon source for the mitochondria in long term exposure to FK866.

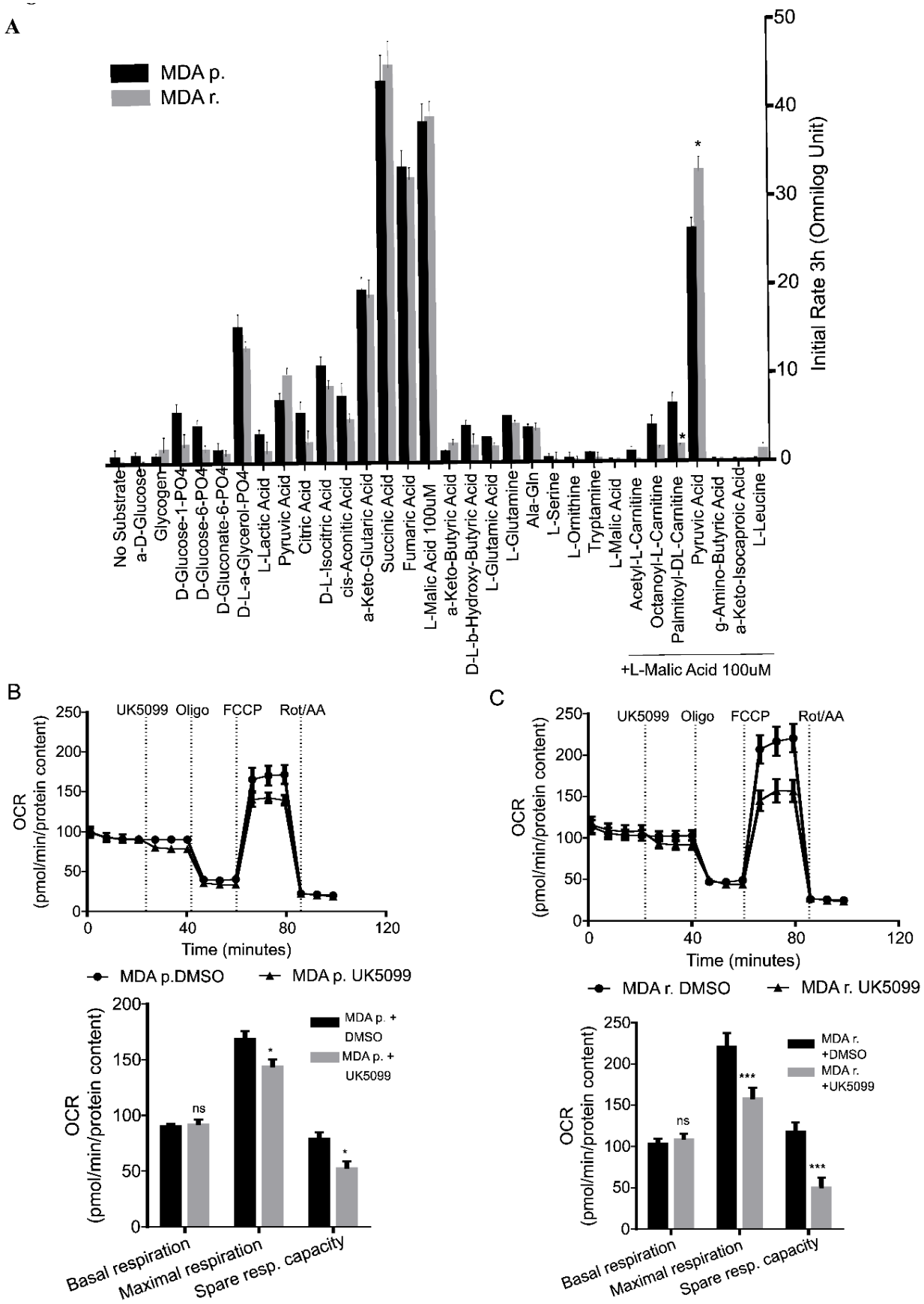

Figure 24 MDA r. show a dependency on pyruvate as carbon source for the TCA. (A) Assessment of mitochondrial dependencies through the Mitoplate S-I to determine the initial mitochondrial substrate oxidation rate between MDA p. and MDA r.. Assay performed on OmniLog® ID System and analyzed on . Repeated measures one-way ANOVA was used to calculate statistical significance (*P<0.05, **P < 0.01, ***P < 0.001) between MDA p. and MDA r..

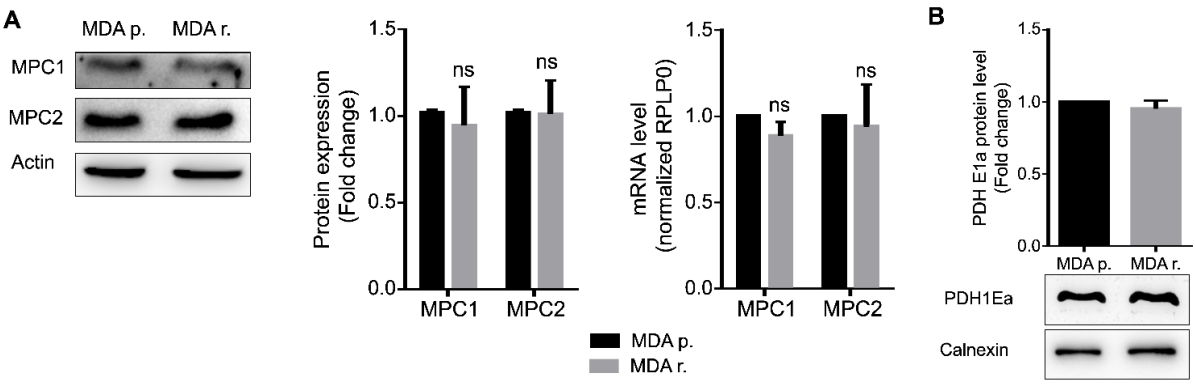

Figure 25 Expression of proteins involved in pyruvate metabolism. (A) Western blot showing the basal levels of MPC1 and MPC2 and (B) PDH1Ea in MDA p. and MDA r.. Either calnexin or actin were used as loading controls. All the experiments were performed in triplicate. Repeated measures one-way ANOVA was used to calculate statistical significance (*P<0.05, **P < 0.01, ***P < 0.001) between MDA p. and MDA r..

The uncoupling of glycolysis and mitochondrial respiration favored by MPC2 blockage induces a FK866 resistant-like phenotype in MDA p. cells

To gain some insights on whether MPC modulates the acquirement of resistance to FK866 in triple negative breast cancer, MDA p. and MDA r. cells were exposed to increasing concentrations of UK5099 for 48h. Both cells showed the same sensitivity to the drug (IC_{50} > 100 µM, **Figure 22**).

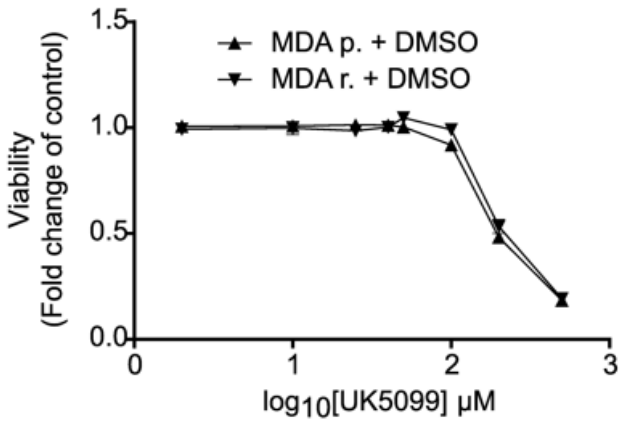

Figure 26 MDA p. and MAD r. present the same sensitivity to UK5099. Dose-response curve of UK5099 upon 48 hours of exposure assessed by the OzBlue assay. Three biological replicates were performed.

However, the treatment of the parental cells with UK5099 in combination with FK866 lead to a significant increase in cell viability when compared to FK866

single administration (Figure 27A). Instead, no significant differences were observed for the co-treatment of MDA r. cells with both small molecules (Figure 27B).

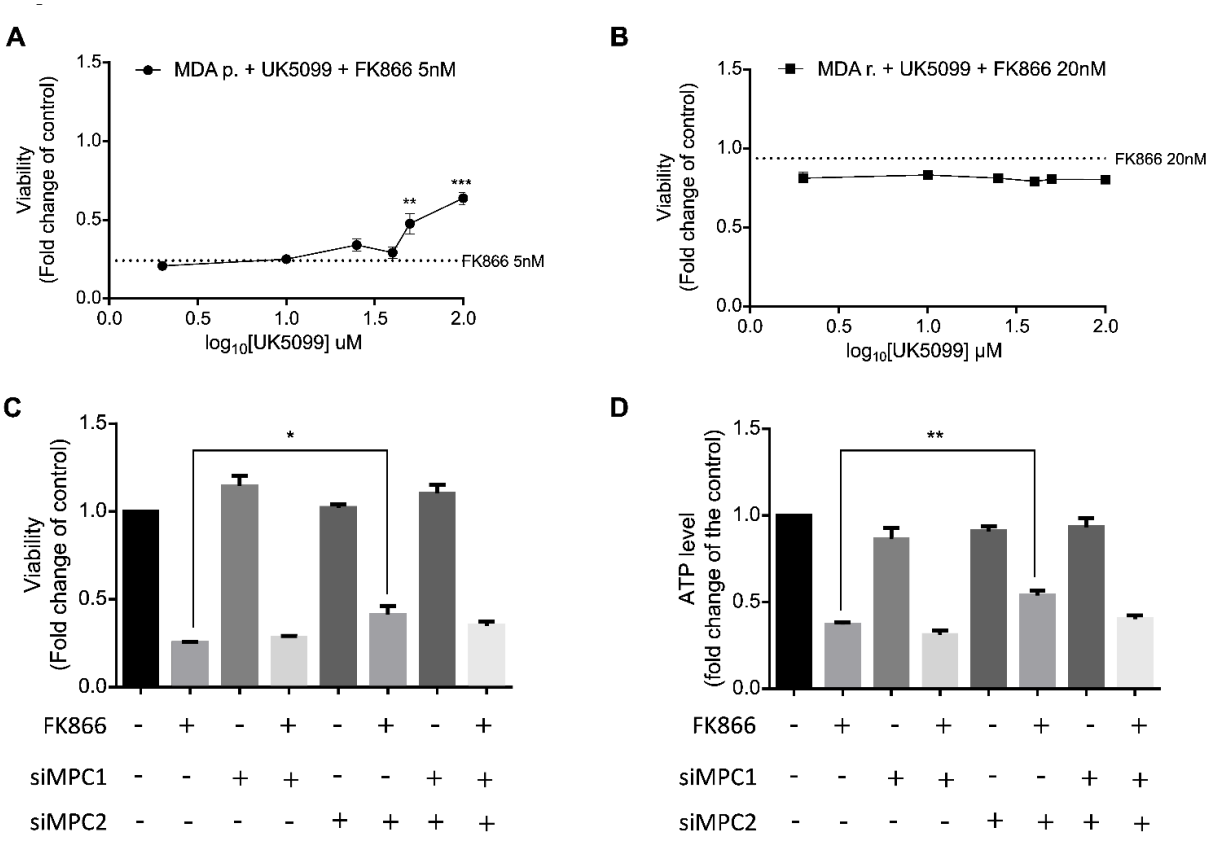

Figure 27 The uncoupling of glycolysis and mitochondrial respiration favored by MPC2 blockage induce a FK866 resistant-like phenotype in MDA p. cells. Co-treatment of MDA p.(A) and MDA r. (B) with UK5099 (0.1-100) µM and FK866 as well as with FK866 single administration (Final concentrations: 5nM for MDA p. and 20nM for MDA r.). Viability assessed by OzBlue assay after 48h and compared with DMSO condition. Effect of MPC1 (siMPC) and/or MPC2 (siMPC2) transient silencing in MDA p. in terms of cell viability (C) and relative ATP level (D), in combination with FK866 5nM. All the experiments were performed in triplicate. Repeated measures one-way ANOVA was used to calculate statistical significance (*P<0.05, **P < 0.01, ***P < 0.001) between DMSO and experimental conditions.

To understand if the acquirement of a FK866-resistant like phenotype in the parental cells was specifically dependent on pyruvate transport, cells were transiently silenced for MPC1 and/or MPC2 and viability and ATP levels were assessed after 48h of FK866 treatment. FK866 treatment reduced both viability and ATP levels in the control condition. Interestingly, the treatment of FK866 upon the silencing of MPC2 partially but significantly rescued the FK866 toxic effect

observed in the control condition. The same trend was obtained for the ATP level measurements. Instead, the silencing of MPC1 or MPC1 and MPC2 did not lead to a significant rescue of FK866 toxicity for the analyzed parameters, even if the dual silencing approach showed an increasing trend (Figure 27C-D). Taken together, this data unravels the pivotal importance of regulating the pyruvate import to mitochondria *via* MPC2 as a mediator of the adaptation of triple negative breast cancer cells to FK866 exposure.

Acquired resistance to FK866 induces dependency on succinate, even in pyruvate-deficiency conditions

To dig deeper into mitochondrial bioenergetic dependencies, we questioned if the observed mitochondrial function in MDA r. was associated with a differential activity of the ETC complexes. The ETC complexes uses NADH and $FADH_2$, produced through the oxidation of carbon sources on the TCA cycle, and generate the MMP to sustain mitochondrial ATP production.

Cells were treated with FK866, UK5099 or the combination of both for 48h, and enzymatic activity of the uncoupled complexes was assessed and normalized to the sample protein content. Complexes I-IV presented the same enzymatic activity for all the treatments performed and among the two cell lines (Figure 28A-D). Conversely, the activity of ATP synthase (Complex V), induced by the pyruvate/malate addition, decreased similarly in MDA p. and MDA r. cells, during either the single treatment with FK866 or UK5099. Instead, combining the exposure of cells to both small molecules, we observed that Complex V activity was less affected in MDA r. cells compared to MDA p. cells (Figure 28E).

We further confirmed that the increased ATP synthase activity is sustained by the maintenance of the MMP, determined spectrophotometrically through the measurement of TMRE fluorescence. This dye accumulates in active mitochondria according with their membrane potential. The co-treatment of MDA r. cells with FK866 and UK5099 did not decrease MMP, indicating a continued mitochondrial ATP production. Instead, in MDA p. cells we observed a significant decrease of the fluorescent counts in the same condition, associated with a diminished ability of these cells to produce energy in the mitochondria when uncoupled from glycolysis. As the ionophore uncoupler of the oxidative phosphorylation, FCCP

was used as positive control. FCCP determined a decrease of MMP for cell lines (Figure 28F).

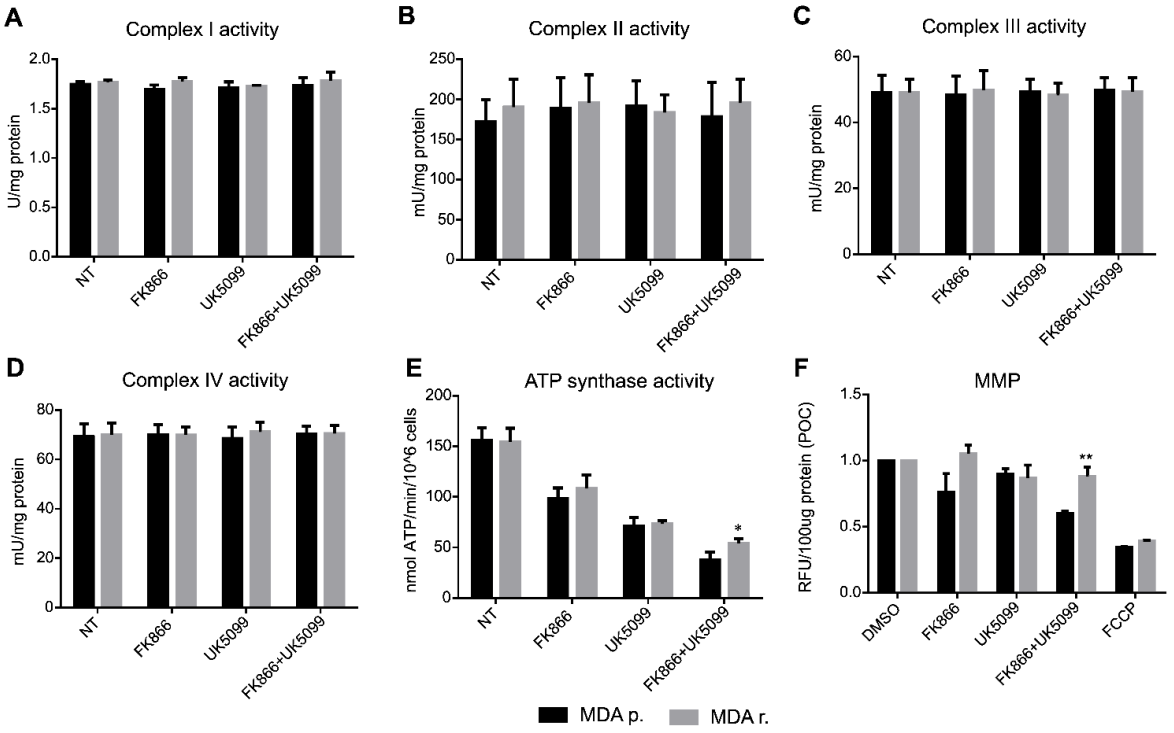

Figure 28 MDA r. present a higher ATP synthase activity even in pyruvate-deprivation conditions. Assessment of Complex I-IV and ATP synthase activities, and Mitochondrial Membrane Potential (MMP). The activities of Complex I-IV (A-D) in MDA p. and MDAr. were measured upon treatment with FK866 and/or UK5099. (E) ATP synthase activity and (F) mitochondrial membrane potential (MMP) were determined in the same conditions. FCCP was used as positive control for the MMP determination. Final concentrations: FK866 - 10nM for MDA p. and 100nM for MDA r.; UK5099 - 100µM for both cell lines. All the experiments were performed in triplicate. Repeated measures one-way ANOVA was used to calculate statistical significance (*P<0.05, **P < 0.01, ***P < 0.001) between MDA p. and MDA r..

These data show that the long-term exposure to FK866 increases the fitness of mitochondria in ATP synthesis through an increase in ATP synthase activity, that is not only sustained by the MPC-dependent pyruvate import, but potentially by alternative metabolic mechanisms that maintain the MMP in pyruvate-deprivation conditions.

Thus, we decided to investigate mitochondrial substrate dependence in the presence of pyruvate/malate and succinate/rotenone during the silencing and inhibition of MPC subunits to identify the pathways led by Complex I and Complex II, respectively (Figure 29).

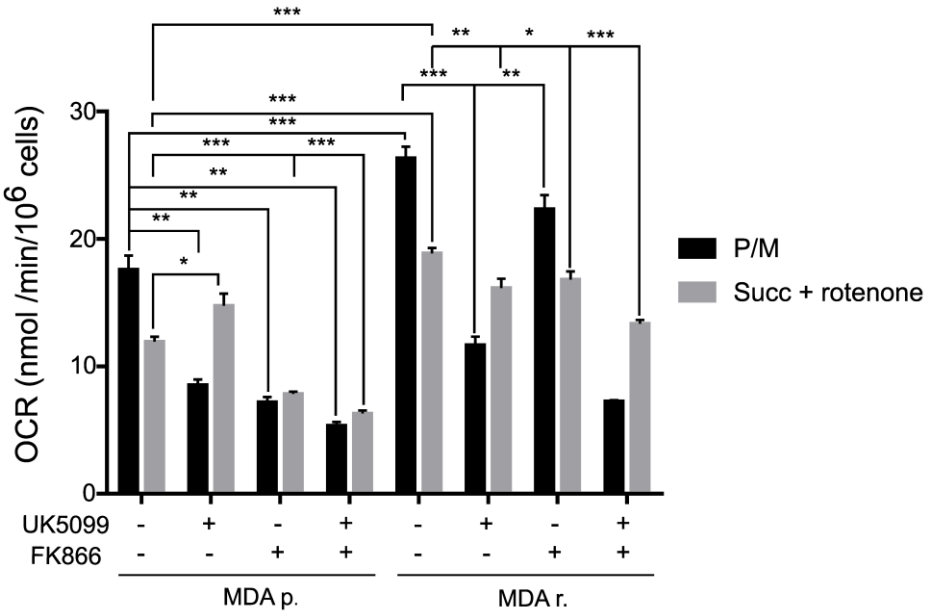

Figure 29 FK866 long-term exposure model increases succinate metabolism. OCR measurements of cells permeabilized with digitonin and treated with UK5099 and/or FK866, in the presence of pyruvate/malate (P/M) or succinate/rotenone (Succ + Rotenone) were also determined. . Final concentrations: FK866 - 10nM for MDA p. and 100nM for MDA r.; UK5099 - 100µM for both cell lines. All the experiments were performed in triplicate. Repeated measures one-way ANOVA was used to calculate statistical significance (*P<0.05, **P < 0.01, ***P < 0.001) between MDA p. and MDA r..

The OCR measurements revealed that mitochondria of MDA r. presented a higher OCR than MDA p., showing a preferential utilization of pyruvate/malate. Reduction of pyruvate entrance into the MDA p. mitochondria, by pharmacological means, decreased the pyruvate plus malate-induced OCR but increased the succinate-dependent respiration, suggesting an attempt to compensate the oxygen consumption decrement through Complex I. In the presence of FK866, however, mitochondria are deprived of the ability to activate both Complex I and II, either in the presence or absence of UK5099. In MDA r. mitochondria, MPC blockage reduced pyruvate dependent OCR, and did not increase succinate utilization, that is already higher than in MDA p.. Interestingly, FK866 treatment was not affecting neither pyruvate nor succinate dependent OCR, further confirming the insensitivity of these cells to NAMPT inhibition. Upon cotreatment with UK5099 and FK866, we still observed succinate exploitation that sustained OCR. Therefore, resistant cells show a higher mitochondrial function than parental ones, sustained by both pyruvate and succinate oxidation.

DISCUSSION

Metabolic rearrangement offers cancer cells the plasticity to respond and adapt to toxic insults[243]. We used a triple negative breast cancer cell line that is resistant to the NAMPT inhibitor FK866 (MDA r.) to dissect molecular mechanisms sustaining the cellular adaptation of prolonged NAD(H) shortage and found that we found that mitochondria rearrange in term of substrate utilization and increase spare respiratory capacity and mass. This model present cross-resistance to CHS-828, another NAMPT inhibitor[244]. However, for some classes of chemotherapeutics commonly used in the clinics for cancer treatment, like 5-fluoruracil (antimetabolite) and cisplatin (alkylating agent), MDA p. and MDA r. presented the same sensitivity, differently from other FK866-resistant models, whose sensitivity to these drugs are increased upon the acquisition of the FK866-resistant phenotype[163]. Canonical mechanisms of pharmacoresistance differ depending on the drug but can often include the increase of transporter pumps, target mutation and mitochondrial alteration, as described for other FK866 resistant models[163,245,246]. In MDA r. cells, *NAMPT* is not mutated. Similarly, the treatment with the drug efflux pumps' inhibitors verapamil and cyclosporine A, did not sensitize MDA r. cells to FK866, excluding the role of multi-drug resistance (MDR) mechanisms in the acquired resistance to FK866 in these cells. Thus, MDA r. present a NAMPT-dependent acquired resistance to FK866, that is not dependent on the canonical mechanisms of acquired resistance.

Importantly, cancer cells' dependency on other enzymes for NAD(H) synthesis like QAPRT or NAPRT can bypass the NAMPT inhibitors' dependent NAD(H) depletion[164,231,247–249]. In our model, QAPRT is not expressed but NMRK1 expression is positively modulated in MDA r., in opposition to NAPRT, that presents the inverse trend. This data is aligned with a recent study that showed that dependence of NAMPT is subject to resistance by NMRK1-dependent synthesis of NAD(H), which can explain the failure of NAMPT inhibitors[108]. However, the stable silencing of NMRK1 in MDA r. did not sensitize these cells to FK866 treatment, and NAD(H) and ATP were kept unaltered. Nevertelhess it is important to notice that our experiments were inspired by the expression levels of these enzymes, and only NMRK1 was found upregulated in MDA r.. Thus, it would

be important to access the activity of these enzymes rather than its expression levels to understand to which extent FK866 is inhibiting NAMPT activity in the resistant model; and if NMRK1 knockdown indeed results in a relevant loss of its activity.

Furthermore, we found that the acquisition of resistance to FK866 determines specific mitochondrial adaptation. Real-time cell metabolic analysis revealed that MDA r. have an increased spare respiratory capacity (SRC) sustained by a higher maximal respiration. Indeed, SRC is a critical component of cellular bioenergetics as it correlates with mitochondrial plasticity and its ability to adapt in response to energetic stress conditions[250,251], with several studies reporting a positive correlation between high levels of SRC and resistance to anti-cancer drugs[252,253]. Similarly, mitochondrial-mediated chemoresistance has also been associated with an increase in the mitochondrial mass[254–256]. Aligned with these studies, we observed an increase in the mitochondrial DNA versus nuclear upon parental cells' treatment with FK866, revealing a FK866-depedent increase of mitochondrial mass. The mtDNA/nDNA ratio was further augmented once cells became fully resistant. An increase of the expression of PGC-1α, TFAM and Sirt1 transcripts and of TOMM20 protein levels were also observed. These results corroborate the hypothesis that prolonged NAD(H) shortage led to an increased mitochondrial biogenesis and content.

Alterations on mitochondria physiology imply the maintenance of the import of carbon sources to sustain the TCA cycle, ETC and ultimately ATP synthesis. Using a Mitoplate-SI, we questioned the mitochondrial substrate dependences of MDA r. and revealed that these cells metabolize pyruvate in combination with low doses of malic acid faster than the parental ones, but this phenotype was not recapitulated by either pyruvate or malic acid alone. In fact, it is described that malic acid acts as a spark for the TCA cycle to have optimal oxidation rates[242], which confirms that MDA r. present a higher dependence on pyruvate metabolism.

Mitochondrial dependence on pyruvate was further confirmed through the inhibition of its uptake by the mitochondrial pyruvate carrier (MPC). MDA r. treated with the MPC inhibitor UK5099 failed to achieve the same levels of maximal respiration as the control, which implied a lower spare respiratory capacity. Although not strictly correlated with differential activity, as the expression of both

subunits of the MPC complex was not altered between the parental and resistant cells, the increased pyruvate oxidation seems not to be associated with an augmented pyruvate uptake through MPC.

Given the role of MPC for the mitochondrial adaptation to NAD lowering agents observed in MDA r., we questioned the effect UK5099 treatment on the sensitivity to FK866 in these cell lines. The cotreatment with the MPC inhibitor and FK866 led to an increase of cellular viability, counteracting FK866 toxicity in parental cells. Moreover, by transient silencing of MPC1 and/or MPC2, we were able to associate the resistant phenotype observed with the subunit 2 of MPC (MPC2) and not with MPC1. Instead, sensitivity to FK866 was not modulated upon MPC inhibition in MDA r.. These data revealed that MPC inhibition is likely important for the immediate/chronic response to FK866 exposure in triple negative breast cancer but does not entirely sustain the resistant phenotype. The blocking of pyruvate entrance into the mitochondria would rather stimulate LDHA activity, allowing the recycling of NAD^+ cytoplasmatic levels, as previously observed in MDA r.[257].

Additionally, we observed that complexes I-IV activities, measured in an uncoupled way, were not altered either with the single or combination treatment of FK866 and UK5099, confirming that the respiratory complexes are not the target of these molecules, and that the FK866 and UK5099 effect of OxPhos function depend on the altered pyruvate and NAD(H) availability. These data might indicate an additional mitochondrial rearrangement not previously considered, in which the presence of respiratory supercomplexes might sustain the higher OCR in MDA r.[258].

We showed that the combination of FK866 and UK5099 treatments in MDA r. led to a higher activity of ATP synthase (Complex V), and consequently ATP production, compared with the parental cells. The increased ATP synthase activity is sustained by the maintenance of the mitochondrial membrane potential (MMP), in the same conditions. Collectively, this data show that MDA r. mitochondria are adapted to maintain MMP and ATP synthesis in MPC-blockage dependent pyruvate-deficiency conditions. Of note, the pyruvate import to the mitochondria is coupled with the symport of one proton[22]. Blocking MPC would prevent not only

the import of pyruvate but also of the proton, which favor the maintenance of a higher MMP and ultimately ATP production by Complex V.

Further analysis of mitochondrial function revealed that MDA r. present higher basal OCR than MDA p. in the presence of succinate, suggesting a mitochondrial adaptation during NAD(H) shortage. Indeed, upon MPC blockage, MDA p. can exploit succinate utilization as carbon source for the TCA cycle. Taken together, our data suggest that acquired resistance to NAMPT inhibition is likely developed through several steps. Initially, the blockage of MPC2, and thus the uncoupling of glycolysis and mitochondrial respiration, results in higher pyruvate cytoplasmatic accumulation. In alignment with previous work from our group, cytoplasmatic pyruvate can be used by LDHA, to keep NAD^+ levels high in the cytoplasm. The lack of pyruvate leads mitochondria to adapt to be able to keep OxPhos, namely through the exploitation of succinate as a carbon source for the TCA cycle and increase of mitochondrial mass. In the last stages of the acquisition of a stable FK866 resistant cell line, both pyruvate and succinate are used to sustain ATP synthesis.

Taken together, our data show that mitochondrial plasticity provides a metabolic advantage to cells' adaptation to NAD(H) shortage.

CONCLUSIONS

In the first project, we developed a model of triple negative breast cancer cells that are resistant to FK866, to dissect the molecular adaptations of cells to NAD(H) shortage. We observed that the acquired resistance to NAMPT inhibition is not sustained by canonical mechanisms of drug resistance or to a compensatory synthesis of NAD^+ by salvage or *de novo* NAD^+ biosynthesis pathways. Instead, MDA r. presented an overall metabolic rewiring sustained by mitochondrial adaptations. These cells presented a higher pyruvate dependency than the parental ones, that sustains an increase of the mitochondrial spare respiratory capacity and mitochondrial mass.

We also showed that the uncoupling between glycolysis and mitochondrial respiration, through the inhibition of MPC2, favors mitochondrial ATP synthesis and allow the parental cell line to acquire a FK866 resistant-like phenotype, during the acute and initial phase of the treatment.

Aligned with previous data from our group, showing that these cells rely on LDHA to overcome resistance to FK866[231], we suggest that MDA r. can modulate the activity of MPC2 and control pyruvate uptake by the mitochondria. Pyruvate is both the substrate of LDHA and the main carbon source for the mitochondrial TCA cycle. During resistance acquisition, the blockage of MPC2 provides a double metabolic advantage to cancer cells experiencing NAD(H) shortage. From one side, pyruvate in the cytoplasm provides the substrate to LDHA allowing the maintenance of NAD(H) levels. From the other side, the initial lack of mitochondrial pyruvate import stimulates a mitochondrial adaptation that can allow OxPhos to proceed. When resistance is acquired, mitochondrial rewiring and concomitant increase of the mitochondrial mass, allow to metabolize pyruvate and succinate more efficiently and sustain ATP synthesis.

Taken together, these data give some insights on the mechanisms developed by cancer cells in response to NAD(H) shortage, which can challenge the NAMPT inhibitors usage in the clinics.

SECOND PROJECT

YAP modulates sensitivity to FK866 in a triple negative breast cancer cell line

BACKGROUND

Disruption of the balance between cell proliferation and cell death disturb cell and tissues homeostasis and often drive pathological conditions[165]. YAP, together with TAZ, are the downstream effectors of the Hippo pathway, and function as transcriptional co-activators of target genes via interaction with the TEA domain family members (TEAD)[172]. YAP/TAZ translocate between cytoplasm and nucleus according with the activation of the Hippo kinases: when the Hippo pathway is "on", a signaling cascade culminate in LATS1/2-mediated YAP phosphorylation at serine 127 and its sequestration in the cytoplasm and degraded. Conversely, inactivation of the Hippo pathway prevents YAP phosphorylation, leading to its nuclear translocation and interaction with TEAD to modulate transcription[181].

YAP has been historically related with increased cell proliferation, a necessary condition for tumor growth. In fact, hyperactivation of YAP and TAZ is widely spread in cancers, which lead to its classification as oncogenes[180,259]. Nevertheless, in the recent years YAP has been reported to present tumor suppressor functions in a context-dependent condition.. Particularly, in TNBC, YAP plays an oncogenic function: it was founded to be upregulated in TNBC but not in estrogen receptor alpha positive breast cancer, whilst its depletion inhibited cell invasion and proliferation[260].

Aligned with the role of YAP/TAZ on the maintenance of energy-consuming processes as cell proliferation and growth and tissue homeostasis, it emerged as a critical node in metabolic regulation[182]. YAP and TAZ coordinate several NAD^+-dependent processes like glycolysis, fatty acid oxidation and glutaminolysis in nutrient-deprivation conditions[261]. However, correlations between NAD(H) levels and YAP/TAZ metabolic function are still poorly understood.

AIMS

Recent studies regarding the Hippo signaling and YAP/TAZ role in tumorigenesis highlighted its contribution to mediate metabolic adaptation to sustain highly energy-consuming cellular processes like glycolysis, fatty acid oxidation and glutaminolysis[182]. Of note, all these energy-producing traits depend on the activity of dehydrogenases (as GAPDH, LDHA, FDH, SDH) and consequently of NAD(H) availability. Nevertheless, a correlation between NAD(H) cellular levels or response to NAD(H) depletion agents, and YAP/TAZ activity are poorly understood.

Previous unpublished data from our lab revealed a potential role of YAP in mediating the sensitivity to the NAMPT inhibitor FK866 in prostate cancer (PC). Nowadays, the standard of care for PC treatment relies initially on prostatectomy and radiotherapy, followed by androgen-deprivation therapy and administration of AR antagonists. Despite the drastic improvement of PC diagnostics and treatment, around 20% of the patients invariably develops metastasis resistant to AR inhibition (metastatic castration-resistant prostate cancer - mCRPC), which lacks therapeutical options[262].

Importantly, we observed that the AR-positive cell line LNCaP was less sensitive to FK866 than the AR-negative, castration resistant cell line PC3. Upon FK866 exposure, PC3 but not LNCaP presented a decreased level of pYAP, consistent with YAP nuclear translocation and transcription of target genes as CTGF and CYR61. Of note, the stable silencing of YAP in PC3 rescued FK866 toxicity in anchorage-independent growth conditions (Annex 1).

Given the mention data obtained for PC cancer models, we hypothesized that YAP could play a role in the acquirement of resistance to FK866 in triple negative breast cancer.

Thus, we aimed to expand the characterize FK866-resistant cancer cell models by:

(1) Confirming the effect of FK866 in YAP phosphorylation status in FK866-sensitive and less sensitive/resistant cancer cell lines.

(2) Modulate YAP levels and evaluate the presence of a mechanistic correlation with FK866 sensitivity.

(3) Investigate the role of YAP on the metabolic rearrangement observed in the FK866-resistant TNBC model.

MATERIALS AND METHODS

The Materials and Methods applied for the second project of the thesis is very similar to the one of the first project. To avoid repetitions, references will be made to the Materials and Methods section of the first project.

Cell lines culture conditions

Culturing of MDA p. and MDA r. were described for the first project. The pancreatic ductal adenocarcinoma cell line PK9 resistant to FK866 (PK9 r.) were obtained from their sensitive parental cells (PK9 p.) using the same strategy[263]. PK9 p. and PK9 r. were cultured in RPMI (Gibco) and supplemented with 10% fetal bovine serum (FBS), 2mM L-glutamine, and 100U/mL penicillin-streptomycin (all from Lonza). The culture media of PK9 r. and was additionally supplemented with 100nM of FK866.

YAP knockdown or overexpressing cells were kept in the same conditions as the original ones. Cells were maintained at 37ºC under humidified conditions with 5% CO_2.

Drug treatments and in vitro cell viability

FK-866 sensitive and resistant cells were treated with FK866 (sc-205325, Santa Cruz Biotechnology) for 48h. As described for the first project, in vitro drug sensitivity was assessed through the OzBlue Cell Viability kit (OzBiosciences) and the surforhodamide B (SRB) assay.

Protein extraction and western blot analysis

Protein extraction and western blot analysis were performed with the same protocol used for the first project. The primary antibodies used were: YAP (sc-101199, Santa Cruz Biotechnologies), pYAP Ser127 (4911S, CST), and actin (BK4970S, CST). Actin was used as protein loading controls. The anti-mouse and anti-rabbit secondary antibodies (111-035-003) used were obtained from Jackson Immunoresearch Laboratories. A representative western blot of three independent biological experiments is shown.

Lenti- and retroviral transfection

HEK293T cells were used to produce lentiviral vector particles (LVP) and retroviral particles (RVP).

For YAP silencing, HEK293T cells were co-transfected with a Δ891 and a VSV-G encoding vector along with the shYAP plasmid. PLKO vector was used as the transfer plasmid.

For YAP overexpression, the plasmid pQCXIH-Myc-YAP5SA was purchased from Addgene. The negative control pQCXIH-Myc-empty was obtained by removing the YAP5SA cassete by digestion with the restriction enzyme BamHI. Digested plasmid was run on 1% agarose gel, extracted and purified. Ligation was carried out with T4 ligase. Plasmids were amplified and sequence was confirmed through Sanger sequencing. HKE293Tcells were co-transfected with pC9 GAG pol and VSV-G encoding vector, along with the pQCXIH-Myc-YAP5SA (YAP5SA) or the transfer plasmid pQCXIH-Myc-empty (empty) to produce the RVP.

Viral supernatants were collected, filtrated, and quantified 72 hours post-transfection. Selection with puromycin (1ug/mL) and hygromycin (500ug/mL) were performed, respectively, on MDA p. stably infected with shSCR/shYAP, and on MDA r. stably infected with empty/YAP5SA plasmids.

Colony formation assay (Soft agarose)

Soft agar assay was carried out in 6-well plates with a double coating of agarose. The base agarose layer presented 0,7% of agarose in 10% FBS supplemented DMEM. 5000 cells per condition were resuspended in 1mL of 0,35% agarose in 10% FBS supplemented DMEM and seeded. Cells were cover with 1mL of media and treated with different concentrations of FK866 (range 1-500nM) every 3 days, for 2 weeks; and constantly kept under selection with either puromycin (1ug/mL) or hygromycin (500ug/mL), for YAP silencing or overexpression, respectively. Total colony number and colony diameter were measured using Operetta and Harmony 3.5.2 software.

RNA extraction and real-time qPCR

RNA extraction, cDNA synthesis and real time qPCR were performed as described for the first project. The sequences of the primers employed in the study are present in **Table 2**. ΔCq method was used for samples' mRNA quantification, with RPLP0 as housekeeping genes.

Gene	Primers
PGC1α	FW: CAAAGGATGCGCTCTCGTTCA
	RV: GGTGTCTGTAGTGGCTTGACT
RPLP0	FW:CATTCTCGCTTCCTGGAG
	RV:CTTGACCTTTTCAGCAAGTGG

Table 2: List of primers used to evaluate the expression of genes of interest by RT-qPCR analysis.

Statistical analysis

Data was expressed as mean ± standard error of mean (SEM) of three independent biological experiments conducted in technical triplicates, unless indicated otherwise. Statistical significance between control and test groups was determined using Student's t-test or one-way ANOVA, considering values of $*p < 0.05$, $**p < 0.01$, and $***p < 0.001$ as significant. Data were plotted by Graph prism 6 software.

RESULTS

Results in the thesis body reflect my personal contribution to the work and experiments performed by collaborators are properly acknowledged. In this second project, some of the biological replicates were performed by the Bachelor students Arianna Buongiorno and Elia Franceschi.

YAP phosphorylation is decreased in FK866-sensitive cancer cell models upon treatment

Phosphorylation at Ser127 is the most common post-translational modification of YAP and it controls its cellular localization: YAP phosphorylation leads to its cytoplasmatic retention, while YAP dephosphorylation allow its migration into the nucleus to activate the expression of its target genes. To assess YAP phosphorylation status as a proxy of its cellular localization and activation, MDA p. and MDA r. were treated for 48h with FK866. Western Blot analysis revealed a decrease of YAP phosphorylation at serine 127 (pYAP) in a dose-dependent fashion, upon MDA p. exposure to the 5 and 10nM of the small molecule. Instead, pYAP levels were not modulated in MDA r., even at the higher concentration of 100nM (Figure 30A). To increase the robustness of the result, we decided to replicate the experiment in a pancreatic ductal adenocarcinoma cell line (PK9).

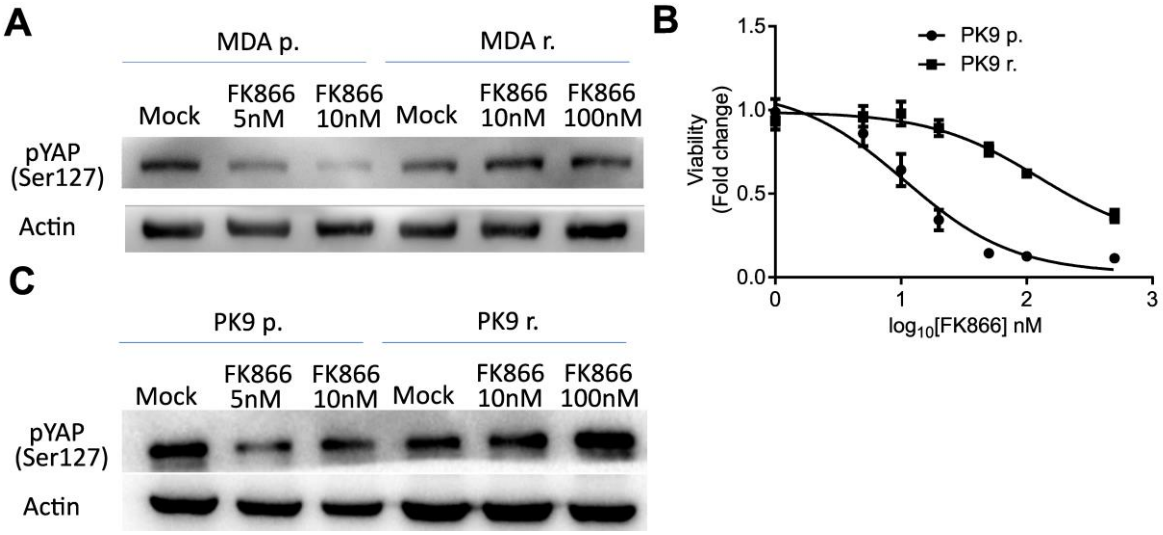

Figure 30 FK866 decrease pYAP (Ser127) in sensitive models. Representative western blot of phosphorylated YAP on serine 127 in MDA p. and MDA r. (A) and PK9 p. and PK9 r. (C) upon 48 hours of exposure to FK866 at the determined concentrations. (B) Dose-response curve of FK866 in PK9 p. and PK9 r. in the same conditions. Three biological replicates were performed

Like the triple negative cancer cell model, also PK9 p. were exposed to increasing concentration of FK866 until resistance was reached (PK9 r.) and *NAMPT* gene was not mutated. However, in this case, full resistance to FK866 could not be obtained (Figure 30B).

FK866-toxicity was assessed for this model upon 48h of exposure to the small molecule and IC_{50} was determined as 10nM for PK9 p. and 150nM for PK9 r. (Figure 30B). pYAP was similarly decreased in PK9 p. when exposed to FK866 at 5 and 10nM, but not on the resistant counterparts (Figure 30C). Taken together, these data confirm the FK866 effect on the modulation of YAP phosphorylate status, and consequent nuclear translocation, on triple negative breast cancer and pancreatic ductal adenocarcinoma, as previously observed for castration-resistant prostate cancer cell models. Moreover, these experiments seem to depict YAP phosphorylation status as an important determinant of FK866 sensitivity, and consequently as a potential mediator of the acquirement of resistance to NAMPT inhibition.

YAP silencing induces a FK866-resistant like phenotype

Hypothesizing a role of YAP in mediating FK866-acquired resistant, we decided to modulate YAP expression levels, through lentiviral-mediated stable silencing of this protein. The FK866 sensitive cell lines MDA p. ad PK9 p. were infected with lentiviral particles containing pLKO shYAP and selected with puromycin for 5 days before starting the experiments. YAP silencing was confirmed by western blot (Figure 31).

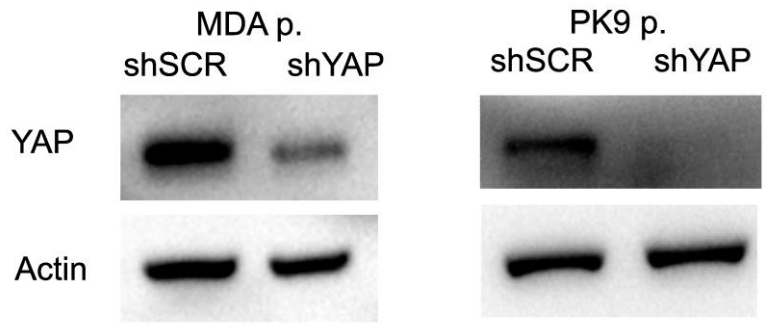

Figure 31 Confirmation of YAP silencing. Representative western blot image of the expression levels of YAP in MDA p. (left) and PK9 p.(right) stably expressing pLKO-shSCR (shSCR) or pLOKO-shYAP (shYAP). Actin was used as loading control.

To assess the effect of YAP silencing on FK866 sensitiveness, both OzBlue and SRB assays were used. While the first measures the activity of dehydrogenase on metabolic active cells, the second determines the total amount of attached cells, in a metabolic-independent fashion. Upon 48 hours treatment with FK866, it was observed an increase of cell viability in cells silenced for YAP, in comparison with the control (shSCR) condition, in both OzBlue (Figure 32A) and SRB assays (Figure 32B). The rescue of FK866-toxicity was more pronounced for the TNBC cell model, as MDA p. shYAP resemble MDA r. phenotype (Figure 13A). Nevertheless, rescue of FK866 toxicity upon YAP silencing was also observed for the pancreatic cancer model, with PK9 p. shYAP viability curve resembling the one of PK9 r (Figures 30B and 32C-D).

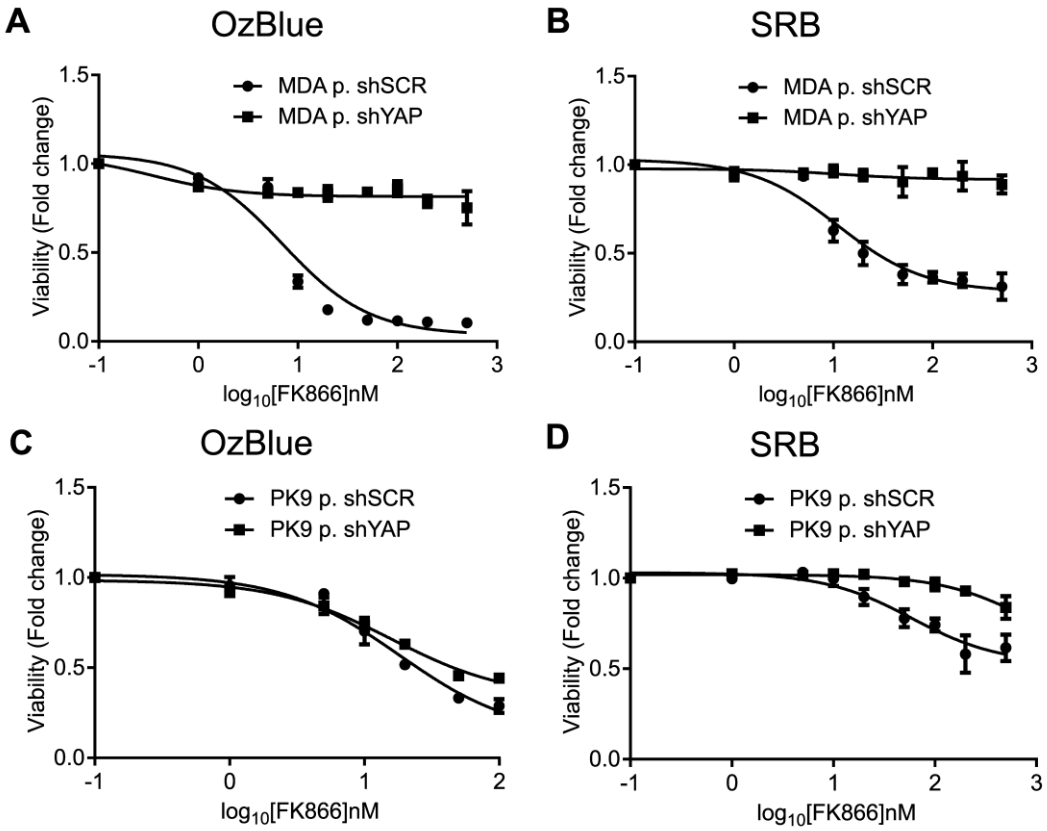

Figure 32 YAP knockdown decreases sensitivity of TNBC cells to FK866. Dose-response curve of 48 hours FK866 treatment in (A-B) TNBC and prostate ductal adenocarcinoma (C-D) cells, stably silenced for YAP, through OzBlue and SRB viability assays. Three biological replicates were performed.

To gain a deeper inside on the effect of YAP silencing on FK866 sensitivity, we performed an *in vitro* clonogenic assay. This experiment determines the ability of

cells to grow into a colony, in attachment-independent conditions, that is a trait of cancer cells with tumor-initiating capabilities[264].

After two weeks of culturing with FK866 treatment every three days, the number of colonies was assessed. We observed that exposure to this NAD(H) depletion agent decreased colony number in a dose-dependent manner in MDA p. shSCR, confirming the sensitivity of these cells to NAMPT inhibition obtained in 2D with the viability assays. Instead, no significant alterations were observed on colony number derived from MDA p. shYAP cells, upon exposure to the small molecule. Interestingly, no significant difference was observed in the non-treated conditions, meaning that YAP silencing *per se* do not affect MDA p. colony formation ability in this cell line (**Figure 33**).

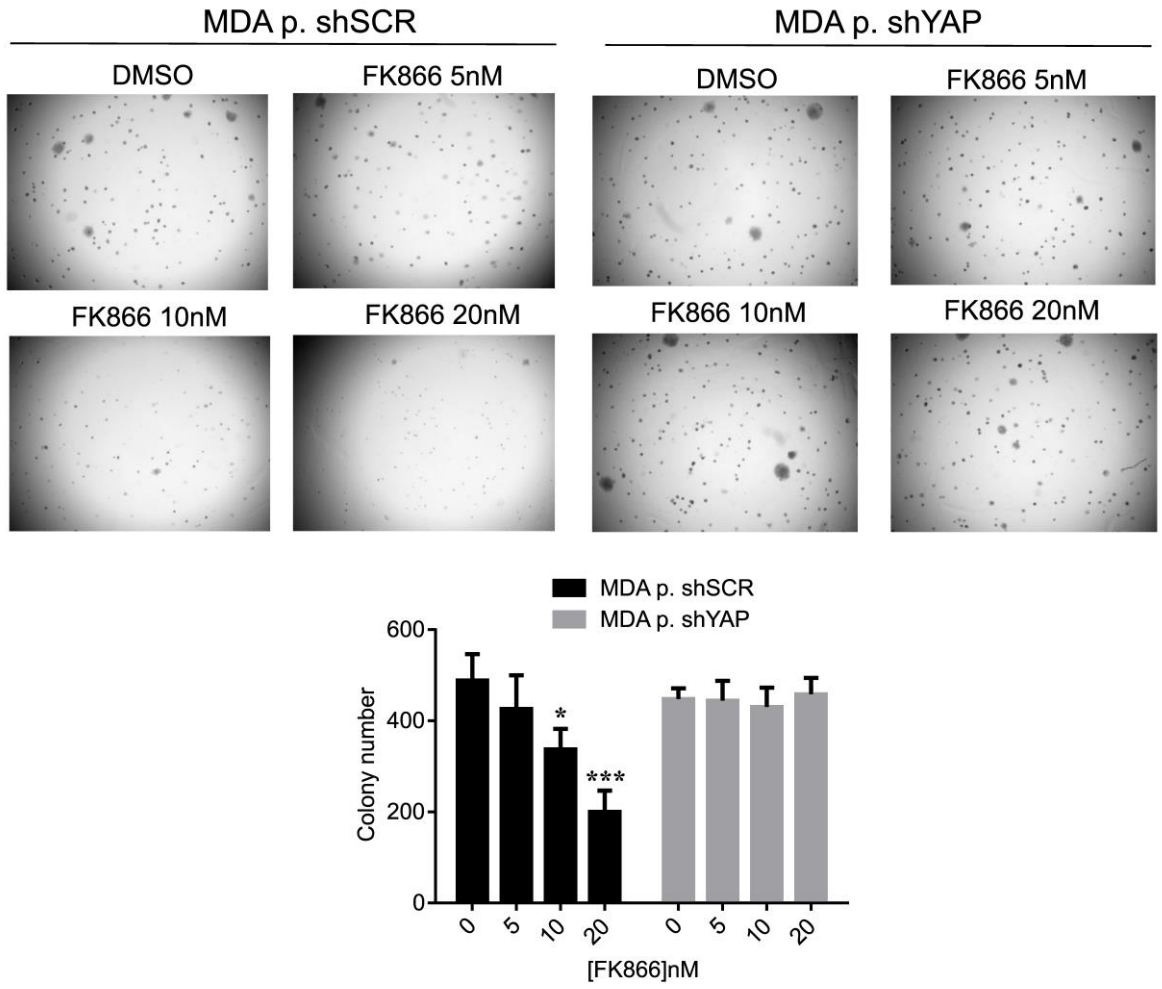

Figure 33 Effect of FK866 treatment on colony formation upon YAP silencing. Representative images of soft agarose assay of MDA p. shSCR (A) and MDA p. shYAP (B) lines. Cells were treated with different concentration of FK866 (5 nM, 10 nM, 20 nM) every three days for a period of three weeks. DMSO was used as negative control. (C) Quantification of normal colony number exposed to the described concentrations of FK866. Colony number was quantified with Operetta and analyzed on Harmony 3.5.2 software. Three biological replicates were performed (*p < 0.05, ***p < 0.001 compared to DMSO condition).

Of note, the clonogenic assay was also performed for PK9 p. shSCR and shYAP, but colonies never fully developed, and no data was acquired.
Overall, these data confirm the role of YAP on the mediation of the cytotoxic response to FK866 treatment both in attachment (2D) and in anchorage-independent conditions (3D).

YAP overexpression rescues FK866-induced toxicity in 2D but not in 3D

The confirmation that YAP activation mediates FK866 cytotoxic effect *in vitro*, reveals its potential role as mediator of the acquirement of resistance to FK866 in TNBC. To confirm the hypothesis, we stablished MDA r. cell lines stably overexpressing a YAP phosphorylation-defective mutant, in which the five individual serine residues within the phosphorylation motifs are replaced by alanine residues. Therefore, YAP phosphorylation on the ectopic protein is prevented, as well as its cytoplasmatic retention, which induces its nuclear translocation and the activation of YAP-dependent transcriptional programs.
MDA r. empty and MDA r. YAP5SA were selected with hygromycin for 5 days before starting the experiments. YAP overexpression was confirmed by western blot (Figure 34).

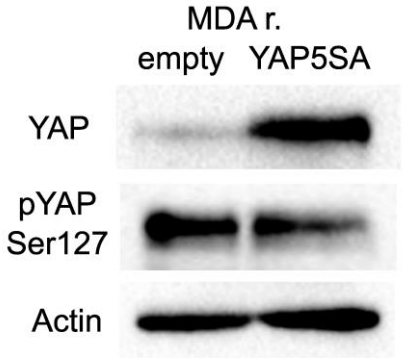

Figure 34 Confirmation of YAP overexpression. Representative western blot image of the expression levels of YAP and pYAP (serine 127) in MDA r. stably expressing pQCXIH-Myc-empty (MDA r. empty) or pQCXIH-Myc-YAP-5SA (YAP5SA). Actin was used as loading control.

Cell viability upon 48 hours of FK866 exposure was once again assessed through OzBlue and SRB assays and similar results were obtained. MDA r. empty presented a lower sensitivity to the NAMPT inhibition for both assays while the overexpression of exogenous non-phosphorylated YAP sensitizes cells to FK866 treatment. Of note, for both assays, the viability curve for MDA r. YAP5SA do not

reach the 0% and presents a plateau for a value of cell viability of approximately 50% of the control (Figure 35).

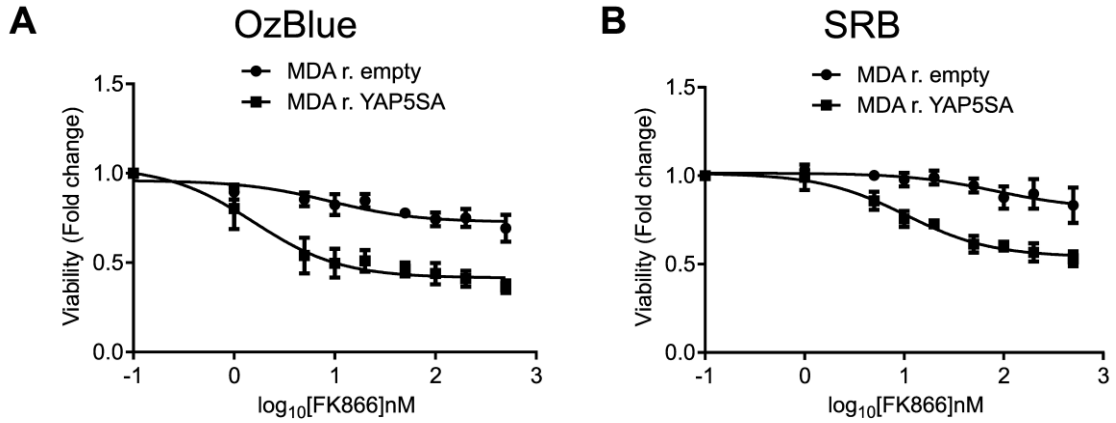

Figure 35 YAP overexpression increases sensitivity of TNBC cells to FK866. Dose-response curve of 48 hours FK866 treatment in MDA r. cells overexpressing YAP, measured through OzBlue (A) and SRB (B) assays. Three biological replicates were performed.

The ability to grow in anchorage-independent conditions was also assessed through the soft agarose assay. Like for the cells silenced for YAP, MDA r. empty and MDA r. YAPSA were grown for two weeks and treated with FK866 every three days (Figure 36). We observed that exposure to this NAD(H) depletion agent had no effect on the colony number in both cell lines, comparing with their correspondent DMSO-treated control. Instead, significant difference was observed in the non-treated conditions, meaning that YAP overexpression *per se* affects MDA r. colony formation ability (Figure 36).

Overall, these data are not aligned with the results obtained for the 2D viability assays, as YAP overexpression do not affect the colony formation ability on a FK866-dependet fashion.

Role of YAP on cancer cells adaptation to NAD(H) shortage: a metabolic perspective

YAP has been widely involved in cellular metabolic regulation. Taking into consideration the data obtained for the first project of this PhD thesis, describing the mitochondrial rewiring in the adaptation to NAD(H) shortage, we decided to further characterize the cancer cell lines modulated for YAP expression at the metabolic level.

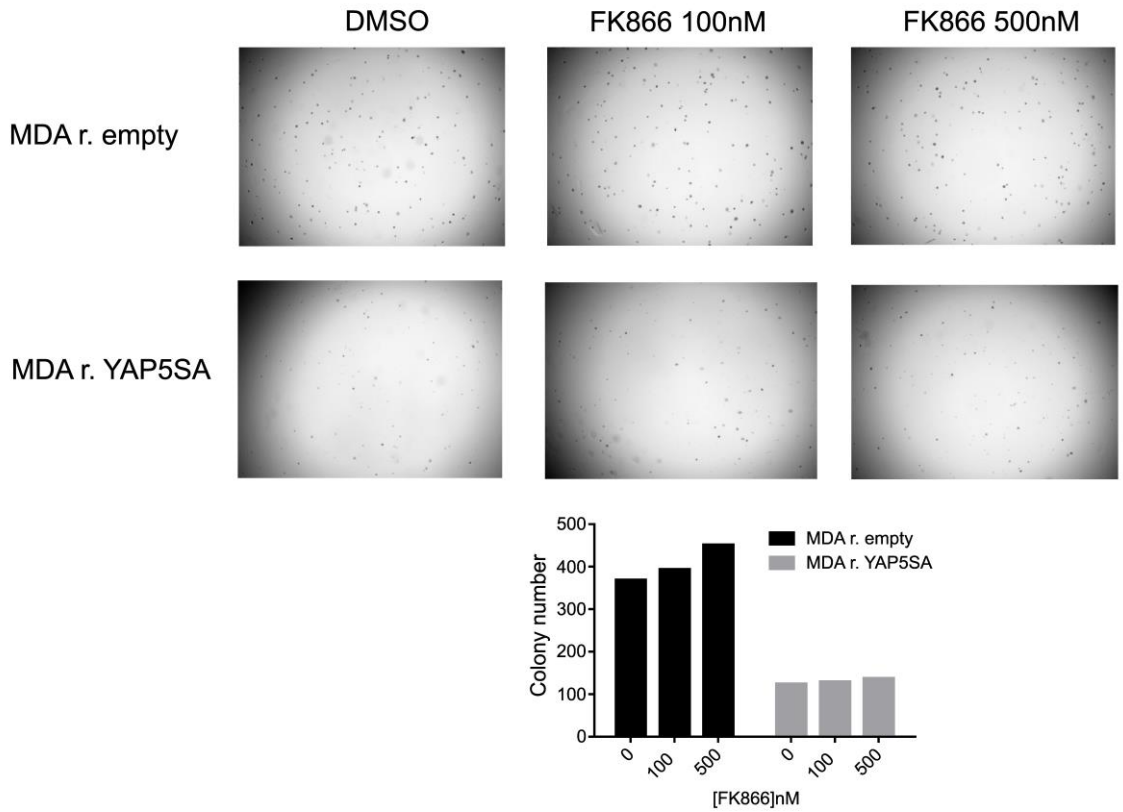

Figure 36 Effect of FK866 treatment on colony formation upon YAP overexpression. Representative images of soft agarose assay of MDA r. empty and YAP5SA cell lines. Cells were treated with different concentration of FK866 (10 nM, 100 nM) every three days for a period of two weeks. DMSO was used as negative contro (top). Quantification of normal colony number exposed to the described concentrations of FK866 (bottom). Colony number was quantified with Operetta and analyzed on Harmony 3.5.2 software. Only one biological replicates was performed so far.

Initial preliminary data revealed that the silencing of YAP in MDA p. induce the expression of the mitochondrial biogenesis regulator PGC1-α in more than 2-fold change, which is further stimulated by 48 hours of FK866 treatment at 10nM (Figure 37A). This gene has been already found upregulated in MDA r (Figure 23C).

PGC1-α expression was also assessed in the cells line overexpressing YAP, MDA r. YAP5SA, but no significative difference was observed either in FK866-treated or non-treated conditions (Figure 37B).

Overall, these data suggests PGC1-α as a factor involved in the response to the energetic stress induced by the FK866 and that can be involved in the process of resistance acquisition. However, it's functional role is yet to be investigated.

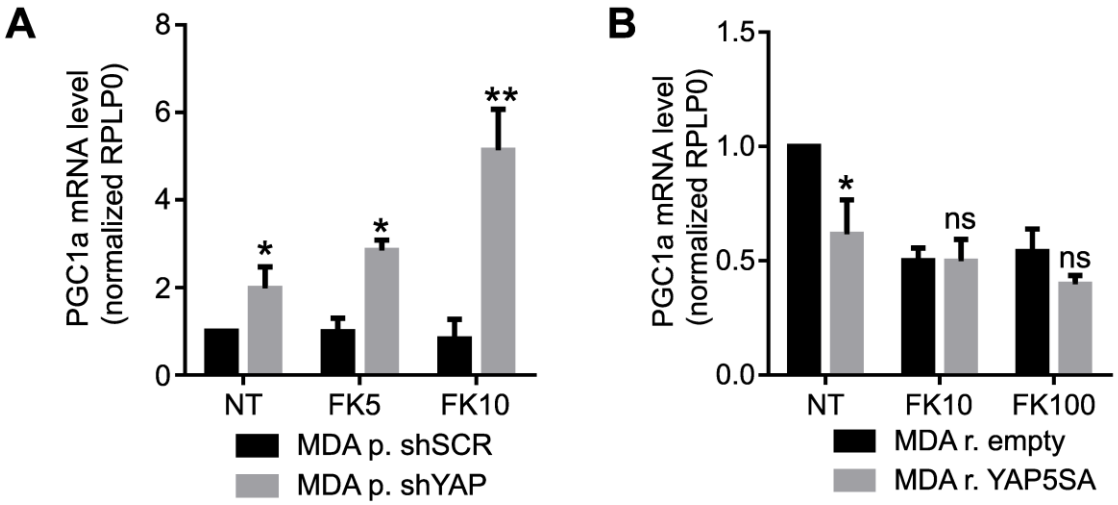

Figure 37 PGC1- α expression is increased in cancer cells with FK866-resistant phenotype. RT-qPCR to determine PGC1-α expression in MDA p. silenced for YAP (A) and in MDA r. overexpressing YAP (B) and treated with FK866. (non treated - NT - and treated for 48h with the determined concentrations of FK866). *RPLP0* was used as a house-keeping gene. All the experiments were performed in triplicate. Repeated measures one-way ANOVA was used to calculate statistical significance (*P<0.05, **P < 0.01, ***P < 0.001) .

DISCUSSION

YAP, the downstream effector of the Hippo pathway, is historically described to promote cell proliferation and tissue homeostasis. Given the indispensability of cellular energy and metabolites for survival and growth, correlations between YAP and metabolic regulation have recently gain interest in the cancer bioenergetics field[182,261]. Likewise, the NAD^+-producing enzyme NAMPT is widely found upregulated in several solid tumors, reflecting its importance for NAD(H) and consequently cancer cell bioenergetics maintenance. Here, we find a correlation between the activation of YAP and the sensitivity to the NAMPT inhibitor FK866 in a cellular model of TNBC, that can play a role on the acquirement of resistance to this small molecule.

YAP activity to promote the co-transcriptional activation of its target genes depends on its cellular localization and consequently of its phosphorylation status. We showed that the treatment with FK866, in TNBC and PDAC cells sensitive to this small molecule but not in their resistant counterparts, decrease YAP phosphorylation at serine 127 (Figures 30A and 30C), which is aligned with YAP nuclear translocation. However, YAP phosphorylation can occur at other sites rather than at serine 127, like at serine 61,109, 164 and 397, either in a LATS1/2-dependent (and consequently Hippo-dependent) or independent fashion[265]. Thus, further experiments, like immunofluorescence and expression of target genes must be performed to confirm YAP nuclear translocation and activity upon FK866 exposure.

Proceeding with the hypothesis that YAP activation results from FK866 exposure, which would be prevented in the resistant cell models, we modulated the levels of YAP (Figures 31 and 34). In fact, we were able to show that the silencing of YAP on the FK866-sensitive cell lines (MDA p. and PK9 p.) decrease the sensitivity to the NAMPT inhibitor in attachment (2D) conditions (Figure 32).

As previously described, the cellular ability to survive and grow in anchorage-independent conditions (resistance to anoikis) is a necessary condition for cancer cell metastasis and a hallmark of the YAP activation[266]. Thus, to reinforce our data, we decided to mirror the viability experiment in a 3D setting, by performing a clonogenic assay in soft agar (Figure 33). Interestingly, the silencing of YAP *per*

se did not decrease the number of colonies formed, as would be expected from an inactivation of the YAP signaling, suggesting that anchorage-independent growth ability in this model is not sustained exclusively by YAP. Nonetheless, it confirmed the results of the cell viability experiments in 2D, with MDA p. shYAP cell rescuing FK866 cytotoxicity. The fact that YAP silencing did not decrease the colony number was previously described in breast cancers. YAP knockdown rendered MDA-MB-231 resistant to anoikis and slightly increased the colony formation ability, confirming that YAP loss also promotes anchorage-independent growth[267].

Overall, it is conceivable to assume that in MDA-MB-231 cells YAP-independent transcriptional programs can sustain their ability to grow in anchorage-independent conditions, as indeed can be explained by the metastatic origin of these cells.

As the knockdown of YAP decreased the sensitivity to FK866, a potential role of this co-transcriptional factor in mediating the acquirement of resistance to the NADH(H) depletion agent is suggested. The overexpression of the mutant non-phosphorylatable YAP in MDA r. indeed sensitizes the cells to FK866 treatment in attachment conditions, pinpointing its importance for the maintenance of the resistant phenotype (Figure 35). Even if only one biological replicate was performed, surprisingly, different results were obtained for the 3D culturing in soft agar. MDA r. YAP5SA cells showed fewer colonies compared with the control ones expressing the vector plasmid, but the FK866 treatment did not further reduce this parameter. These data revealed that YAP activation indeed deregulate cellular responses involved in the acquirement of resistance to FK866 in MDA r., but it is not the only mediator of this process, as FK866 did not reacquire its full toxicity.

Finally, we checked the expression level of PGC1-α, that we had previously shown to be overexpressed in MDA r. to investigate downstream effects of YAP modulation on the acquirement of resistance to FK866 in TNBC, at the metabolic level. In fact, we were able to confirm that PGC1-α is differentially expressed according with YAP activation, being upregulated upon YAP silencing, which is once more consistent with the FK866-resistant phenotype. Interestingly, PGC1-α expression levels reflect the results obtained in anchorage-independent conditions: cells overexpressing mutated YAP present a lower number of colonies

and a lower expression of PGC1-α; while the treatment with FK866, at each concentration, is not affecting none of the parameters (Figures 36 and 37).
Overall, these data seem to highlight a role of YAP on the acquisition of resistance to FK866, but not as the main player of its maintenance.

CONCLUSIONS

In the second project, we investigated the potential role of YAP in the modulation of the sensitivity to FK866 in cancer cell models.

We showed that FK866 treatment decrease YAP phosphorylation status at serine 127, thus increasing its nuclear translocation and target gene expression, in cancer cell models of triple negative breast cancer (MDA p.) and pancreatic ductal adenocarcinoma (PK9 p.), that are sensitive to the NAMPT inhibitor. These results were in agreement with previously unpublished data from our lab, using prostate cancer cell models.

Additionally, we demonstrated that stable silencing of YAP in FK866-sensitive cell lines, rescued its toxicity both in 2D and in 3D culturing, promoting a dose dependent FK866-resistant like phenotype. By the other side, the overexpression of YAP in FK866-resistant TNBC cells only rescued the cytotoxicity of the NAD(H) lowering agent in attachment, but not in anchorage-independent conditions.

Moreover, the silencing of YAP on MDA p. induces the FK866-dependent expression of the mitochondrial biogenesis gene PGC1-α, previously associated with TNBC FK866-resistant phenotype.

In conclusion, we were able to identify a connection between YAP activation and sensitivity to FK866, that can in part sustain the acquirement of resistance to FK866 in TNBC, likely through the modulation of mitochondrial metabolic traits.

CONCLUSIONS AND FUTURE PERSPECTIVES

Until the 2000's, cancer biology was focused on the characterization of two distinct classes of cancer genes, that could either result in cellular gain or loss of function, and thus be characterized as oncogenes or oncosupressors, to explain cancer initiation and progression. Hanahan and Weinberg were the first to propose an organized list of biological traits that sustain the multistep development of human tumors, which has been lastly updated in 2022[2]. Nonetheless, it is since 2011 that the deregulation of cellular bioenergetics has been considered an hallmark of cancer[214]. However, this reprogramming of energy metabolism is context-dependent and goes far beyond the Warburg effect, as initially proposed[13].

In our model of FK866-resistant TNBC, obtained by increasing exposure to the NAD(H) depletion agent, we indeed observed a hybrid glycolytic/OXPHOS phenotype. Previous published data from our lab showed that FK866 resistance, namely in the TNBC model, invariably induces dependence on LDHA, but not a shift towards a Warburg-like metabolism[133]. As LDHA recycles NAD^+ through the conversion of pyruvate to lactate, contributing for the maintenance of NAD/NADH pool in the cytoplasm, which could explain its increase expression in MDA r..

In fact, pyruvate utilization is a critical node for the maintenance of cellular bioenergetics due to double usage as substrate for LDHA or as carbon source for the TCA cycle. We showed that the acute treatment of MDA p. with the MPC inhibitor UK5099 counteracts FK866 cytotoxicity and induces a resistant like phenotype, presumably because MPC blockage increases pyruvate cytoplasmatic availability. Similar results were obtained for MPC2 but not to MPC1 silencing.

Nevertheless, we were not able to demonstrate that loss of function of MPC sustain the observed FK866 acquired resistance. Instead, we showed that MDA r. are more dependent on pyruvate metabolism than MDA p., and that pyruvate contributes to the maintenance of their higher mitochondrial respiration. Apart from pyruvate, these cells also present a higher OCR in the presence of succinate, the substrate of Complex II of the ETC, similarly revealed as a metabolic dependency of MDA r.. It is however not excluded that additional anaplerotic reactions might contribute to mitochondrial bioenergetics, by sustaining the TCA cycle. This hypothesis should be further explored.

Interestingly, the activity of the uncoupled ETC complexes was not different between MDA p. and MDA r..

In line with the observed rewiring of mitochondria in response to FK866, we further showed an increased expression of the mitochondrial biogenesis genes PGC1-α and TFAM, as well as of the mitochondrial versus nuclear ratios, indicative of an increased mitochondrial mass. These results are aligned with the literature, that reports increased PGC1-α, and consequently mitochondrial mass, to counteract nutrient stress conditions[268]. Although the importance of PGC1-α to sustain the acquired-resistance to FK866 is yet to be confirmed through loss of function assays, it seems to be a marker of the stress response induced by FK866 as observed in the second project of this thesis.

Giving the observed hybrid glycolytic/OXPHOS phenotype in the FK866-resistant model, through the contribution of both cytoplasmatic and mitochondrial compartments for the maintenance of bioenergetics, further characterization of the model should focus on their mechanistic connection, and on the relevance of MPC.

Nevertheless, the results of this thesis highly emphasize the role of mitochondria for metabolic adaptation to stress stimuli. In fact, mitochondria have been historically seen as the powerhouse of the cells, but its functions in cancer initiation, growth, survival and metastasis goes far beyond energy production. More than alterations in fuel utilization, mitochondria offers cancer cells the flexibility to adapt to adverse conditions like starvation and exposure to chemotherapeutics, by modulating cell death susceptibility and oxidative stress[70]. FK866 treatment has been previously described to induce ROS production in several cancer models[269]. Similarly, it was shown that cytotoxic stress inducing ROS production can subsequently activate YAP in TNBC cell models, leading to mitochondrial disfunction[270]. Importantly, the formation of the mitochondrial supercomplexes are indeed described to reduce the production of ROS apart from their role in increasing the ETC efficiency[258]. Thus, it is of our interested to understand how oxidative stress is managed in FK866-resistant cancer cells and as well as its response to YAP modulation.

Furthermore, it is important to note that with our experimental settings, we are not studying the progressive acquirement of resistance to FK866, but rather

comparing the initial and final timepoints. The response to chronic FK866 exposure, acquisition of the resistance and its maintenance, shall be considered as temporal process, with specific contributions for the ultimate FK866-resistant phenotype. This means that we can't exclude a potential role of MPC or NMRK1 in the acute phase of the treatment. One can hypothesize that the first cellular responses to the FK866-induced metabolic stress is the blockage of MPC and the upregulation of NMRK1 to maintain the NAD/NADH cytoplasmatic pool. In fact, the compartmentalization of the NAD/NADH is mainly sustained due to the impermeability of the mitochondria outer membrane[92]. NAD^+ concentrations in the mitochondria is around 400µM, while in the cytoplasm is 100µM; and the NAD/NADH ratio are, respectively 60-700 in the cytoplasm and 7-8 in the mitochondria[271–273]. This compartmentalization of the NAD/NADH pools leads to different responses to genotoxic stress in the distinct subcellular compartments, with NAD^+ being usually firstly observed in the cytoplasm and later in mitochondria[92]. This way, we can hypothesize that upon acute treatment with FK866, cells respond by stimulating processes that maintain the cytoplasmatic NAD/NADH pools, as the increase activity of LDHA through the blocking of MPC2, and eventually NMRK1 gain of function. FK866 also induce the nuclear translocation of YAP and activation of its target genes, likely pro-apoptotic, in line with its role of oncosupressor gene observed in this model. We hypothesize, that the FK866-induced decrease of the cytoplasmatic NAD/NADH pools and consequent utilization of the mitochondrial ones would stimulate the exploitation of pyruvate and succinate as carbon sources to keep the TCA cycle and mitochondrial respiration running. Additionally, we observe that FK866-sensitive cells knocked-down for YAP present an overexpression of PGC1-α, reported to promote mitochondrial biogenesis and increase of the mitochondrial mass to sustain mitochondrial NAD/NADH pools. Thus, specifically measuring the basal NAD^+/NADH pools in the cytoplasm and in the mitochondria, as well as upon FK866 treatment, rather than the total cellular content, could give some clues on both cytoplasmic and mitochondria roles to sustain the FK866-resistant phenotype.

The data present in this thesis also supports a connection between the YAP activation and the sensitivity to FK866 in cancer cell models of breast, prostate

and pancreatic tumors, but upstream and downstream YAP signaling is yet to be assessed.

Taking together this assumption and the previously reported role of YAP on metabolic reprogramming, we would further like to explore the YAP downstream metabolic targets. We were able to show that an upregulation of PGC1-α, found upregulated in the FK866-resistant phenotype (MDA r.), is observed in a FK866-dose dependent manner in the YAP silenced cells but not in the control ones. Moreover, the overexpression of YAP in MDA r. leads to a decrease in both colony number and PGC1- α expression. Interestingly, the upregulation of mitochondrial proteins and, particularly PGC1-α, was identified through proteomic analysis of breast cancer cell lines grown in anchorage-independent conditions[274]. Aligned with these data, the mitochondrial rewiring observed in the FK866-resistant phenotype and mimicked by YAP silencing can play a role on the anchorage-independent growth ability of these models. By the other side, the upregulation of YAP and consequent downregulation of PGC1- α in MDA r. would explain the decrease of colony number in MDA r. YAP5SA. Once more, PGC1-α functional loss and gain of function assays still have to be performed to confirm its expression and function modulation by YAP. Additional metabolic experiments to determine mitochondrial spare respiratory capacity, metabolic dependency and mass could potentially reveal supplemental similitudes between the two cell phenotypes with different FK866 sensitiveness: MDA p./MDA r. YAP5SA and MDA r./MDA p. shYAP.

Furthermore, we are interested in deciphering the YAP upstream signaling cascade. In TNBC, YAP is reported to be activated by the glucocorticoid receptor (GR) signaling[275], whose relevance is likewise reported in the acquirement of resistance to AR targeted therapies in prostate cancer. As members of the steroid receptor superfamily of ligand-regulated transcription factors, both the AR and the GR present similar structural, functional, and consequently, compensatory properties[276]. In fact, the synthetic glucocorticoid (GC) dexamethasone suppresses the proliferation and migration of the AR^- prostate cancer cell line PC3, but not of the AR^+ LNCaP[277].

These reports are aligned with previous nonpublished data from our lab, in which we observed that leukemia cells resistant to FK866 are co-resistant to

glucocorticoids. Thus, we hypothesize that the acquirement of resistance to FK866 and the inactivation of the GR signaling and consequently of YAP are related events, that we would further like to explore.

Finally, it will be of crucial importance to validate the data obtained in this thesis with other NAMPT inhibitors, as FK866 was prevented to be used in the clinics due to its poor pharmacokinetic profile and secondary effects. Nonetheless, other NAMPT inhibitors are currently being developed and tested for clinical application (like OT-82), and chemoresistance is a common problem of the usage chemotherapy for anti-cancer treatment. Thus, the insights obtained can be used for improved rational design of these small molecules. The validation of the data obtained on different FK866-resistant cancer cell models would also be of relevance to increase the robustness of the results and the transversal exploitation of the identified fragilities on other FK866-resistant tumors.

To conclude, we would like to emphasize that the characterization of the molecular mechanisms of resistance to FK866 reveals cancer cells strategies to counteract and adapt to NAD(H) depletion, a common feature of highly proliferating tumors, that can be further explored for anti-cancer therapy.

CONTRIBUTION PROJECTS

During my PhD I have also been involved in four other side projects, two in the host laboratory and two in collaboration with Prof. Dr. Vincent Timmerman and Dr. Michele Cea, respectively. A brief description of the projects is presented.

1st project: development of an novel method to isolate extracellular vesicles from serum (Annex 2).

2nd project: *in vitro* validation of small molecules targeting the RAN translation, with clinical applications for the treatment of Amyotrophic Lateral Sclerosis (ALS).

3rd project: collaboration with Prof. Dr. Vincent Timmerman to identify modulators of autophagy through a high-throughput screening, clinically relevant for the treatment of Charcot-Marie-Tooth type 2L (CMT2L) disease.

4th project: on going collaboration with Dr. Michele Cea and Dr. Debora Soncini to develop multiple myeloma cancer cell lines resistant to ARQ531, to further study the mechanisms of acquired resistance to this small molecule.

LIST OF PUBLICATIONS

Agata SA Carreira, Silvia Ravera, Chiara Zucal, Natthakan Thongon, Irene Caffa, Cecilia Astigiano, Nadia Bertola, Arianna Buongiorno, Barbara Pardini, Alessio Nencioni, Santina Bruzzone, Alessandro Provenzani. Mitochondrial rewiring drives metabolic adaptation to NAD(H) shortage in triple negative breast cancer cells, Neoplasia, 2023 (in revision)

Agata SA Carreira, Natthakan Thongon, Alessandro Provenzani. YAP modulates sensitivity to FK866 in cancer cell lines. (in preparation)

GRANT SUPPORT

This project has received funding from the European Union's Horizon 2020 research and innovation program under grant agreement No 813284.

ANNEX 1

Results in this Annex reflect my personal contribution to the work.

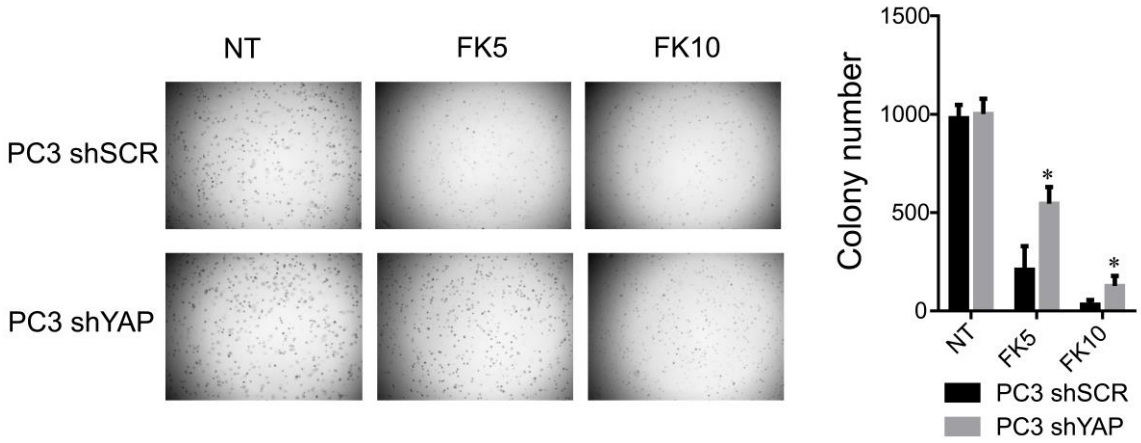

Figure 38 Effect of FK866 treatment on colony formation upon YAP silencing. Representative images of soft agarose assay of PC3 shSCR and PC3 shYAP lines (left). Cells were treated with different concentration of FK866 (5 nM and 10 nM) every three days for a period of three weeks. DMSO was used as negative control. Quantification of normal colony number exposed to the described concentrations of FK866 (right). Colony number was quantified with Operetta and analyzed on Harmony 3.5.2 software. Three biological replicates were performed (*p < 0.05 compared to DMSO condition).

ANNEX 2

Results in this Annex reflect my personal contribution to the work.

Extracellular vesicles (EVs) are lipid-bilayer structures secreted by cells to the extracellular spaces. EVs mediate cell-to-cell communication by transferring biological cargo (proteins, lipids, nucleic acids) from donor to receiving cells, thus mediating both physiological and pathological processes[278–280]. In fact, these structures have been widely reported to have critical roles in cancer development by sustaining the growth, invasion and metastasis of cancer cells in a myriad of cancer types[281–284]. Importantly, EVs can be found on and isolated from biological fluids like blood, urine and cerebrospinal fluid (CSF), and applied as biomarkers for the diagnosis, prognostication, and surveillance of cancer, as well as response to treatment, making them an important tool for liquid biopsies and precise medicine[285–287]. The gold-standard method for EVs isolation is ultracentrifugation, even if other methods based on polymer-based precipitation, size-exclusion chromatography, or density gradient centrifugation are currently being optimized and applied[288]. Nonetheless, a plethora of challenges are still to be addressed, namely the optimization of the isolation protocol duration, the separation of EVs from serum proteins and non-EVs particles, and the reduction of the amount of sample needed for the analysis[289,290].

EVs isolation procedures exploiting the negative charges of this structures were proven to reduce protein contaminants in comparison with ultracentrifugation[291–293]. Behind these approaches rely the premise that EVs display negative fluctuations of zeta potential (ZP), under physiological conditions (pH>5) and thus are able to bind to positively charged specimens, and further released by modulation the pH and the ionic strength in the elution buffer [294].

Thus, we developed a graphene-based magnetic isolation (GBMI) method to isolate EVs from serum samples. This method explores the positive-charge of polyethyleneimine (PEI), covering the surface of graphene-coated magnetic beads, to bind and capture heterogenous EVs population from limited amount of

serum. A graphical illustration of the procedure used for the optimization of the method with FBS samples is shown (Figure 39).

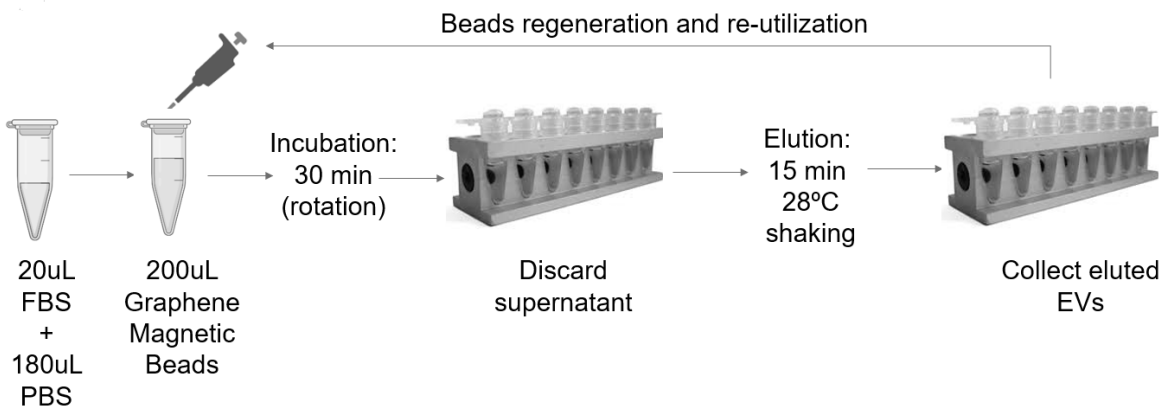

Figure 39 GBMI protocol. Schematic representation of GBMI protocol.

Shortly, 20µL of commercial FBS (Gibco) were aliquoted and diluted in 180 µL of PBS. An equal volume of graphene magnetic beads solution were added and the mix was incubated for 30 minutes on a circular rotating wheel. The samples were then placed in a magnetic rack to immobilize the graphene-beads bond to the FBS EVs, and the supernatant was discarded. Tubes were collected and incubated for 15 minutes at 28ºC with the elution solution on a shaking thermoblock. Ended the incubation time, samples were again placed on the magnetic rack and the EVs-enriched supernatant was collected and stored at 4ºC. The remaining magnetic beads are then washed with the regenerating solution and PBS and can be reused for further isolations.

To assure that GBMI was indeed able to grab a high number of EVs from the FBS samples, we measured EV number eluted with increasing concentrations of urea through Nanoparticle Tracking Analysis (NTA), using NanoSight. We confirmed that the number of eluted EVs was proportional to the urea concentration on the elution buffer in a range from 0 to 8M. Moreover, at the highest urea concentration used, the yield of recovered EVs is 92% of the EVs present on the 20 µL FBS input (Figure 40A).

Regardless the confirmation of the method ability on grabbing the EVs from FBS, elution buffers with high concentration of urea are not suitable for further EVs biological characterization or application. Thus, we proceed for the optimization of the EVs elution process.

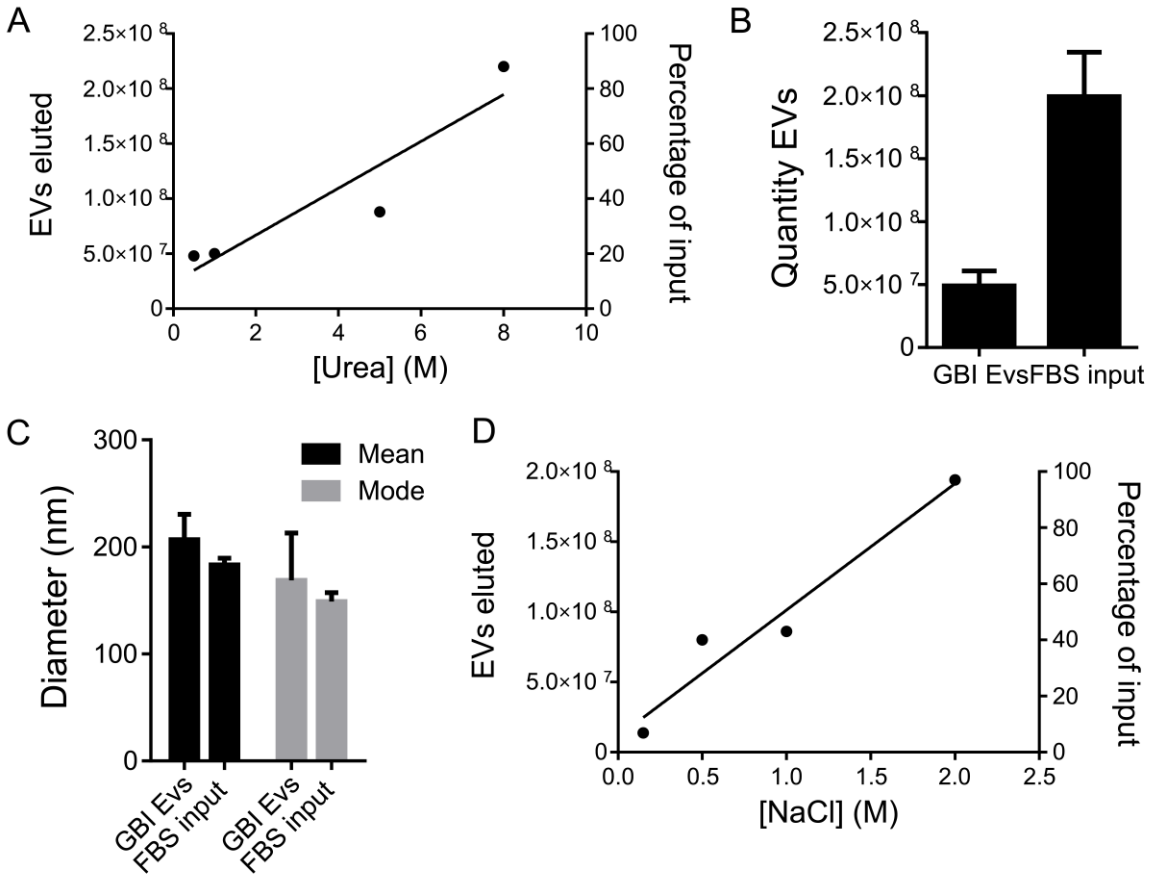

Figure 40 Quality control of GBMI protocol. FBS EVs were eluted with different elution buffer. (A) The number of EVs recovered is directly correlated with the concentration of urea used as elution buffer, and represent a percentage of the initial FBS input. (B) EVs quantity obtained from the elution with a containing chelating agents is lower than the number of EVs on the FBS input, even presenting the same mean and mode diameter (C). The usage of NaCl as elution buffer allow the recovery of high percentage of EVs (compared with the FBS input) and is directly proportional to the concentration of NaCl (D).

As a first approach, we used an elution buffer with chelating agents, as described in [293], but a low yield of EVs was recovered. NTA revealed that only around 25% of the EVs present in the FBS input were isolated (Figure 40B). Nonetheless, GBMI allowed the isolation of sample's representative and heterogenous EVs populations, as confirmed by the similar mean and mode diameter of the EVs presented in the elution solution and in the FBS input (Figure 40C).

We further optimized the elution solution by selecting a biological compatible salt, sodium chloride (NaCl), to compete with EVs for the binding with the functionalized magnetic beads, and promote it's elution. NaCl concentrations ranging from 0 to 2M enable EVs isolation and a full recovery (99%) of the FBS

sample EVs at 2M (Figure 40D). It is important to notice that physiologic sodium concentration is around 1,4 mM, meaning that the utilization of NaCl 2M may induce osmotic pressure and consequent disruption of the EVs, which may become challenge for further EVs applications[295].

Given the satisfactory preliminary data obtained for the development of the method, we are now assessing the presence of co-eluted contaminants, as well as the integrity of the EVs. Further validation of the method is expected to be performed in clinical samples, to evaluate its potential to isolate EVs from serum, as well as it’s usage for biomarker detection.

REFERENCES

1. Hanahan, D. & Weinberg, R. A. Leading Edge Review Hallmarks of Cancer: The Next Generation. (2011) doi:10.1016/j.cell.2011.02.013.

2. Hanahan, D. Hallmarks of Cancer: New Dimensions. *Cancer Discov.* **12**, 31–46 (2022).

3. Cantor, J. R. & Sabatini, D. M. Cancer cell metabolism: One hallmark, many faces. *Cancer Discov.* **2**, 881–898 (2012).

4. De Berardinis, R. J. & Chandel, N. S. Fundamentals of cancer metabolism. *Sci. Adv.* **2**, (2016).

5. Arfin, S. *et al.* Oxidative stress in cancer cell metabolism. *Antioxidants* **10**, 1–28 (2021).

6. Ju, H. Q., Lin, J. F., Tian, T., Xie, D. & Xu, R. H. NADPH homeostasis in cancer: functions, mechanisms and therapeutic implications. *Signal Transduct. Target. Ther.* **5**, 1–12 (2020).

7. Lu, J., Tan, M. & Cai, Q. The Warburg effect in tumor progression: Mitochondrial oxidative metabolism as an anti-metastasis mechanism. *Cancer Lett.* **356**, 156–164 (2015).

8. Vaupel, P., Schmidberger, H. & Mayer, A. The Warburg effect: essential part of metabolic reprogramming and central contributor to cancer progression. *Int. J. Radiat. Biol.* **95**, 912–919 (2019).

9. Pascale, R. M., Calvisi, D. F., Simile, M. M., Feo, C. F. & Feo, F. The warburg effect 97 years after its discovery. *Cancers (Basel).* **12**, 1–33 (2020).

10. Potter, M., Newport, E. & Morten, K. J. The Warburg effect: 80 years on. *Biochem. Soc. Trans.* **44**, 1499–1505 (2016).

11. Ward, P. S. & Thompson, C. B. Metabolic Reprogramming: A Cancer Hallmark Even Warburg Did Not Anticipate. *Cancer Cell* **21**, 297–308 (2012).

12. Koppenol, W. H., Bounds, P. L. & Dang, C. V. Otto Warburg's contributions to current concepts of cancer metabolism. *Nat. Rev. Cancer* **11**, 325–337 (2011).

13. Vaupel, P. & Multhoff, G. Revisiting the Warburg effect: historical dogma versus current understanding. *J. Physiol.* **599**, 1745–1757 (2021).

14. Courtnay, R. *et al.* Cancer metabolism and the Warburg effect: the role of HIF-1 and PI3K. *Mol. Biol. Rep.* **42**, 841–851 (2015).

15. Semenza, G. L. HIF-1: upstream and downstream of cancer metabolism. *Curr. Opin. Genet. Dev.* **20**, 51–56 (2010).

16. Hoxhaj, G. & Manning, B. D. The PI3K–AKT network at the interface of oncogenic signalling and cancer metabolism. *Nat. Rev. Cancer* **20**, 74–88 (2020).

17. Sano, H. *et al.* Insulin-stimulated phosphorylation of a Rab GTPase-activating protein regulates GLUT4 translocation. *J. Biol. Chem.* **278**, 14599–14602 (2003).

18. Filigheddu, N. *et al.* Cytokine Stimulation Promotes Glucose Uptake via Phosphatidylinositol-3 Kinase/Akt Regulation of Glut1 Activity and Traffickin. *Mol. Biol. Cell* **18**, 986–994 (2007).

19. Gottlob, K. *et al.* Inhibition of early apoptotic events by Akt/PKB is dependent on the first committed step of glycolysis and mitochondrial hexokinase. *Genes Dev.* **15**, 1406–1418 (2001).

20. Deprez, J., Vertommen, D., Alessi, D. R., Hue, L. & Rider, M. H. Phosphorylation and activation of heart 6-phosphofructo-2-kinase by protein kinase B and other protein kinases of the insulin signaling cascades. *J. Biol. Chem.* **272**, 17269–17275 (1997).

21. Laughner, E., Taghavi, P., Chiles, K., Mahon, P. C. & Semenza, G. L. HER2 (neu) Signaling Increases the Rate of Hypoxia-Inducible Factor 1 ⎵ (HIF-1 ⎵) Synthesis : Novel Mechanism for HIF-1-Mediated Vascular Endothelial Growth Factor Expression. **21**, 3995–4004 (2001).

22. Kim, J. & Dang, C. V. Cancer ' s Molecular Sweet Tooth and the Warburg Effect. 8927–8930 (2006) doi:10.1158/0008-5472.CAN-06-1501.

23. Anderson, N. M. & Simon, M. C. ll Magazine The tumor microenvironment ll. *Curr. Biol.* **30**, R921–R925 (2020).

24. Baghban, R., Roshangar, L., Jahanban-esfahlan, R., Seidi, K. & Ebrahimi-kalan, A. Tumor microenvironment complexity and therapeutic implications at a glance. **4**, 1–19 (2020).

25. Cruz-lópez, K. G. De & Castro-muñoz, L. J. Lactate in the Regulation of Tumor Microenvironment and Therapeutic Approaches. **9**, (2019).

26. Brown, T. P. & Ganapathy, V. Pharmacology & Therapeutics Lactate / GPR81 signaling and proton motive force in cancer : Role in angiogenesis , immune escape , nutrition , and Warburg phenomenon. *Pharmacol. Ther.* **206**, 107451 (2020).

27. Chen, Y. *et al.* mitochondria. **12**, (2016).

28. Senyilmaz, D. & Teleman, A. A. Chicken or the egg: Warburg effect and

mitochondrial dysfunction. *F1000Prime Rep.* **7**, 1–13 (2015).

29. Olson, K. A., Schell, J. C., Rutter, J., City, S. L. & City, S. L. Selective Cancer Therapies. *Trends Biochem Sci* **41**, 219–230 (2016).

30. Cairns, R. A., Harris, I. S. & Mak, T. W. Regulation of cancer cell metabolism. *Nat. Rev. Cancer* **11**, 85–95 (2011).

31. Christofk, H. R. *et al.* The M2 splice isoform of pyruvate kinase is important for cancer metabolism and tumour growth. *Nature* **452**, 230–233 (2008).

32. Kaplon, J. *et al.* A key role for mitochondrial gatekeeper pyruvate dehydrogenase in oncogene-induced senescence. *Nature* **498**, 109–112 (2013).

33. Hitosugi, T. *et al.* Tyrosine Phosphorylation of Mitochondrial Pyruvate Dehydrogenase Kinase 1 Is Important for Cancer Metabolism. *Mol. Cell* **44**, 864–877 (2011).

34. Scientific, E. & Company, P. INHIBITION OF M I T O C H O N D R I A L PYRUVATE T R A N S P O R T BY P H E N Y L P Y R U V A T E AND ~ -KETO1SOCAPROATE I . Pyruvate oxidation by coupled rat heart and brain mitochondria is inhibited by phenylpyruvate and c ¢ -ketoisocaproate but not by . **367**, 102–108 (1974).

35. Herzig, S. *et al.* Identification and functional expression of the mitochondrial pyruvate carrier. *Science (80-.).* **336**, 93–96 (2012).

36. Bowie, D. References and Notes. *Reform Revolt City Dreaming Spires* **337**, 277–313 (2019).

37. Gyimesi, G. & Hediger, M. A. Sequence features of mitochondrial transporter protein families. *Biomolecules* **10**, 1–19 (2020).

38. Tang, X. P. *et al.* Mitochondrial pyruvate carrier 1 functions as a tumor suppressor and predicts the prognosis of human renal cell carcinoma. *Lab. Investig.* **99**, 191–199 (2019).

39. Schell, J. C. *et al.* A role for the mitochondrial pyruvate carrier as a repressor of the warburg effect and colon cancer cell growth. *Mol. Cell* **56**, 400–413 (2014).

40. Vacanti, N. M. *et al.* Regulation of substrate utilization by the mitochondrial pyruvate carrier. *Mol. Cell* **56**, 425–435 (2014).

41. Yang, C. *et al.* Glutamine oxidation maintains the TCA cycle and cell survival during impaired mitochondrial pyruvate transport. *Mol. Cell* **56**, 414–424 (2014).

42. Wang, L. *et al.* MPC1, a key gene in cancer metabolism, is regulated by COUP-TFII in human prostate cancer. *Oncotarget* **7**, 14673–14683 (2016).

43. Xiao, B. *et al.* Downregulation of COUP-TFII inhibits glioblastoma growth via targeting MPC1. *Oncol. Lett.* **15**, 9697–9702 (2018).

44. Koh, E., Kim, Y. K., Shin, D. & Kim, K. S. MPC1 is essential for PGC-1α-induced mitochondrial respiration and biogenesis. *Biochem. J.* **475**, 1687–1699 (2018).

45. Park, S. *et al.* Inhibition of ERRα Prevents Mitochondrial Pyruvate Uptake Exposing NADPH-Generating Pathways as Targetable Vulnerabilities in Breast Cancer. *Cell Rep.* **27**, 3587-3601.e4 (2019).

46. Li, D. *et al.* PGC1α promotes cholangiocarcinoma metastasis by upregulating PDHA1 and MPC1 expression to reverse the Warburg effect. *Cell Death Dis.* **9**, (2018).

47. Liang, L., Li, Q., Huang, L., Li, D. & Li, X. Sirt3 binds to and deacetylates mitochondrial pyruvate carrier 1 to enhance its activity. *Biochem. Biophys. Res. Commun.* **468**, 807–812 (2015).

48. Vadvalkar, S. S. *et al.* Decreased mitochondrial pyruvate transport activity in the diabetic heart: Role of Mitochondrial Pyruvate Carrier 2 (MPC2) acetylation. *J. Biol. Chem.* **292**, 4423–4433 (2017).

49. Halestrap, A. P. & Denton, R. M. Specific inhibition of pyruvate transport in rat liver mitochondria and human erythrocytes by α cyano 4 hydroxycinnamate. *Biochem. J.* **138**, 313–316 (1974).

50. Halestrap, A. P. The mechanism of the inhibition of the mitochondrial pyruvate transporter by α cyanocinnamate derivatives. *Biochem. J.* **156**, 181–183 (1976).

51. Hildyard, J. C. W., Ämmälä, C., Dukes, I. D., Thomson, S. A. & Halestrap, A. P. Identification and characterisation of a new class of highly specific and potent inhibitors of the mitochondrial pyruvate carrier. *Biochim. Biophys. Acta - Bioenerg.* **1707**, 221–230 (2005).

52. Divakaruni, A. S. *et al.* Thiazolidinediones are acute, specific inhibitors of the mitochondrial pyruvate carrier. *Proc. Natl. Acad. Sci. U. S. A.* **110**, 5422–5427 (2013).

53. Corbet, C. *et al.* Interruption of lactate uptake by inhibiting mitochondrial pyruvate transport unravels direct antitumor and radiosensitizing effects. *Nat. Commun.* **9**, 1–11 (2018).

54. Tompkins, S. C. *et al.* Disrupting Mitochondrial Pyruvate Uptake Directs Glutamine into the TCA Cycle away from Glutathione Synthesis and Impairs Hepatocellular Tumorigenesis. *Cell Rep.* **28**, 2608-2619.e6 (2019).

55. Tai, Y. Y. *et al.* Enhanced mitochondrial pyruvate transport elicits a robust ROS production to sensitize the antitumor efficacy of interferon-γ in colon cancer. *Redox Biol.* **20**, 451–457 (2019).

56. Ward, P. S. *et al.* Article The Common Feature of Leukemia-Associated IDH1 and IDH2 Mutations Is a Neomorphic Enzyme Activity Converting a -Ketoglutarate to 2-Hydroxyglutarate. *Cancer Cell* **17**, 225–234 (2010).

57. Dang, L. *et al.* Cancer-associated IDH1 mutations produce 2-hydroxyglutarate. *Nature* **462**, (2009).

58. Tseng, P., Wu, W., Hu, T., Chen, C. & Cheng, H. Decreased succinate dehydrogenase B in human hepatocellular carcinoma accelerates tumor malignancy by inducing the Warburg effect. *Sci. Rep.* 1–16 (2018) doi:10.1038/s41598-018-21361-6.

59. Linehan, W. M. & Rouault, T. A. Molecular Pathways : Fumarate Hydratase -De fi cient Kidney Cancer — Targeting the Warburg Effect in Cancer. 3345–3352 (2013) doi:10.1158/1078-0432.CCR-13-0304.

60. Lebleu, V. S. *et al.* PGC-1 α mediates mitochondrial biogenesis and oxidative phosphorylation in cancer cells to promote metastasis. **16**, (2014).

61. Maiuri, M. C. & Kroemer, G. Previews Essential Role for Oxidative Phosphorylation in Cancer Progression. *Cell Metab.* **21**, 11–12 (2015).

62. Yu, L. *et al.* Modeling the genetic regulation of cancer metabolism: Interplay between glycolysis and oxidative phosphorylation. *Cancer Res.* **77**, 1564–1574 (2017).

63. Kruspig, B., Zhivotovsky, B. & Gogvadze, V. Mitochondrion Mitochondrial substrates in cancer : Drivers or passengers ? *MITOCH* **19**, 8–19 (2014).

64. Ahn, C. S. & Metallo, C. M. Mitochondria as biosynthetic factories for cancer proliferation. 1–10 (2015) doi:10.1186/s40170-015-0128-2.

65. Porporato, P. E., Filigheddu, N., Pedro, J. M. B. & Kroemer, G. Mitochondrial metabolism and cancer. *Nat. Publ. Gr.* **28**, 265–280 (2017).

66. Yang, L. *et al.* Metabolic shifts toward glutamine regulate tumor growth , invasion and bioenergetics in ovarian cancer. 1–23 (2014).

67. Fan, J. *et al.* Glutamine-driven oxidative phosphorylation is a major ATP source in transformed mammalian cells in both normoxia and hypoxia. *Mol. Syst. Biol.* **9**, 1–11 (2013).

68. Camarda, R. *et al.* Inhibition of fatty acid oxidation as a therapy for MYC-overexpressing triple-negative breast cancer. *Nat. Med.* **22**, (2016).

69. Chan, D. C. Mitochondria: Dynamic Organelles in Disease, Aging, and Development. *Cell* **125**, 1241–1252 (2006).

70. Diering, Maxson & Mitchell & Freeman. Mitochondria and cancer. *Physiol. Behav.* **176**, 139–148 (2018).

71. Nemoto, K. & Sato, K. I. A 2.5PPM fully integrated CMOS analog TCXO. *Proc. Annu. IEEE Int. Freq. Control Symp.* **98**, 740–743 (2001).

72. Schreiber, S. N. *et al.* The estrogen-related receptor α (ERRα) functions in PPARγ coactivator 1α (PGC-1α)-induced mitochondrial biogenesis. *Proc. Natl. Acad. Sci. U. S. A.* **101**, 6472–6477 (2004).

73. Daly, M. J. *et al.* PGC-1α-responsive genes involved in oxidative phosphorylation are coordinately downregulated in human diabetes. *Nat. Genet.* **34**, 267–273 (2003).

74. Vega, R. B., Huss, J. M. & Kelly, D. P. The Coactivator PGC-1 Cooperates with Peroxisome Proliferator-Activated Receptor α in Transcriptional Control of Nuclear Genes Encoding Mitochondrial Fatty Acid Oxidation Enzymes. *Mol. Cell. Biol.* **20**, 1868–1876 (2000).

75. Tan, Z. *et al.* The role of PGC1α in cancer metabolism and its therapeutic implications. *Mol. Cancer Ther.* **15**, 774–782 (2016).

76. Zhang, Y. *et al.* PGC-1α induces apoptosis in human epithelial ovarian cancer cells through a PPARγ-dependent pathway. *Cell Res.* **17**, 363–373 (2007).

77. D'Errico, I. *et al.* Bax is necessary for PGC1α pro-apoptotic effect in colorectal cancer cells. *Cell Cycle* **10**, 2937–2945 (2011).

78. LaGory, E. L. *et al.* Suppression of PGC-1α Is Critical for Reprogramming Oxidative Metabolism in Renal Cell Carcinoma. *Cell Rep.* **12**, 116–127 (2015).

79. Jiang, W. G., Douglas-Jones, A. & Mansel, R. E. Expression of peroxisome-proliferator activated receptor-gamma (PPARγ) and the PPARγ co-activator, PGC-1, in human breast cancer correlates with clinical outcomes. *Int. J. Cancer* **106**, 752–757 (2003).

80. Oliveira, G. L., Coelho, A. R., Marques, R. & Oliveira, P. J. Cancer cell metabolism: Rewiring the mitochondrial hub. *Biochim. Biophys. Acta - Mol. Basis Dis.* **1867**, 166016 (2021).

81. Li, F. *et al.* Myc Stimulates Nuclearly Encoded Mitochondrial Genes and Mitochondrial Biogenesis. *Mol. Cell. Biol.* **25**, 6225–6234 (2005).

82. Mancias, J. D. & Kimmelman, A. C. Mechanisms of Selective Autophagy in Normal Physiology and Cancer. *J. Mol. Biol.* **428**, 1659–1680 (2016).

83. Boulton, D. P. & Caino, M. C. Mitochondrial Fission and Fusion in Tumor Progression to Metastasis. *Front. Cell Dev. Biol.* **10**, 1–19 (2022).

84. Gomes, L. C., Benedetto, G. Di & Scorrano, L. During autophagy mitochondria elongate, are spared from degradation and sustain cell viability. *Nat. Cell Biol.* **13**, 589–598 (2011).

85. Osteryoung, K. W. & Nunnari, J. The Division of Endosymbiotic Organelles. *Science (80-.).* **302**, 1698–1704 (2003).

86. Rambold, A. S., Kostelecky, B., Elia, N. & Lippincott-Schwartz, J. Tubular network formation protects mitochondria from autophagosomal degradation during nutrient starvation. *Proc. Natl. Acad. Sci. U. S. A.* **108**, 10190–10195 (2011).

87. Nikiforov, A., Kulikova, V. & Ziegler, M. The human NAD metabolome : Functions , metabolism and compartmentalization. **9238**, 284–297 (2015).

88. Chiarugi, A., Dölle, C., Felici, R. & Ziegler, M. The NAD metabolome — a key determinant of cancer cell biology. *Nat. Publ. Gr.* **12**, (2012).

89. Chen, S. & Yu, X. Human DNA ligase IV is able to use NAD + as an alternative adenylation donor for DNA ends ligation. **47**, 1321–1334 (2019).

90. Bird, J. G. *et al.* The mechanism of RNA 5′ capping with NAD+, NADH and desphospho-CoA. *Nature* **535**, 444–447 (2016).

91. Pollak, N. & Olle, C. D. The power to reduce : pyridine nucleotides – small molecules with a. **218**, 205–218 (2007).

92. Hopp, A. & Hottiger, M. O. Regulation of Glucose Metabolism by NAD + and ADP-Ribosylation 1 2. 1–23 (2019).

93. Morrison, M. J. & Weerapana, E. cysteine-reactive chemical probes †. 972–982 (2022) doi:10.1039/d2cb00091a.

94. Macdonald, M. J. & Donald, M. J. M. A. C. Evidence for the Malate Aspartate Shuttle in Pancreatic Islets Glucose is the most potent physiological insulin secretagogue for the pancreatic p cell and is believed to stimulate sustained of , for example , only its interaction with p cell . Some of the. **213**, 643–649 (1982).

95. Macdonalds, M. J. Dehydrogenase in Pancreatic Islets and Its Inhibition by. **2**,.

96. Luongo, T. S. *et al.* SLC25A51 is a mammalian mitochondrial NAD + transporter. *Nature* **588**, (2020).

97. Manuscript, A. NIH Public Access. **324**, 1029–1033 (2010).

98. Zhao, Q., Lan, T., Su, S. & Rao, Y. Induction of apoptosis in MDA-MB-231 breast cancer cells by a PARP1-targeting PROTAC small molecule. *Chem. Commun.* **55**, 369–372 (2019).

99. Hu, Y. *et al.* PARP1-driven poly-ADP-ribosylation regulates BRCA1 function in homologous recombination–mediated DNA repair. *Cancer Discov.* **4**, 1430–1447 (2014).

100. Bian, C. *et al.* NADP + is an endogenous PARP inhibitor in DNA damage response and tumor suppression. *Nat. Commun.* **10**, 1–14 (2019).

101. Singh, N. Enhanced poly ADP-ribosylation in human leukemia lymphocytes and ovarian cancers. *Cancer Lett.* **58**, 131–135 (1991).

102. Yalcintepe, L. *et al.* Changes in NAD/ADP-ribose metabolism in rectal cancer. *Brazilian J. Med. Biol. Res.* **38**, 361–365 (2005).

103. Carafa, V., Altucci, L. & Nebbioso, A. Dual tumor suppressor and tumor promoter action of sirtuins in determining malignant phenotype. *Front. Pharmacol.* **9**, 1–14 (2019).

104. Wang, B. *et al.* NAMPT overexpression in prostate cancer and its contribution to tumor cell survival and stress response. *Oncogene* **30**, 907–921 (2011).

105. Dobbin, M. M. *et al.* SIRT1 collaborates with ATM and HDAC1 to maintain genomic stability in neurons. *Nat. Neurosci.* **16**, 1008–1015 (2013).

106. Mottahedeh, J. *et al.* CD38 is methylated in prostate cancer and regulates extracellular NAD+. *Cancer Metab.* **6**, 1–17 (2018).

107. Kanayama, M. & Luo, J. CD38-Induced Apoptosis and Mitochondrial Damage is Restored by Nicotinamide in Prostate Cancer. *Front. Mol. Biosci.* **9**, 1–10 (2022).

108. Chowdhry, S. *et al.* NAD metabolic dependency in cancer is shaped by gene amplification and enhancer remodelling. *Nature* **569**, 570–575 (2019).

109. Human, T. H. E. Short communications. **20**, 2903–2906 (1971).

110. Gaut, Z. N. & Solomon, H. M. Inhibition of Nicotinate Phosphoribosyl Transferase by Nonsteroidal Anti-Inflammatory Drugs : A Possible Mechanism of Action. **60**, 1887–1888 (1971).

111. Ghanem, M. S. *et al.* Identification of NAPRT Inhibitors with Anti-Cancer Properties by In Silico Drug Discovery. (2022).

112. Galli, U. *et al.* Recent Advances in NAMPT Inhibitors : A Novel Immunotherapic Strategy. **11**, 1–20 (2020).

113. Preiss, J. & Handler, P. ENZYMATIC SYNTHESIS OF NICOTINAMIDE MONONUCLEOTIDE. *J. Biol. Chem.* **225**, 759–770.

114. Revollo, J. R. *et al.* Nampt/PBEF/Visfatin Regulates Insulin Secretion in β Cells as a Systemic NAD Biosynthetic Enzyme. *Cell Metab.* **6**, 363–375 (2007).

115. Sethi, C. J. K., Genazzani, A. A. & Piemonte, U. Extracellular nicotinamide phosphoribosyltransferase , a new cancer metabokine Tables of Links.

(2016) doi:10.1111/bph.13505.

116. Samal, B., Sun, Y., Stearns, G., Suggs, S. & Mcniece, I. A. N. Cloning and Characterization of the cDNA Encoding a Novel Human Pre-B-Cell Colony-Enhancing Factor. **14**, 1431–1437 (1994).

117. Audrito, V. *et al.* Extracellular nicotinamide phosphoribosyltransferase (eNAMPT) is a novel marker for patients with BRAF-mutated metastatic melanoma. *Oncotarget* (2018) doi:10.18632/oncotarget.24871.

118. Soncini, D. *et al.* Nicotinamide phosphoribosyltransferase promotes epithelial-to-mesenchymal transition as a soluble factor independent of its enzymatic activity. *J. Biol. Chem.* **289**, 34189–34204 (2014).

119. Audrito, V. *et al.* Extracellular nicotinamide phosphoribosyltransferase (NAMPT) promotes M2 macrophage polarization in chronic lymphocytic leukemia. *Blood* **125**, 111–123 (2015).

120. Tian, W. *et al.* Visfatin, a potential biomarker and prognostic factor for endometrial cancer. *Gynecol. Oncol.* **129**, 505–512 (2013).

121. Reddy, P. S. *et al.* PBEF1/NAmPRTase/Visfatin: A potential malignant astrocytoma/glioblastoma serum marker with prognostic value. *Cancer Biol. Ther.* **7**, 663–668 (2008).

122. Garten, A. *et al.* Physiological and pathophysiological roles of NAMPT and NAD metabolism. *Nat. Rev. Endocrinol.* **11**, 535–546 (2015).

123. Audrito, V., Messana, V. G. & Deaglio, S. NAMPT and NAPRT: Two Metabolic Enzymes With Key Roles in Inflammation. *Front. Oncol.* **10**, 1–17 (2020).

124. Ramsey, K. M. *et al.* Circadian clock feedback cycle through NAMPT-Mediated NAD+ biosynthesis. *Science (80-.).* **324**, 651–654 (2009).

125. Kim, S. R. *et al.* Visfatin promotes angiogenesis by activation of extracellular signal-regulated kinase 1/2. *Biochem. Biophys. Res. Commun.* **357**, 150–156 (2007).

126. Lucena-Cacace, A., Otero-Albiol, D., Jiménez-García, M. P., Peinado-Serrano, J. & Carnero, A. NAMPT overexpression induces cancer stemness and defines a novel tumor signature for glioma prognosis. *Oncotarget* **8**, 99514–99530 (2017).

127. Zhou, S. J., Bi, T. Q., Qin, C. X., Yang, X. Q. & Pang, K. Expression of NAMPT is associated with breast invasive ductal carcinoma development and prognosis. *Oncol. Lett.* **15**, 6648–6654 (2018).

128. Hasmann, M. & Schemainda, I. FK866, a Highly Specific Noncompetitive Inhibitor of Nicotinamide Phosphoribosyltransferase, Represents a Novel Mechanism for Induction of Tumor Cell Apoptosis. *Cancer Res.* **63**, 7436–

7442 (2003).

129. Kim, M. K. *et al.* Crystal Structure of Visfatin/Pre-B Cell Colony-enhancing Factor 1/Nicotinamide Phosphoribosyltransferase, Free and in Complex with the Anti-cancer Agent FK-866. *J. Mol. Biol.* **362**, 66–77 (2006).

130. Olesen, U. H. *et al.* Target enzyme mutations are the molecular basis for resistance towards pharmacological inhibition of nicotinamide phosphoribosyltransferase. *BMC Cancer* **10**, 1–13 (2010).

131. Lee, J. *et al.* Selective Cytotoxicity of the NAMPT Inhibitor FK866 Toward Gastric Cancer Cells With Markers of the Epithelial-Mesenchymal Transition, Due to Loss of NAPRT. *Gastroenterology* **155**, 799-814.e13 (2018).

132. Sauer, H., Kampmann, H., Khosravi, F., Sharifpanah, F. & Wartenberg, M. The nicotinamide phosphoribosyltransferase antagonist FK866 inhibits growth of prostate tumour spheroids and increases doxorubicin retention without changes in drug transporter and cancer stem cell protein expression. *Clin. Exp. Pharmacol. Physiol.* **48**, 422–434 (2021).

133. Thongon, N. *et al.* Cancer cell metabolic plasticity allows resistance to NAMPT inhibition but invariably induces dependence on LDHA. *Cancer Metab.* (2018) doi:10.1186/s40170-018-0174-7.

134. Liberti, M. V *et al.* Article A Predictive Model for Selective Targeting of the Warburg Effect through GAPDH Inhibition with a Article A Predictive Model for Selective Targeting of the Warburg Effect through GAPDH Inhibition with a Natural Product. *Cell Metab.* **26**, 648-659.e8 (2017).

135. Tan, B. *et al.* Pharmacological inhibition of nicotinamide phosphoribosyltransferase (NAMPT), an enzyme essential for NAD+ biosynthesis, in human cancer cells: Metabolic basis and potential clinical implications. *J. Biol. Chem.* **288**, 3500–3511 (2013).

136. Gehrke, I. *et al.* On-target effect of FK866, a nicotinamide phosphoribosyl transferase inhibitor, by apoptosis-mediated death in chronic lymphocytic leukemia cells. *Clin. Cancer Res.* **20**, 4861–4872 (2014).

137. Cloux, A. J. *et al.* Reactive oxygen/nitrogen species contribute substantially to the antileukemia effect of APO866, a NAD lowering agent. *Oncotarget* **10**, 6723–6738 (2019).

138. Moore, Z. *et al.* NAMPT inhibition sensitizes pancreatic adenocarcinoma cells to tumor-selective, PAR-independent metabolic catastrophe and cell death induced by β-lapachone. *Cell Death Dis.* **6**, 1–10 (2015).

139. Cea, M. *et al.* Targeting NAD+ salvage pathway induces autophagy in multiple myeloma cells via mTORC1 and extracellular signal-regulated kinase (ERK1/2) inhibition. *Blood* **120**, 3519–3529 (2012).

140. Travelli, C. *et al.* Reciprocal potentiation of the antitumoral activities of FK866, an inhibitor of nicotinamide phosphoribosyltransferase, and etoposide or cisplatin in neuroblastoma cells. *J. Pharmacol. Exp. Ther.* **338**, 829–840 (2011).

141. Billington, R. A., Genazzani, A. A., Travelli, C. & Condorelli, F. NAD depletion by FK866 induces autophagy. *Autophagy* **4**, 385–387 (2008).

142. Kozako, T. *et al.* High expression of NAMPT in adult T-cell leukemia/lymphoma and anti-tumor activity of a NAMPT inhibitor. *Eur. J. Pharmacol.* **865**, 172738 (2019).

143. Daniels, V. W. *et al.* Metabolic perturbations sensitize triple-negative breast cancers to apoptosis induced by BH3 mimetics. *Sci. Signal.* **14**, (2021).

144. Holen, K., Saltz, L. B., Hollywood, E., Burk, K. & Hanauske, A. R. The pharmacokinetics, toxicities, and biologic effects of FK866, a nicotinamide adenine dinucleotide biosynthesis inhibitor. *Invest. New Drugs* **26**, 45–51 (2008).

145. Goldinger, S. M. *et al.* Efficacy and safety of apo866 in patients with refractory or relapsed Cutaneous t-cell lymphoma: A phase 2 clinical trial. *JAMA Dermatology* **152**, 837–839 (2016).

146. Von Heideman, A., Berglund, Å., Larsson, R., Nygren, P. & Larsson, R. Safety and efficacy of NAD depleting cancer drugs: Results of a phase i clinical trial of CHS 828 and overview of published data. *Cancer Chemother. Pharmacol.* **65**, 1165–1172 (2010).

147. Parisotto, M. *et al.* The NAMPT Inhibitor FK866 Increases Metformin Sensitivity in Pancreatic Cancer Cells. (2022).

148. Dong, G. *et al.* Small Molecule Inhibitors Simultaneously Targeting Cancer Metabolism and Epigenetics: Discovery of Novel Nicotinamide Phosphoribosyltransferase (NAMPT) and Histone Deacetylase (HDAC) Dual Inhibitors. *J. Med. Chem.* **60**, 7965–7983 (2017).

149. Zoppoli, G. *et al.* Potent synergistic interaction between the Nampt inhibitor APO866 and the apoptosis activator TRAIL in human leukemia cells. *Exp. Hematol.* **38**, 979–988 (2010).

150. Neumann, C. S. *et al.* Targeted delivery of cytotoxic NAMPT inhibitors using antibody–drug conjugates. *Mol. Cancer Ther.* **17**, 2633–2642 (2018).

151. Korotchkina, L. *et al.* OT-82, a novel anticancer drug candidate that targets the strong dependence of hematological malignancies on NAD biosynthesis. *Leukemia* **34**, 1828–1839 (2020).

152. Oita, R. C. *et al.* Novel mechanism for nicotinamide phosphoribosyltransferase inhibition of TNF-α-mediated apoptosis in human lung endothelial cells. *Am. J. Respir. Cell Mol. Biol.* **59**, 36–44 (2018).

153. Liu, C., Jin, Y. & Fan, Z. The Mechanism of Warburg Effect-Induced Chemoresistance in Cancer. *Front. Oncol.* **11**, 1–16 (2021).

154. Alfarouk, K. O. *et al.* Resistance to cancer chemotherapy: Failure in drug response from ADME to P-gp. *Cancer Cell Int.* **15**, 1–13 (2015).

155. Wu, Q., Yang, Z., Nie, Y., Shi, Y. & Fan, D. Multi-drug resistance in cancer chemotherapeutics: Mechanisms and lab approaches. *Cancer Lett.* **347**, 159–166 (2014).

156. Vadlapatla, R., Vadlapudi, A., Pal, D. & Mitra, A. Mechanisms of Drug Resistance in Cancer Chemotherapy: Coordinated Role and Regulation of Efflux Transporters and Metabolizing Enzymes. *Curr. Pharm. Des.* **19**, 7126–7140 (2013).

157. Jacob B. Williams, C. M. B. and W. G. P. Codelivery of Doxorubicin and Verapamil for Treating Multidrug Resistant Cancer Cells. *Pharm. Nanotechnol.* **6**, 116.123 (2018).

158. Qadir, M. *et al.* Cyclosporin A is a broad-spectrum multidrug resistance modulator. *Clin. Cancer Res.* **11**, 2320–2326 (2005).

159. Helleday, T., Petermann, E., Lundin, C., Hodgson, B. & Sharma, R. A. DNA repair pathways as targets for cancer therapy. *Nat. Rev. Cancer* **8**, 193–204 (2008).

160. Wang, X., Zhang, H. & Chen, X. Drug resistance and combating drug resistance in cancer. *Cancer Drug Resist.* **2**, 141–160 (2019).

161. Wang, W. *et al.* Structural basis for resistance to diverse classes of NAMPT inhibitors. *PLoS One* **9**, (2014).

162. Ogino, Y., Sato, A., Uchiumi, F. & Tanuma, S. I. Cross resistance to diverse anticancer nicotinamide phosphoribosyltransferase inhibitors induced by FK866 treatment. *Oncotarget* **9**, 16451–16461 (2018).

163. Ogino, Y. *et al.* Association of ABC transporter with resistance to FK866, a NAMPT inhibitor, in human colorectal cancer cells. *Anticancer Res.* **39**, 6457–6462 (2019).

164. Guo, J. *et al.* Identification of novel resistance mechanisms to NAMPT inhibition via the de novo NAD+ biosynthesis pathway and NAMPT mutation. *Biochem. Biophys. Res. Commun.* **491**, 681–686 (2017).

165. Snigdha, K., Gangwani, K. S., Lapalikar, G. V., Singh, A. & Kango-Singh, M. Hippo signaling in cancer: Lessons from Drosophila models. *Front. Cell Dev. Biol.* **7**, 1–16 (2019).

166. Kango-Singh, M. & Singh, A. Regulation of organ size: Insights from the drosophila hippo signaling pathway. *Dev. Dyn.* **238**, 1627–1637 (2009).

167. Justice, R. W., Zilian, O., Woods, D. F., Noll, M. & Bryant, P. J. The Drosophila tumor suppressor gene warts encodes a homolog of human myotonic dystrophy kinase and is required for the control of cell shape and proliferation. *Genes Dev.* **9**, 534–546 (1995).

168. Tian Xu, Weiyi Wang, Sheng Zhang, Rodney A. Stewart & Wan Yu. Identifying tumor suppressors in genetic mosaics: the Drosophila lats gene encodes a putative protein kinase. *Development* **121**, 1053–1063 (1995).

169. Edgar, B. A. From cell structure to transcription: Hippo Forges a new path. *Cell* **124**, 267–273 (2006).

170. Huang, J., Wu, S., Barrera, J., Matthews, K. & Pan, D. The Hippo signaling pathway coordinately regulates cell proliferation and apoptosis by inactivating Yorkie, the Drosophila homolog of YAP. *Cell* **122**, 421–434 (2005).

171. Sudol, M. Yes-associated protein (YAP65) is a proline-rich phosphoprotein that binds to the SH3 domain of the Yes proto-oncogene product. *Oncogene* **9**, 2145–2152 (1994).

172. Moroishi, T., Hansen, C. G. & Guan, K. L. The emerging roles of YAP and TAZ in cancer. *Nat. Rev. Cancer* **15**, 73–79 (2015).

173. Chen, L. *et al.* Structural basis of YAP recognition by TEAD4 in the Hippo pathway. *Genes Dev.* **24**, 290–300 (2010).

174. Lehmann, W. *et al.* ZEB1 turns into a transcriptional activator by interacting with YAP1 in aggressive cancer types. *Nat. Commun.* **7**, (2016).

175. Downward, J. & Basu, S. YAP and p73: A Complex Affair. *Mol. Cell* **32**, 749–750 (2008).

176. Li, Z. *et al.* Structural insights into the YAP and TEAD complex. *Genes Dev.* **24**, 235–240 (2010).

177. Cheng, Y., Mao, M. & Lu, Y. The biology of YAP in programmed cell death. *Biomark. Res.* **10**, 1–10 (2022).

178. Zhao, B. *et al.* Inactivation of YAP oncoprotein by the Hippo pathway is involved in cell contact inhibition and tissue growth control. *Genes Dev.* **21**, 2747–2761 (2007).

179. Oka, T., Mazack, V. & Sudol, M. Mst2 and Lats kinases regulate apoptotic function of Yes kinase-associated protein (YAP). *J. Biol. Chem.* **283**, 27534–27546 (2008).

180. Johnson, R. & Halder, G. The two faces of Hippo: Targeting the Hippo pathway for regenerative medicine and cancer treatment. *Nat. Rev. Drug Discov.* **13**, 63–79 (2014).

181. Oren, M. & Aylon, Y. The hippo signaling pathway and cancer. *Hippo Signal. Pathw. Cancer* **15**, 1–354 (2014).

182. Koo, J. H. & Guan, K. L. Interplay between YAP/TAZ and Metabolism. *Cell Metab.* **28**, 196–206 (2018).

183. Overholtzer, M. *et al.* Transforming properties of YAP, a candidate oncogene on the chromosome 11q22 amplicon. *Proc. Natl. Acad. Sci. U. S. A.* **103**, 12405–12410 (2006).

184. St John, M. A. R. *et al.* Mice deficient of Lats1 develop soft-tissue sarcomas, ovarian tumours and pituitary dysfunction. *Nat. Genet.* **21**, 182–186 (1999).

185. Lu, L. *et al.* Hippo signaling is a potent in vivo growth and tumor suppressor pathway in the mammalian liver. *Proc. Natl. Acad. Sci. U. S. A.* **107**, 1437–1442 (2010).

186. Pei, T. *et al.* YAP is a critical oncogene in human cholangiocarcinoma. *Oncotarget* **6**, 17206–17220 (2015).

187. Hiemer, S. E. *et al.* A YAP/TAZ-regulated molecular signature is associated with Oral squamous cell carcinoma. *Mol. Cancer Res.* **13**, 957–968 (2015).

188. Zhang, W. *et al.* YAP promotes malignant progression of Lkb1-deficient lung adenocarcinoma through downstream regulation of survivin. *Cancer Res.* **75**, 4450–4457 (2015).

189. Mizuno, T. *et al.* YAP induces malignant mesothelioma cell proliferation by upregulating transcription of cell cycle-promoting genes. *Oncogene* **31**, 5117–5122 (2012).

190. Lin, L. *et al.* The Hippo effector YAP promotes resistance to RAF- and MEK-targeted cancer therapies. *Nat. Genet.* **47**, 250–256 (2015).

191. Azzolin, L. *et al.* YAP/TAZ incorporation in the β-catenin destruction complex orchestrates the Wnt response. *Cell* **158**, 157–170 (2014).

192. Imajo, M., Miyatake, K., Iimura, A., Miyamoto, A. & Nishida, E. A molecular mechanism that links Hippo signalling to the inhibition of Wnt/β-catenin signalling. *EMBO J.* **31**, 1109–1122 (2012).

193. Tomlinson, V. *et al.* JNK phosphorylates Yes-associated protein (YAP) to regulate apoptosis. *Cell Death Dis.* **1**, e29-9 (2010).

194. Basu, S., Totty, N. F., Irwin, M. S., Sudol, M. & Downward, J. Akt Phosphorylates the Yes-Associated Protein, YAP, to Induce Interaction with 14-3-3 and Attenuation of p73-Mediated Apoptosis some of the metabolic effects of Akt, whereas BAD can account for some of the survival-promoting effects. The most convincingly. *Mol. Cell* **11**, 11–23 (2003).

195. Matallanas, D. *et al.* RASSF1A Elicits Apoptosis through an MST2 Pathway

Directing Proapoptotic Transcription by the p73 Tumor Suppressor Protein. *Mol. Cell* **27**, 962–975 (2007).

196. Cottini, F. *et al.* Rescue of Hippo coactivator YAP1 triggers DNA damage-induced apoptosis in hematological cancers. *Nat. Med.* **20**, 599–606 (2014).

197. Huang, H. *et al.* YAP suppresses lung squamous cell carcinoma progression via deregulation of the DNP63-GPX2 axis and ros accumulation. *Cancer Res.* **77**, 5769–5781 (2017).

198. Ming Zhu, Ruiqing Peng, Xin Liang, Zhengdao Lan, Ming Tang, Pingping Hou, Jian H. Song, Celia Sze Ling Mak, Jiwon Park, Shui-er Zheng, Ailing Huang, Xingdi Ma, Ruidong Chen, Qing Chang, Christopher J. Logothetis, Abhinav K. Jain, Sue-Hwa Lin, Hiroyuki Kat, S. H. & G. W. P4HA2-induced prolyl hydroxylation suppresses YAP1-mediated prostate cancer cell migration, invasion, and metastasis. *Oncogene* **40**, 6049–56 (2021).

199. White, S. M. *et al.* YAP/TAZ Inhibition Induces Metabolic and Signaling Rewiring Resulting in Targetable Vulnerabilities in NF2-Deficient Tumor Cells. *Dev. Cell* **49**, 425-443.e9 (2019).

200. Mo, J. S. *et al.* Cellular energy stress induces AMPK-mediated regulation of YAP and the Hippo pathway. *Nat. Cell Biol.* **17**, 500–510 (2015).

201. Wang, W. *et al.* AMPK modulates Hippo pathway activity to regulate energy homeostasis. *Nat. Cell Biol.* **17**, 490–499 (2015).

202. deRan, M. *et al.* Energy stress regulates Hippo-YAP signaling involving AMPK-mediated regulation of angiomotin-like 1 protein. *Cell Rep.* **9**, 495–503 (2014).

203. Butkinaree, C., Park, K. & Hart, G. W. O-linked β-N-acetylglucosamine (O-GlcNAc): Extensive crosstalk with phosphorylation to regulate signaling and transcription in response to nutrients and stress. *Biochim. Biophys. Acta - Gen. Subj.* **1800**, 96–106 (2010).

204. Hanover, J. A., Krause, M. W. & Love, D. C. Bittersweet memories: Linking metabolism to epigenetics through O-GlcNAcylation. *Nat. Rev. Mol. Cell Biol.* **13**, 312–321 (2012).

205. Lee, C. kun *et al.* Tumor metastasis to lymph nodes requires YAP-dependent metabolic adaptation. *Science (80-.).* **363**, 644–649 (2019).

206. Shu, Z. *et al.* A functional interaction between Hippo-YAP signalling and SREBPs mediates hepatic steatosis in diabetic mice. *J. Cell. Mol. Med.* **23**, 3616–3628 (2019).

207. Yuan, L. *et al.* Palmitic acid dysregulates the Hippo-YAP pathway and inhibits angiogenesis by inducing mitochondrial damage and activating the cytosolic DNA sensor cGAS-STING-IRF3 signaling mechanism. *J. Biol. Chem.* **292**, 15002–15015 (2017).

208. Chan, P. *et al.* Autopalmitoylation of TEAD proteins regulates transcriptional output of the Hippo pathway. *Nat. Chem. Biol.* **12**, 282–289 (2016).

209. Yang, C. *et al.* Glutamine-utilizing transaminases are a metabolic vulnerability of TAZ/YAP-activated cancer cells. *EMBO Rep.* **19**, (2018).

210. Puspitarini. 済無No Title No Title No Title. *Angew. Chemie Int. Ed. 6(11), 951–952.* **2**, 65–70 (1967).

211. Hansen, C. G., Ng, Y. L. D., Lam, W. L. M., Plouffe, S. W. & Guan, K. L. The Hippo pathway effectors YAP and TAZ promote cell growth by modulating amino acid signaling to mTORC1. *Cell Res.* **25**, 1299–1313 (2015).

212. Nagaraj, R. *et al.* Control of mitochondrial structure and function by the Yorkie/YAP oncogenic pathway. *Genes Dev.* **26**, 2027–2037 (2012).

213. von Eyss, B. *et al.* A MYC-Driven Change in Mitochondrial Dynamics Limits YAP/TAZ Function in Mammary Epithelial Cells and Breast Cancer. *Cancer Cell* **28**, 743–757 (2015).

214. Hanahan, D. & Weinberg, R. A. Hallmarks of cancer: The next generation. *Cell* **144**, 646–674 (2011).

215. Heiden, M. G. V., Cantley, L. C. & Thompson, C. B. Understanding the warburg effect: The metabolic requirements of cell proliferation. *Science (80-.).* **324**, 1029–1033 (2009).

216. Not a simple switch. **1653**, 2020 (2020).

217. Vasan, K., Werner, M. & Chandel, N. S. Mitochondrial Metabolism as a Target for Cancer Therapy. *Cell Metab.* **32**, 341–352 (2020).

218. Hopp, Grüter & Hottiger. Erratum: Hopp, A.K., et al. Regulation of Glucose Metabolism by NAD+ and ADP-Ribosylation. Cells 2019, 8, 890. *Cells* **8**, 1371 (2019).

219. Xu, M. *et al.* NAD kinase sustains lipogenesis and mitochondrial metabolismthrough fatty acid synthesis. *Cell Rep.* **37**, (2021).

220. Gameiro, P. A., Laviolette, L. A., Kelleher, J. K., Iliopoulos, O. & Stephanopoulos, G. Cofactor balance by nicotinamide nucleotide transhydrogenase (NNT) coordinates reductive carboxylation and glucose catabolism in the tricarboxylic acid (TCA) cycle. *J. Biol. Chem.* **288**, 12967–12977 (2013).

221. Zhang, T. & Kraus, W. L. SIRT1-dependent regulation of chromatin and transcription: Linking NAD+ metabolism and signaling to the control of cellular functions. *Biochim. Biophys. Acta - Proteins Proteomics* **1804**, 1666–1675 (2010).

222. Zhang, X. N. *et al.* Discovery of an NAD+analogue with enhanced specificity

for PARP1. *Chem. Sci.* **13**, 1982–1991 (2022).

223. Hogan, K. A., Chini, C. C. S. & Chini, E. N. The Multi-faceted Ecto-enzyme CD38: Roles in immunomodulation, cancer, aging, and metabolic diseases. *Front. Immunol.* **10**, 1–12 (2019).

224. Bieganowski, P. & Brenner, C. Discoveries of Nicotinamide Riboside as a Nutrient and Conserved NRK Genes Establish a Preiss-Handler Independent Route to NAD in Fungi and Humans it became clear that Sir2 and Sir2-related enzymes termed Sirtuins deacetylate lysine residues with consumpt. *Cell* **117**, 495–502 (2004).

225. Ghanem, M. S., Monacelli, F. & Nencioni, A. *Advances in nad-lowering agents for cancer treatment*. *Nutrients* vol. 13 (2021).

226. Verdin, E. NAD+ in aging, metabolism, and neurodegeneration. *Science (80-.).* **350**, 1208–1213 (2015).

227. Audrito, V. *et al.* Tumors carrying BRAF-mutations over-express NAMPT that is genetically amplified and possesses oncogenic properties. *J. Transl. Med.* **20**, 1–13 (2022).

228. Sawicka-Gutaj, N. *et al.* Nicotinamide phosphorybosiltransferase overexpression in thyroid malignancies and its correlation with tumor stage and with survivin/survivin DEx3 expression. *Tumor Biol.* **36**, 7859–7863 (2015).

229. Bi, T. Q. *et al.* Overexpression of Nampt in gastric cancer and chemopotentiating effects of the Nampt inhibitor FK866 in combination with fluorouracil. *Oncol. Rep.* **26**, 1251–1257 (2011).

230. Gibson, A. E. *et al.* Inhibition of nicotinamide phosphoribosyltransferase (NAMPT) with OT-82 induces DNA damage, cell death, and suppression of tumor growth in preclinical models of Ewing sarcoma. *Oncogenesis* **9**, (2020).

231. Thongon, N. *et al.* Cancer cell metabolic plasticity allows resistance to NAMPT inhibition but invariably induces dependence on LDHA. 40170 (2018).

232. Villa, F. *et al.* The Human Fetal and Adult Stem Cell Secretome Can Exert Cardioprotective Paracrine Effects against Cardiotoxicity and Oxidative Stress from Cancer Treatment. (2021).

233. Amaroli, A. *et al.* Photobiomodulation and Oxidative Stress : 980nm Diode Laser Light Regulates Mitochondrial Activity and Reactive Oxygen Species Production. **2021**, (2021).

234. Cappelli, E. *et al.* Redox Biology The passage from bone marrow niche to bloodstream triggers the metabolic impairment in Fanconi Anemia mononuclear cells. *Redox Biol.* **36**, 101618 (2020).

235. Soleilhac, E. *et al.* Quantitative Automated Assays in Living Cells to Screen for Inhibitors of Hemichannel Function. *SLAS Discov.* **26**, 420–427 (2021).

236. Han, Y. *et al.* Identification of SARS-CoV-2 inhibitors using lung and colonic organoids. *Nature* **589**, 270–275 (2021).

237. Zhang, J. H., Chung, T. D. Y. & Oldenburg, K. R. A simple statistical parameter for use in evaluation and validation of high throughput screening assays. *J. Biomol. Screen.* **4**, 67–73 (1999).

238. Roush, G. C., Buddharaju, V., Ernst, M. E. & Holford, T. R. Chlorthalidone: Mechanisms of action and effect on cardiovascular events. *Curr. Hypertens. Rep.* **15**, 514–521 (2013).

239. Shahin, M. H. & Johnson, J. A. Mechanisms and pharmacogenetic signals underlying thiazide diuretics blood pressure response. *Curr. Opin. Pharmacol.* **27**, 31–37 (2016).

240. Jin, P. *et al. Mitochondrial adaptation in cancer drug resistance: prevalence, mechanisms, and management*. *Journal of Hematology and Oncology* vol. 15 (2022).

241. Park, S. H. *et al.* TOMM20 as a potential therapeutic target of colorectal cancer. *BMB Rep.* **52**, 712–717 (2019).

242. Journal, T. H. E. The Oxidation of Fatty Acids Combined bv Isolated Rat Liver Mitochondria * with Albumin. **241**, (1966).

243. Morandi, A. & Indraccolo, S. Biochimica et Biophysica Acta Linking metabolic reprogramming to therapy resistance in cancer. *BBA - Rev. Cancer* **1868**, 1–6 (2017).

244. Olesen, U. H. *et al.* Anticancer agent CHS-828 inhibits cellular synthesis of NAD. *Biochem. Biophys. Res. Commun.* **367**, (2008).

245. Zheng, H. C. The molecular mechanisms of chemoresistance in cancers. *Oncotarget* **8**, 59950–59964 (2017).

246. Ogino, Y., Sato, A., Uchiumi, F. & Tanuma, S.-I. Cross resistance to diverse anticancer nicotinamide phosphoribosyltransferase inhibitors induced by FK866 treatment. *Oncotarget* **9**, 16451–16461 (2018).

247. Piacente, F. *et al.* Nicotinic acid phosphoribosyltransferase regulates cancer cell metabolism, susceptibility to NAMPT inhibitors and DNA repair. *Cancer Res.* canres.3079.2016 (2017) doi:10.1158/0008-5472.CAN-16-3079.

248. O'Brien, T. *et al.* Supplementation of nicotinic acid with NAMPT inhibitors results in loss of in vivo efficacy in NAPRT1-deficient tumor models. *Neoplasia (United States)* **15**, 1314–1329 (2013).

249. Shames, D. S. *et al.* Loss of NAPRT1 expression by tumor-specific promoter

methylation provides a novel predictive biomarker for NAMPT inhibitors. *Clin. Cancer Res.* **19**, 6912–6923 (2013).

250. Marchetti, P., Fovez, Q., Germain, N., Khamari, R. & Kluza, J. Mitochondrial spare respiratory capacity: Mechanisms, regulation, and significance in non-transformed and cancer cells. *FASEB J.* **34**, 13106–13124 (2020).

251. Pfleger, J., He, M. & Abdellatif, M. Mitochondrial complex II is a source of the reserve respiratory capacity that is regulated by metabolic sensors and promotes cell survival. *Cell Death Dis.* **6**, 1–14 (2015).

252. Teh, J. T., Zhu, W. L., Newgard, C. B., Casey, P. J. & Wang, M. Respiratory capacity and reserve predict cell sensitivity to mitochondria inhibitors: Mechanism-based markers to identify metformin-responsive cancers. *Mol. Cancer Ther.* **18**, 693–705 (2019).

253. Salunkhe, S. *et al.* Metabolic rewiring in drug resistant cells exhibit higher OXPHOS and fatty acids as preferred major source to cellular energetics. *Biochim. Biophys. Acta - Bioenerg.* **1861**, 148300 (2020).

254. Farge, T. *et al.* Chemotherapy-resistant human acute myeloid leukemia cells are not enriched for leukemic stem cells but require oxidative metabolism. *Cancer Discov.* **7**, 716–735 (2017).

255. Xu, Y. *et al.* ABT737 reverses cisplatin resistance by targeting glucose metabolism of human ovarian cancer cells. *Int. J. Oncol.* **53**, 1055–1068 (2018).

256. Farnie, G., Sotgia, F. & Lisanti, M. P. High mitochondrial mass identifies a sub-population of stem-like cancer cells that are chemo-resistant. **6**,.

257. Thongon, N. *et al.* Cancer cell metabolic plasticity allows resistance to NAMPT inhibition but invariably induces dependence on LDHA. doi:10.1186/s40170-018-0174-7.

258. Novack, G. V., Galeano, P., Castaño, E. M. & Morelli, L. Mitochondrial Supercomplexes: Physiological Organization and Dysregulation in Age-Related Neurodegenerative Disorders. *Front. Endocrinol. (Lausanne).* **11**, 1–9 (2020).

259. Harvey, K. F., Zhang, X. & Thomas, D. M. The Hippo pathway and human cancer. *Nat. Rev. Cancer* **13**, 246–257 (2013).

260. Wang, Z. *et al.* Regulation of Hippo signaling and triple negative breast cancer progression by an ubiquitin ligase RNF187. *Oncogenesis* **9**, (2020).

261. Ibar, C. & Irvine, K. D. Integration of Hippo-YAP Signaling with Metabolism. *Dev. Cell* **54**, 256–267 (2020).

262. Henríquez, I. *et al.* Current and emerging therapies for metastatic castration-resistant prostate cancer (Mcrpc). *Biomedicines* **9**, 1–13 (2021).

263. Thongon, N. *et al.* The GSK3β inhibitor BIS I reverts YAP-dependent EMT signature in PDAC cell lines by decreasing SMADs expression level. **7**,.

264. Franken, N. A. P., Rodermond, H. M., Stap, J., Haveman, J. & van Bree, C. Clonogenic assay of cells in vitro. *Nat. Protoc.* **1**, 2315–2319 (2006).

265. Hao, Y., Chun, A., Cheung, K., Rashidi, B. & Yang, X. Tumor suppressor LATS1 is a negative regulator of oncogene YAP. *J. Biol. Chem.* **283**, 5496–5509 (2008).

266. Zhao, B. *et al.* Cell detachment activates the Hippo pathway via cytoskeleton reorganization to induce anoikis. *Genes Dev.* **26**, 54–68 (2012).

267. Yuan, M. *et al.* Yes-associated protein (YAP) functions as a tumor suppressor in breast. *Cell Death Differ.* **15**, 1752–1759 (2008).

268. Boland, M. L., Chourasia, A. H. & Macleod, K. F. Mitochondrial dysfunction in cancer. *Front. Oncol.* **3 DEC**, 1–28 (2013).

269. Audrito, V. *et al.* Nicotinamide Phosphoribosyltransferase (NAMPT) as a Therapeutic Target in BRAF-Mutated Metastatic Melanoma. *J. Natl. Cancer Inst.* **110**, 290–303 (2018).

270. Wang, L. *et al.* Curcumin derivative WZ35 inhibits tumor cell growth via ROS-YAP-JNK signaling pathway in breast cancer. *J. Exp. Clin. Cancer Res.* **38**, 1–17 (2019).

271. Di Lisa, F., Menabò, R., Canton, M., Barile, M. & Bernardi, P. Opening of the Mitochondrial Permeability Transition Pore Causes Depletion of Mitochondrial and Cytosolic NAD+ and Is a Causative Event in the Death of Myocytes in Postischemic Reperfusion of the Heart. *J. Biol. Chem.* **276**, 2571–2575 (2001).

272. Rodrigues, T. B. & Ballesteros, P. Journal of Neuroscience Research 85:3244–3253 (2007). *J. Neurosci. Res.* **3253**, 3244–3253 (2007).

273. Sallin, O. *et al.* Semisynthetic biosensors for mapping cellular concentrations of nicotinamide adenine dinucleotides. *Elife* **7**, 1–32 (2018).

274. Lamb, R. *et al.* Mitochondria as new therapeutic targets for eradicating cancer stem cells: Quantitative proteomics and functional validation via MCT1/2 inhibition. *Oncotarget* **5**, 11029–11037 (2014).

275. Sorrentino, G. *et al.* Glucocorticoid receptor signalling activates YAP in breast cancer. *Nat. Commun.* **8**, (2017).

276. Pak, S. *et al.* Glucocorticoid receptor and androgen receptor-targeting therapy in patients with castration-resistant prostate cancer. *Front. Oncol.* **12**, 1–9 (2022).

277. Guo, J. *et al.* Androgen receptor reverts dexamethasone-induced inhibition of prostate cancer cell proliferation and migration. *Mol. Med. Rep.* **17**, 5887–5893 (2018).

278. Doyle, L. M. & Wang, M. Z. Overview of extracellular vesicles, their origin, composition, purpose, and methods for exosome isolation and analysis. *Cells* **8**, 29–39 (2019).

279. Van Niel, G., D'Angelo, G. & Raposo, G. Shedding light on the cell biology of extracellular vesicles. *Nat. Rev. Mol. Cell Biol.* **19**, 213–228 (2018).

280. Zhang, X. *et al.* The Biology and Function of Extracellular Vesicles in Cancer Development. *Front. Cell Dev. Biol.* **9**, 1–9 (2021).

281. Xavier, C. P. R. *et al.* The Role of Extracellular Vesicles in the Hallmarks of Cancer and Drug Resistance. *Cells* **9**, 1–34 (2020).

282. Campos, A. *et al.* Caveolin-1-containing extracellular vesicles transport adhesion proteins and promote malignancy in breast cancer cell lines. *Nanomedicine* **13**, 2597–2609 (2018).

283. Yoshimura, A. *et al.* Exosomal miR-99a-5p is elevated in sera of ovarian cancer patients and promotes cancer cell invasion by increasing fibronectin and vitronectin expression in neighboring peritoneal mesothelial cells. *BMC Cancer* **18**, 1–13 (2018).

284. Setti, M. *et al.* Extracellular vesicle-mediated transfer of CLIC1 protein is a novel mechanism for the regulation of glioblastoma growth. *Oncotarget* **6**, 31413–31427 (2015).

285. König, L. *et al.* Elevated levels of extracellular vesicles are associated with therapy failure and disease progression in breast cancer patients undergoing neoadjuvant chemotherapy. *Oncoimmunology* (2017) doi:10.1080/2162402X.2017.1376153.

286. Tian, F. *et al.* Protein analysis of extracellular vesicles to monitor and predict therapeutic response in metastatic breast cancer. *Nat. Commun.* **12**, 1–13 (2021).

287. Ekström, K. *et al.* Characterization of surface markers on extracellular vesicles isolated from lymphatic exudate from patients with breast cancer. *BMC Cancer* **22**, 1–17 (2022).

288. Brennan, K. *et al.* A comparison of methods for the isolation and separation of extracellular vesicles from protein and lipid particles in human serum. *Sci. Rep.* **10**, 1–13 (2020).

289. Allelein, S. *et al.* Potential and challenges of specifically isolating extracellular vesicles from heterogeneous populations. *Sci. Rep.* **11**, 1–12 (2021).

290. Ludwig, N., Whiteside, T. L. & Reichert, T. E. Challenges in exosome isolation and analysis in health and disease. *Int. J. Mol. Sci.* **20**, (2019).

291. Kosanović, M., Milutinović, B., Goč, S., Mitić, N. & Janković, M. Ion-exchange chromatography purification of extracellular vesicles. *Biotechniques* **63**, 65–71 (2017).

292. Heath, N. *et al.* Rapid isolation and enrichment of extracellular vesicle preparations using anion exchange chromatography. *Sci. Rep.* **8**, 1–12 (2018).

293. Notarangelo, M. *et al.* Ultrasensitive detection of cancer biomarkers by nickel-based isolation of polydisperse extracellular vesicles from blood. *EBioMedicine* (2019) doi:10.1016/j.ebiom.2019.04.039.

294. Předota, M., Machesky, M. L. & Wesolowski, D. J. Molecular Origins of the Zeta Potential. *Langmuir* **32**, 10189–10198 (2016).

295. E Langhoff, J. L. Sodium activity, sodium concentration, and osmolality in plasma in acute and chronic renal failure. *Clin. Chem.* **31**, 1811–1814 (1985).